Scientific Reports

https://doi.org/10.1038/s41598-026-43763-7

Article in Press

A tri-level stochastic framework for planning integrated electricity, gas, and heating networks with enhanced resilience and renewable integration

Received: 30 November 2025

Accepted: 6 March 2026

Published online: 24 April 2026

Cite this article as: Moshkelgosha M., Niknam T. & Bahmani-Firouzi B. A tri-level stochastic framework for planning integrated electricity, gas, and heating networks with enhanced resilience and renewable integration. *Sci Rep* (2026). https://doi.org/10.1038/s41598-026-43763-7

Mahmoud Moshkelgosha, Taher Niknam & Bahman Bahmani-Firouzi

A Tri-Level Stochastic Framework for Planning Integrated Electricity, Gas, and Heating Networks with Enhanced Resilience and Renewable Integration

Mahmoud Moshkelgosha[1], Taher Niknam[2*], Bahman Bahmani-Firouzi[1]

[1]Department of Electrical Engineering, Marv. C., Islamic Azad University, Marvdasht, Iran.

[2]Department of Electrical Engineering, Shiraz University of Technology, Shiraz, 11456-7856, Fars, Iran.

[*]Correspondences: niknam@sutech.ac.ir (T.N)

Abstract: In this work, a new tri-level stochastic optimization formulation is developed for the capacity expansion (CE) planning of an integrated multi-carrier energy system comprising electricity, natural gas, and district heating (DH) networks that explicitly captures the trade-off between economic optimality and system resilience in the face of extreme events. When prior works on the (dis)integration of energy vectors often consider energy vectors independently or overlook disrupted system recovery dynamics, the present research develops an integrated multi-carrier framework that simultaneously determines long-term investment decisions, short-term operational dispatch, and emergency reconfiguration measures. The problem is formulated in a hierarchical manner: the upper level searches for optimal capacity expansion for lines, pipelines, and conversion technologies (CHP, P2G, heat pumps), the middle level solves minimum operational cost problem under ordinary stochastic conditions, and the lower-level deals with maximum load restoration in N-k contingencies by a quantitative resiliency measure. To make the difficult mixed-integer problem computationally tractable, we employ an iterative Column-and-Constraint Generation (C&CG) algorithm. A numerical example of a coupled test system over a ten-year time period displays the feasibility of the presented approach. It is shown that the combined resilience-oriented design planning decreases the total expected costs as well as the resilience cost penalty by ca. 8.4% over the single-energy-system design and even surpasses the performance of deterministic methods considering system resilience, although with increasing costs. Critically, the framework features an endogenous, quantifiable resilience metric that is co-optimized with economic objectives, transforming resilience from a passive design constraint into an active driver of investment decisions. In addition, the framework enables a significant increase in renewables penetration (from 18% to 54%) through exploiting multi-carrier flexibility to buffer intermittency. These results can help guide policy makers on the importance of cross-sectoral coupling to increase infrastructure robustness and demonstrate that such resilience-focused investments are instrumental in enabling deep decarbonization of the energy system.

Keywords: multi-carrier energy systems; integrated electricity-gas-heat networks; tri-level stochastic optimization; resilience assessment; renewable integration; column-and-constraint generation.

Nomenclature

Sets and Indices:

T: Set of planning years, indexed by t.

S: Set of seasonal periods, indexed by s.

H: Set of hourly time steps, indexed by h.

N^{e}: Set of electrical buses, indexed by i,j.

N^{g}: Set of gas nodes, indexed by m,n.

N^{h}: Set of heating nodes, indexed by p,q.

L^{e}: Set of electrical transmission lines, indexed by l^{e}.

L^{g}: Set of gas pipelines, indexed by l^{g}.

L^{h}: Set of heating pipes, indexed by l^{h}.

G^{conv}: Set of conventional generators, indexed by g.

G^{wind}: Set of wind farms, indexed by w.

G^{solar}: Set of solar installations, indexed by pv.

G^{chp}: Set of combined heat and power (CHP) units, indexed by c.

G^{gas}: Set of gas-fired generators.

U^{p2g}: Set of power-to-gas facilities, indexed by k.

U^{boiler}: Set of gas boilers, indexed by b.

U^{hp}: Set of heat pumps, indexed by hp.

$U^{storage,e}$: Set of electrical storage systems, indexed by es.

$U^{storage,g}$: Set of gas storage facilities, indexed by gs.

$U^{storage,h}$: Set of thermal storage units, indexed by hs.

Ω: Set of operational scenarios, indexed by ω.

Ξ: Set of disruption scenarios, indexed by ξ.

C: Set of candidate investment options, indexed by ι.

C^{harden}: Subset of candidate hardening investments.

Z: Set of network zones for resilience assessment, indexed by z.

$Z^{critical}$: Set of critical zones.

$Z^{microgrid}$: Set of microgrid zones.

M^{supply}: Set of gas supply nodes.

$N^{critical,e}$: Set of electrical buses with critical loads.

$P_{i,j}^{path}$: Set of lines in a path connecting buses i and j.

C^{cut}: A cutset in the electrical network.

N^{island}: Set of buses forming an island.

Parameters:

C_{ι}^{inv}: Investment cost for candidate option ι.

$C_{g,t}^{fuel}$: Fuel cost for generator g in year t.

$C_{g}^{startup}$: Startup cost for generator g.

$C_{g}^{shutdown}$: Shutdown cost for generator g.

$C_{m,t}^{gas}$: Cost of gas supply at node m in year t.

$C_{c,t}^{fuel,chp}$: Fuel cost for CHP unit c.

$C_{w}^{curtail,wind}$: Penalty for wind power curtailment.

$C_{pv}^{curtail,solar}$: Penalty for solar power curtailment.

$C_{es}^{degrade}$: Degradation cost for electrical storage es.

$C_{gs}^{operate}$: Operating cost for gas storage gs.

$C_{t,s,h}^{curtail,e}$: Penalty for electrical load curtailment.

$C_{t,s,h}^{curtail,g}$: Penalty for gas load curtailment.

$C_{t,s,h}^{curtail,h}$: Penalty for heating load curtailment.

$C_{l^e}^{switch}$: Cost of switching electrical line l^e.

$C_{l}^{blackstart}$: Cost associated with black start capability at bus l.

$C_{z}^{resilience}$: Resilience cost for zone z.

C_{g}^{attack}: Cost for attacker to disable generator g.

$C_{l^e}^{attack}$: Cost for attacker to disable line l^e.

$\overline{P}_{g}$: Maximum power output of generator g.

$\underline{P}_{g}$: Minimum power output of generator g.

R_{g}^{up}: Ramp-up rate of generator g.

R_{g}^{down}: Ramp-down rate of generator g.

T_{g}^{up}: Minimum up time of generator g.

T_{g}^{down}: Minimum down time of generator g.

η_{g}^{heat}: Heat rate of generator g.

η_{c}^{elec}: Electrical efficiency of CHP unit c.

η_{c}^{heat}: Thermal efficiency of CHP unit c.

$\overline{\Gamma}_{c}^{H2P}$, $\underline{\Gamma}_{c}^{H2P}$: Maximum and minimum heat-to-power ratio for CHP unit c.

η_{k}^{p2g}: Efficiency of power-to-gas facility k.

η_{b}^{boiler}: Efficiency of gas boiler b.

COP_{hp}: Coefficient of performance for heat pump hp.

η_{es}^{charge}: Charging efficiency of electrical storage es.

$\eta_{es}^{discharge}$: Discharging efficiency of electrical storage es.

ρ_{es}^{decay}: Self-discharge rate of electrical storage es.

ϱ_{es}^{E2P}: Energy-to-power ratio for electrical storage es.

$\overline{F}_{l^e}$: Capacity of electrical line l^e.

X_{l^e}: Reactance of electrical line l^e.

$l_{l^e}^{loss}$: Fractional transmission loss on line l^e.

$\overline{Q}_{l^g}$: Capacity of gas pipeline l^g.

K_{l^g}: Pipeline constant for gas pipeline l^g.

$\overline{H}_{l^h}$: Capacity of heating pipe l^h.

Λ_{l^h}: Thermal loss coefficient for heating pipe l^h.

$\underline{Pr}_m^{g,min}$, $\overline{Pr}_m^{g,max}$: Minimum and maximum gas pressure at node m.

$T_p^{h,min}$, $T_p^{h,max}$: Minimum and maximum temperature at heating node p.

$\overline{E}_{es}$: Energy capacity of electrical storage es.

$\overline{P}_{es}^{ch}$, $\overline{P}_{es}^{dis}$: Charging/Discharging power limit of electrical storage es.

$\overline{V}_{gs}$, $\underline{V}_{gs}$: Maximum and minimum volume capacity of gas storage gs.

$\overline{Q}_{gs}^{inj}$, $\overline{Q}_{gs}^{with}$: Injection/Withdrawal rate limit of gas storage gs.

$\overline{Q}_{hs}$: Capacity of thermal storage hs.

$P_{i,t,s,h,\omega}^{d,e}$: Electrical demand at bus i.

$Q_{m,t,s,h,\omega}^{d,g}$: Gas demand at node m.

$H_{p,t,s,h,\omega}^{d,h}$: Heating demand at node p.

$\overline{P}_w^{wind}$: Capacity of existing wind farm w.

$\overline{P}_{pv}^{solar}$: Capacity of existing solar installation pv.

$\overline{P}_c^{chp}$: Electrical capacity of CHP unit c.

$\overline{Q}_c^{chp}$: Thermal capacity of CHP unit c.

$\overline{Q}_b^{boiler}$: Capacity of gas boiler b.

$\overline{P}_{hp}^{hp}$: Electrical capacity of heat pump hp.

$\overline{Q}_{hp}^{hp}$: Thermal capacity of heat pump hp.

$\overline{P}_k^{p2g}$: Capacity of power-to-gas facility k.

$Q_m^{supply,base}$: Base gas supply capacity at node m.

$p_{w,t,s,h,\omega}^{avail,wind}$: Available wind power generation.

$p_{pv,t,s,h,\omega}^{avail,solar}$: Available solar power generation.

$\overline{\kappa}_{l^e}^{max,e}$, $\overline{\kappa}_{l^e}^{total,e}$: Maximum annual and total capacity expansion for electrical line l^e.

$\overline{\kappa}_{l^g}^{max,g}$, $\overline{\kappa}_{l^g}^{total,g}$: Maximum annual and total capacity expansion for gas pipeline l^g.

$\underline{\kappa}_g^{min,gen}$, $\overline{\kappa}_g^{max,gen}$: Minimum and maximum capacity expansion for generator g.

$\overline{P}_g^{total}$: Technical maximum capacity for generator g.

B_t^{budget}: Available investment budget for year t.

$N_i^{min,connect}$: Minimum number of connections required for bus i.

$\overline{Q}_m^{inject,max}$: Maximum allowable gas injection at node m.

RM^e, RM^g, RM^h: Electrical, gas, and heating planning reserve margins.

α^{wind}: Capacity credit factor for wind generation.

β_t^{RES}: Minimum renewable penetration ratio in year t.

γ_z^{gen}: Minimum local generation ratio for zone z.

$\chi_t^{harden,min}$: Minimum fraction of investment allocated to hardening.

$\varsigma^{reserve,g}$: Required gas reserve duration (hours).

$\varepsilon^{p2g,min}$: Minimum power-to-gas capacity ratio relative to wind capacity.

$N_z^{lines,total}$: Total number of lines in zone z.

π_ω: Probability of operational scenario ω.

π_ξ: Probability of disruption scenario ξ.

$A_{l^e,\xi}$: Availability of electrical line l^e under disruption ξ.

$A_{l^g,\xi}$: Availability of gas pipeline l^g.

$A_{g,\xi}$: Availability of generator g.

$A_{m,\xi}^{supply}$: Availability of gas supply at node m.

$\Gamma_\xi^{duration}$: Duration of disruption scenario ξ.

$\Psi_z^{critical}$: Criticality weight of zone z.

$P^{min,island}$: Minimum generation required to form an energized island.

$\alpha_i^{critical}$: Criticality factor for bus i.

$\Delta_i^{max,curtail}$: Maximum allowable cumulative electrical load curtailment.

$\Phi^{min,resil}$: Minimum acceptable system resilience.

$\epsilon^{carrier,balance}$: Maximum allowable imbalance between energy carrier curtailments.

$A_{l^e,\xi}^{base}$: Baseline availability of component l^e.

$\beta_z^{microgrid}$: Resilience enhancement factor from microgrid capability.

B^{attack}: Attacker's resource budget.

$R_{t,s,h}^{spin,up}$, $R_{t,s,h}^{spin,down}$: Upward and downward spinning reserve requirements.

δ_t: Discount factor for year t.

D_s: Duration of season s in days.

η_h: Weight of hour h within seasonal representation.

M^{big}: A sufficiently large constant (Big-M).

First Level Variables (Investment Planning):

$x_{\iota,t}$: Binary investment decision for candidate option ι in year t.

$y^{inv,e}_{l^e,t}$: Binary decision to invest in electrical line l^e.

$y^{inv,g}_{l^g,t}$: Binary decision to invest in gas pipeline l^g.

$y^{inv,gen}_{g,t}$: Binary decision to invest in generator g.

$y^{inv,chp}_{c,t}$: Binary decision to invest in CHP unit c.

$y^{harden,line}_{l^e,t}$: Binary hardening decision for electrical line l^e.

$\kappa^{cap,e}_{l^e,t}$: Continuous capacity expansion for electrical line l^e.

$\kappa^{cap,g}_{l^g,t}$: Capacity expansion for gas pipeline l^g.

$\kappa^{cap,gen}_{g,t}$: Capacity expansion for generator g.

$\kappa^{cap,wind}_{w,t}$: Capacity expansion for wind farm w.

$\kappa^{cap,solar}_{pv,t}$: Capacity expansion for solar installation pv.

$\kappa^{elec,chp}_{c,t}$, $\kappa^{heat,chp}_{c,t}$: Electrical and thermal capacity expansion for CHP unit c.

$\kappa^{supply,g}_{m,t}$: Gas supply capacity expansion at node m.

$\kappa^{cap,p2g}_{k,t}$: Capacity expansion for power-to-gas facility k.

$\kappa^{cap,boiler}_{b,t}$: Capacity expansion for gas boiler b.

$\kappa^{cap,hp}_{hp,t}$: Capacity expansion for heat pump hp.

$\kappa^{power,es}_{es,t}$, $\kappa^{energy,es}_{es,t}$: Power and energy capacity expansion for electrical storage es.

$\kappa^{cap,gs}_{gs,t}$: Capacity expansion for gas storage gs.

$\kappa^{cap,h}_{l^h,t}$: Capacity expansion for heating pipe l^h.

Second Level Variables (Operational Optimization):

$p^{gen}_{g,t,s,h,\omega}$: Power output of conventional generator g.

$u^{gen}_{g,t,s,h,\omega}$: Binary commitment status of generator g.

$v^{startup}_{g,t,s,h,\omega}$, $v^{shutdown}_{g,t,s,h,\omega}$: Binary startup/shutdown variables for generator g.

$p^{chp,e}_{c,t,s,h,\omega}$: Electrical output of CHP unit c.

$q^{chp,h}_{c,t,s,h,\omega}$: Heat output of CHP unit c.

$p^{wind}_{w,t,s,h,\omega}$: Power output of wind farm w.

$p^{solar}_{pv,t,s,h,\omega}$: Power output of solar installation pv.

$p^{p2g}_{k,t,s,h,\omega}$: Power consumption of power-to-gas facility k.

$q^{p2g,out}_{k,t,s,h,\omega}$: Gas production from power-to-gas facility k.

$f^{e}_{l^e,t,s,h,\omega}$: Power flow on electrical line l^e.

$\theta^{e}_{i,t,s,h,\omega}$: Voltage angle at electrical bus i.

$q^{g}_{l^g,t,s,h,\omega}$: Gas flow in pipeline l^g.

$pr^{g}_{m,t,s,h,\omega}$: Gas pressure at node m.

$h^{h}_{l^h,t,s,h,\omega}$: Heat flow in heating pipe l^h.

$\tau^{h}_{p,t,s,h,\omega}$: Temperature at heating node p.

$q^{supply}_{m,t,s,h,\omega}$: Gas supply from external source at node m.

$p^{ch}_{es,t,s,h,\omega}$, $p^{dis}_{es,t,s,h,\omega}$: Charging/Discharging power of electrical storage es.

$e^{soc}_{es,t,s,h,\omega}$: State of charge of electrical storage es.

$q^{inj}_{gs,t,s,h,\omega}$, $q^{with}_{gs,t,s,h,\omega}$: Gas injection/withdrawal for gas storage gs.

$v^{level}_{gs,t,s,h,\omega}$: Storage level of gas storage gs.

$q^{boiler,in}_{b,t,s,h,\omega}$: Gas input to boiler b.

$q^{boiler,out}_{b,t,s,h,\omega}$: Heat output from boiler b.

$p^{hp}_{hp,t,s,h,\omega}$: Electricity consumption of heat pump hp.

$q^{hp,out}_{hp,t,s,h,\omega}$: Heat output from heat pump hp.

$q^{ch,h}_{hs,t,s,h,\omega}$, $q^{dis,h}_{hs,t,s,h,\omega}$: Charging/Discharging heat for thermal storage hs.

$f^{chp,fuel}_{c,t,s,h,\omega}$: Fuel (gas) input to CHP unit.

Third Level Variables (Resilience Assessment):

$\lambda^{curtail,e}_{i,t,s,h,\omega,\xi}$: Electrical load curtailment at bus i.

$\lambda^{curtail,g}_{m,t,s,h,\omega,\xi}$: Gas load curtailment at node m.

$\lambda^{curtail,h}_{p,t,s,h,\omega,\xi}$: Heating load curtailment at node p.

$\sigma^{switch,e}_{l^e,t,s,h,\omega,\xi}$: Binary switching status of electrical line l^e under disruption.

$\sigma^{switch,g}_{l^g,t,s,h,\omega,\xi}$: Binary switching status of gas pipeline l^g.

$\sigma^{switch,h}_{l^h,t,s,h,\omega,\xi}$: Binary switching status of heating pipe l^h.

$\nu^{connect,e}_{i,j,t,s,h,\omega,\xi}$: Binary connectivity indicator between electrical buses i and j.

$\hat{p}^{gen}_{g,t,s,h,\omega,\xi}$: Adjusted power output of generator g under disruption.

$\hat{f}^{e}_{l^e,t,s,h,\omega,\xi}$: Adjusted power flow on electrical line l^e under disruption.

$\hat{q}^{g}_{l^g,t,s,h,\omega,\xi}$: Adjusted gas flow in pipeline l^g under disruption.

$\hat{h}^{h}_{l^h,t,s,h,\omega,\xi}$: Adjusted heat flow in heating pipe l^h under disruption.

$\zeta^{island,e}_{i,z,t,\omega,\xi}$: Binary variable indicating if bus i belongs to island z.

$\mu^{restore}_{z,t,\omega,\xi}$: Fraction of load restored in zone z.

$\phi^{resiliency}_{t,\omega,\xi}$: Overall system resiliency metric.

Abbreviations:

CHP: Combined Heat and Power

COP: Coefficient of Performance

DC: Direct Current (referring to the power flow model)

P2G: Power-to-Gas

RES: Renewable Energy Sources

RM: Reserve Margin

SOC: State of Charge

1-Introduction

The decarbonization of energy systems will require a bulk integration of Variable Renewable Energy sources (VRE), making the demand for operational flexibility more intense. At the same time, the electrification and interweaving of the natural gas and district heating networks – through technologies such as Combined Heat and Power (CHP) units, Power-to-Gas (P2G) plants, heat pumps – have led to the development of a complex Multi-Carrier Energy System (MCES) from the energetic infrastructure. Although this coupling has synergistic effects for flexibility and efficiency, it also brings with a compounded vulnerability, in which failures in one network could cascade on to others and magnify the severity of impact of high-impact low-probability (HILP) events [1]. As such, classical planning methods that consider these systems separately or with deterministic assumptions are no longer sufficient. There is an urgent growing of the need for integrated planning approaches that are capable of addressing the trade-off between long-term investments, short-term operational performance and system robustness in the face of extreme perturbations.

The choice of the proposed tri-level stochastic framework solution based on the Column-and-Constraint Generation (C&CG) algorithm is motivated by the inadequacy of other methods to address the intricacies of modern MCES planning. First, the tri-level structure is better than traditional sequential planning methods (investment, operation and resilience are solved sequentially and independently) as it considers the dependency of decisions; sequential methods lead to unexpected operational flexibility requirements out of disruptions, which results in sub-optimal resilience indices as shown in our comparative analysis (Section 4). Second, unlike Robust Optimization (RO)—a methodology that concentrates on worst-case scenarios and usually produces investment plans that are too conservative and aggressive from an economic point of view—an appropriate stochastic method allows for a risk-neutral economic evaluation in which the costs of investment are balanced by the expected cost of load curtailment. Third, with respect to the solution methodology, traditional Benders Decomposition (BD), commonly employed in related research, is outperformed by C&CG. As the proposed third-level problem (resilience) contains binary variables associated with the network reconfiguration and islanding, typical Benders cuts are on the one hand weak and on the other hand invalid (due to the non-convexity of the subproblem). The C&CG algorithm addresses this deficiency by generating variables and constraints dynamically, resulting in tighter relaxations and significantly faster convergence for policies with mixed-integer recourse, and thus guaranteeing the tractability of the large-scale optimization considered here.

1-1 Research Motivation

The decarbonization of energy systems requires a substantial integration of variable renewable energy sources, which increases the operational flexibility needs of the system and brings new reliability challenges to the system. At the same time, energy systems are more vulnerable to extreme weather events, cyber-physical attacks, and other disturbances, highlighting the significance of resilience. Due to the strong interdependence between electricity, gas, and heat networks, the disruption of one energy carrier may propagate to others, reinforcing the impact. Thus, the inspiration of this work is the lack of a comprehensive planning method capable of exploring the economic, operational, and resilience trade-offs in the context of designing and running integrated multi-carrier energy systems under deep uncertainty.

The planning problem addressed in this work operates under conditions of deep uncertainty, where future system states cannot be predicted by a single forecast and are influenced by multiple, irreducible sources of randomness with potentially severe consequences. We explicitly model two distinct strata of this uncertainty, each with its own risk profile:

The tri-level optimization framework mathematically balances the costs associated with these two uncertainty layers. The objective function (Eq. 1a) minimizes the sum of investment costs and the *expected* costs arising from both operational variability (second level, Eq. 2a) and disruptive events (third level, Eq. 3a). This expected-value formulation provides a risk-neutral economic trade-off. Additionally, a minimum resilience constraint (Eq. 3t) enforces a risk-averse performance guarantee against disruptions. By co-optimizing over both uncertainty sets, the model ensures that investment decisions are economically efficient under normal conditions while being robust against extreme contingencies.

Furthermore, the findings challenge the common perception that investments in system resilience and decarbonization are competing priorities. The model demonstrates that the multi-carrier flexibility, storage, and conversion technologies essential for robust response to extreme events are the same assets that enable high penetration of variable renewables. By proving that resilience-oriented design can simultaneously increase renewable integration from 18% to 54% in the studied case, this work provides a critical policy insight: strategic resilience investments are not merely defensive costs but are fundamental enablers of a secure, low-carbon energy transition. This reframes the policy imperative towards integrated planning that unlocks synergies between security and sustainability.

1-2 Research Background

Research in multi-carrier energy systems (MCES) has evolved across several interconnected dimensions, including hybrid energy integration, long-term planning, hydrogen-based systems, stochastic optimization, and resilience-oriented operation. Early research primarily focused on enhancing energy coordination and techno-economic performance. For instance, [1] proposed a multi-objective optimization model for a complementary biomass–solar–wind system to achieve efficient rural multi-energy utilization, while [2] studied building-integrated photovoltaic (BIPV) optimization for high-rise buildings to facilitate load shifting. At the microgrid scale, [3] presented a coordinated multi-timescale planning model incorporating battery storage, hydrogen technologies, and demand response to enhance flexibility under high renewable penetration.

Hydrogen has emerged as a pivotal energy carrier for deep decarbonization and sector coupling. A comparative techno-economic evaluation of hydrogen and ammonia in multi-generation systems is reported in [4]. The coordination of operations for hydrogen-based MCES was enhanced in [5] via a multi-agent deep reinforcement learning algorithm. The development of hydrogen-based multi-energy systems remains a key research frontier, with [11] providing a review of cooperative planning for hydrogen energy chain systems. Long-term planning of hydrogen capacity with hourly balancing constraints was proposed in [12], and [13] formulated a risk-averse resilient expansion planning model for integrated distribution networks with energy hubs. The system-level integration of hydrogen hubs was further considered in a coordinated planning model [16].

Investigations into long-term performance and resilience have also advanced. [6] presented a life-cycle assessment method for building-integrated energy systems considering equipment degradation, and [7] formulated an optimal planning approach for dairy-farm micro-energy systems that aligns energy and material flows. Cooperative resilience-oriented planning for integrated distribution systems and multi-carrier microgrids with energy trading was addressed in [8]. Robust, IoT-enabled planning utilizing green hydrogen to enhance system reliability was studied in [9]. Marine-energy-supported multi-energy generation for coastal areas was presented in [14], and scenario-based stochastic expansion planning for microgrids considering incentive-based financing was analyzed in [15].

Market interactions and advanced operational coordination under uncertainty constitute another major research strand. A market-based optimization model for MCES was formulated in [18], and multi-stage investment planning for community-scale systems has been proposed in [19]. Cooperative scheduling under distributional uncertainty was studied in [20] using transfers of mobile hydrogen storage to improve reliability. Campus-scale emission-constrained planning was investigated in [21], and a two-stage coordinated scheduling approach for user-side integrated energy systems was presented in [22]. Further examination of market- and hub-level coordination in the presence of uncertainty was performed in [33] using a distributionally robust decentralized scheduling model. [34] demonstrated that decentralized coordinated scheduling with incentive schemes can optimize port-level MCES, and [36] proposed a local hybrid power–hydrogen market design via an uncertainty control approach.

Finally, research continues actively in residential, large-scale, and sector-integration applications. An integrated solar solution for zero-energy homes within a multi-objective framework was developed in [23]. For large-scale systems, [24] proposed a two-step robust synthesis model for carbon capture, utilization, and storage (CCUS) and hydrogen production. Pareto-based optimization for hybrid renewable systems with hydrogen integration was introduced in [25]. Multi-objective capacity configuration considering economic and environmental performance is investigated in [26], while a hydrogen-based MCES configuration using solid oxide electrolyzers with efficiency degradation is studied in [27]. Thermal–electrical integration has been advanced through methods such as the bi-level scheduling approach considering thermal and hydraulic transients proposed in [28] and the stochastic coordination framework in [29] for smart microgrids. Community-scale planning with demand-side management is explored in [31], and a probabilistic two-step approach for activating demand response in renewable-intensive systems is presented in [32]. At the residential level, [37] developed a robust optimization framework for smart home energy management. The impact of electrolyzer allocation on transmission systems is analyzed in [38], and a comprehensive report on e-mobility deployment and its impact on European grids is provided in [39]. Flexibility enhancement of urban energy systems through coordinated space heating aggregation is studied in [40]. Finally, [41] presents an optimal supply chain design using machine learning, risk assessment, and optimization.

1-3 Study Gaps

Although advances have been made in the area, there remain large gaps. First, many of the integrated planning models do not have a hierarchical structure that integrates the cascading strategic investment decision with the operational and post-disruption reconfiguration layers. Second, resilience is frequently addressed qualitatively or relegated to an a posteriori assessment rather than being an endogenous objective in the optimization. Third, the solution of large-scale, tri-level stochastic problems with mixed-integer recourse and a large number of scenarios is often computationally intractable, which may cause the introduction of simplifications that reduce the fidelity of the model and/or the quality of the solution. Finally, a shortage of frameworks that yield a quantitative, scenario-based resilience metric to capture the performance of all linked energy carriers during and after disruptive events exists. A critical methodological gap this work addresses is the inadequacy of standard bi-level optimization formulations for this integrated planning problem. A bi-level structure is incapable of capturing the nested feedback loop between operational flexibility and post-disruption reconfiguration. If operation and resilience are combined into a single lower level, the model implicitly assumes the system is perpetually under duress, leading to overly conservative and economically inefficient investment. Conversely, if resilience is evaluated as a separate, post-hoc analysis following investment and operational planning, the resulting investments are blind to a critical fact: the system's recovery capability is fundamentally constrained by the pre-disturbance operational state (e.g., storage state of charge, generator commitment). This decoupling fails to value—and therefore fails to incentivize investment in—operational flexibility that also serves as resilience capacity. Our tri-level hierarchy explicitly models this three-stage decision sequence, ensuring that resilience is not an add-on cost but an endogenous outcome of coordinated investment and operational planning. In Table 1, the novelty of the proposed framework is highlighted through a comparative analysis based on four key methodological dimensions. In contrast to existing literature, our contribution is the only one that simultaneously integrates a tri-level decision hierarchy,

models resilience as an endogenous and quantifiable objective, employs a customized C&CG algorithm to solve the resulting large-scale mixed-integer problem, and performs fully coordinated long-term planning for integrated electricity, gas, and heating networks. This synthesis enables a holistic simulation of infrastructure responses to both operational variability and disruptive events.

Table (1) Comparative analysis of the proposed tri-level resilient planning model and related studies based on key methodological innovations

Ref.	Year	Method/Model Focus	TL	ER	C&CG	MC
Our Paper	2025	**Resilient Tri-Level Stochastic Planning of Integrated Electricity–Gas–Heating Networks**	**Yes**	**Yes**	**Yes**	**Yes**
[1]	2025	Multi-objective biomass–solar–wind hybrid planning	No	No	No	Yes
[2]	2024	BIPV optimization for load shifting	No	No	No	No
[3]	2025	Multi-timescale BESS–H□ planning	No	No	No	Yes
[4]	2025	Techno-economic hydrogen/ammonia comparison	No	No	No	Yes
[5]	2025	Hydrogen IES with Multi-Agent Deep Reinforcement Learning	No	No	No	Yes
[6]	2026	Life-cycle performance with degradation	No	No	No	No
[7]	2025	Dairy-farm micro-energy system planning	No	No	No	Yes
[8]	2024	Cooperative resilience-oriented planning for integrated systems	No	Yes	No	Yes
[9]	2026	Renewable multi-carrier system with IoT	No	No	No	Yes
[10]	2025	Transactive multi-carrier energy scheduling	No	No	No	Yes
[11]	2025	Hydrogen chain planning review	No	No	No	No
[12]	2025	Urban H□ multi-region capacity planning	No	No	No	Yes
[13]	2025	Risk-averse resilient expansion planning	No	Yes	No	Yes
[14]	2025	Marine-energy-supported multi-energy system	No	No	No	Yes
[15]	2025	Robust scenario-based MC planning	No	No	No	Yes
[16]	2025	IES with hydrogen hub planning	No	No	No	Yes
[17]	2025	Long-term planning with vehicle-to-grid	No	No	No	Yes
[18]	2025	Market-based multi-carrier optimization	No	No	No	Yes
[19]	2024	Multi-stage investment for multi-energy carriers	No	No	No	Yes
[20]	2025	DRO cooperative multi-carrier scheduling	No	No	No	Yes
[21]	2023	Environment-constrained campus planning	No	No	No	Yes
[22]	2025	Two-stage IES scheduling	No	No	No	Yes
[23]	2025	Solar residential multi-objective optimization	No	No	No	No
[24]	2025	IES with CCUS and H□ robust configuration	No	No	No	Yes
[25]	2025	H□-enabled multi-objective Pareto framework	No	No	No	Yes
[26]	2022	Harvest-heat system planning	No	No	No	No
[27]	2026	SOE-based H□ MES with degradation	No	No	No	Yes
[28]	2022	Bi-level electric-thermal regulation	No	No	No	Yes
[29]	2023	Stochastic MC microgrid optimization	No	No	No	Yes
[30]	2025	Cloud MPC for multi-carrier home EMS	No	No	No	Yes
[31]	2024	Multi-objective community IES	No	No	No	Yes
[32]	2024	Probabilistic DR-enabled IES	No	No	No	Yes
[33]	2023	DRO decentralized scheduling	No	No	No	Yes
[34]	2025	Two-tier coordinated port IES	No	No	No	Yes
[35]	2024	Real-world H□ microgrid deployment	No	No	No	Yes
[36]	2024	Local energy market for H□ microgrids	No	No	No	Yes

Abbreviations: TL: Tri-level integrated decision-making (Investment–Operation–Resilience); ER: Endogenous & Quantifiable Resilience within optimization; C&CG: Solution via Column-and-Constraint Generation for MIP recourse; MC: Comprehensive Multi-Carrier (Electricity, Gas, Heat) coupling.

1-4 Research Contributions

We propose a full tri-level stochastic optimization model for the co-planning of electricity, natural gas and district heating networks, and our work contributes to energy systems analysis in the following ways:

1. Novel tiered modeling approach: We present a tri-level stochastic programming model which captures the sequential and interrelated decision process in the multi-carrier energy systems. The first level solves for long term strategic investment and capacity augmentation decisions for all infrastructures. The second stage performs the short-term operational dispatch optimization for a multiplicity of typical operating conditions, under detailed physical system constraints and interdependencies among different energy networks at the same time. Based on an analysis of

system viability under a specified set of high-impact/low-probability disruption events, the third stage prescribes optimal post-disruption system reconfiguration and load restoration strategies. The proposed hierarchical structure guarantees that investment decisions will be investment decisions responsive to their consequences for both routine operation and extreme event response, an critical coupling rarely captured in previous work.

2. Endogenous and Quantifiable Resilience Metric: A major novelty is the definition of a quantitative, probabilistic resiliency index that is inherently captured by the optimization objective. This metric is a weighted average of the restored load fractions in multiple subareas where load percentages are weighted with zonal criticality. By translating the typically qualitative notion of resilience into a computable and optimizable number, our framework enables a direct economic comparison between the cost of investing in resilience (e.g., hardening, redundancy, flexible assets) and the anticipated cost of load curta ilment during disruptions. This goes beyond post-analysis resilience evaluation, making resilience an equal driver of the planning process as economic efficiency.

3. An Efficient Solution Approach: We develop a customized solution algorithm based on the column-and-constraint generation (C&CG) algorithm to address the enormous computational burden of the resulting tri-level mixed-integer program. This procedure is accelerated on a number of fronts: (i) splitting of the operational subproblem by season with a progressive hedging approach to address temporal coupling, (ii) dualization-based reformulation of the resilience subproblem to treat its bi-level nature, and (iii) the embedding of valid inequalities (e.g. network cutset constraints) in the form of branch-and-cut scheme to strengthen the relaxation. As a result, the proposed high-fidelity model is amenable to solution for system of realistic sizes while avoiding oversimplifying assumptions.

4. Detailed Empirical Validation and Policy Implications: We rigorously substantiate the practical value of the proposed framework with an extensive case study of a prototypic urban energy system. The results demonstrates not only substantial improvement of economic (e.g., lower operating costs) and environmental (e.g., higher renewable penetration) performance, but also significant enhancement of system resilience, as evidenced by lower load curtailment and shorter restoration duration under multiple disruption scenarios. In addition, scalability results are presented to illustrate the application to larger-scale systems, a sensitivity analysis is undertaken to determine effects of crucial parameters such as discount rates and fuel prices, and a comparison with established planning approaches is conducted to quantify the benefit of the integrated, resilient, and stochastic planning approach.

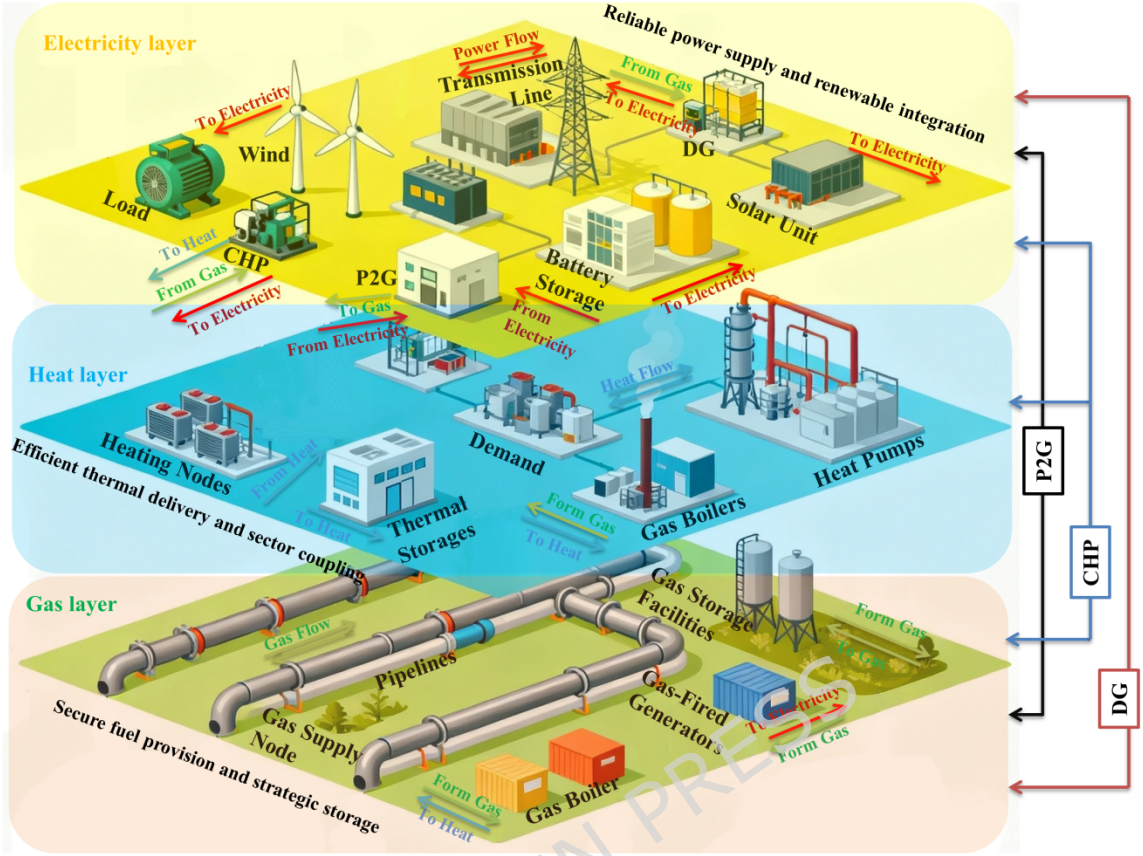

Fig. 1. Integrated multi-carrier energy network: coupled electricity, gas, and heat subsystems with energy conversion links

The architecture of the integrated multi-carrier energy system is shown in Figure (1). It depicts the coupled electricity, natural gas, and district heating networks, which form a single, co-optimized infrastructure. The electricity subsystem includes power generation, transmission, and storage facilities that include distributed generator, solar units, wind turbines, batteries, and lines connecting buses and loads over which electricity is delivered. It also accommodates coupling techniques like combined heat and power devices (CHP) and power to gas (P2G) converters connecting the power system to the gas network. Here, the middle layer is the heating network with heating nodes, thermal storage units, heat pumps and gas boilers that serve the thermal loads of the consumers. This layer is energized with electricity from the electricity layer via electric heat pumps and energy from the gas layer via gas boilers and CHPs. The lower layer depicts the gas system with pipelines, gas supply nodes, storage facilities, and gas fired generators. Devices of energy conversion such as producer/ consumer of electricity CHPs, P2G units, are the physical links between all three layers allowing bidirectional exchanges of e.g., electricity to produce gas via P2G, and gas to produce electricity by gas fired generators and CHPs as well as use of both gas and electricity to produce heat through boilers or heat pumps. The flowchart thus captures the co-optimized energy system whereby multi carrier energy interactions within coupled networks are coordinated to improve operation, enhance efficiency, and increase system resilience.

1-5 Paper Organization

The rest of the paper is organized as follows. The proposed tri-level stochastic optimization model for the integrated multi-carrier system is described in Section 2. Solution methodology is described in Section 3 based on the column-and-constraint generation (C&CG) and the related acceleration techniques. Section 4 is devoted to a detailed illustrative numerical example the consists in setting parameters, scenarios definition, computational implementation and finally an analysis of results from investments, operations

and resilience. It also contain sensitivity, scalability, and comparative analysis. Finally, in Section 5, the paper is concluded by summarizing the key contributions and by suggesting several potential future research.

2-Proposed Model

The proposed framework is structured as a tri-level optimization model for the integrated multi-carrier energy system, hierarchically coordinating strategic investment, operational scheduling, and post-disturbance mitigation, which is also a main analytical tool of this work. The first stage solves the long-term investment planning problem by choosing optimal capacity expansion and infrastructure strengthening measures within electricity, gas, and heating networks subject to budget, policy, and technical feasibility constraints. The second level models the operational planning, simulating the short-term joint operation of the generation, storage and conversion units for a large number of normal operating conditions, considering the physical constraints and coupling interactions of the connected networks in detail. In the third stage the resilience evaluation is conducted, wherein performance of the system is assessed against different disruption scenarios and the method is used to identify the best network reconfiguration and load recovery strategies to reduce the severity of outages. These stages are coupled through a set of shared variables and constraints, thus capturing explicitly the operational feasibility and resilience robustness of the investment decisions, which yields a single, cohesive planning framework spanning long-term strategy to short-run and contingency operations.

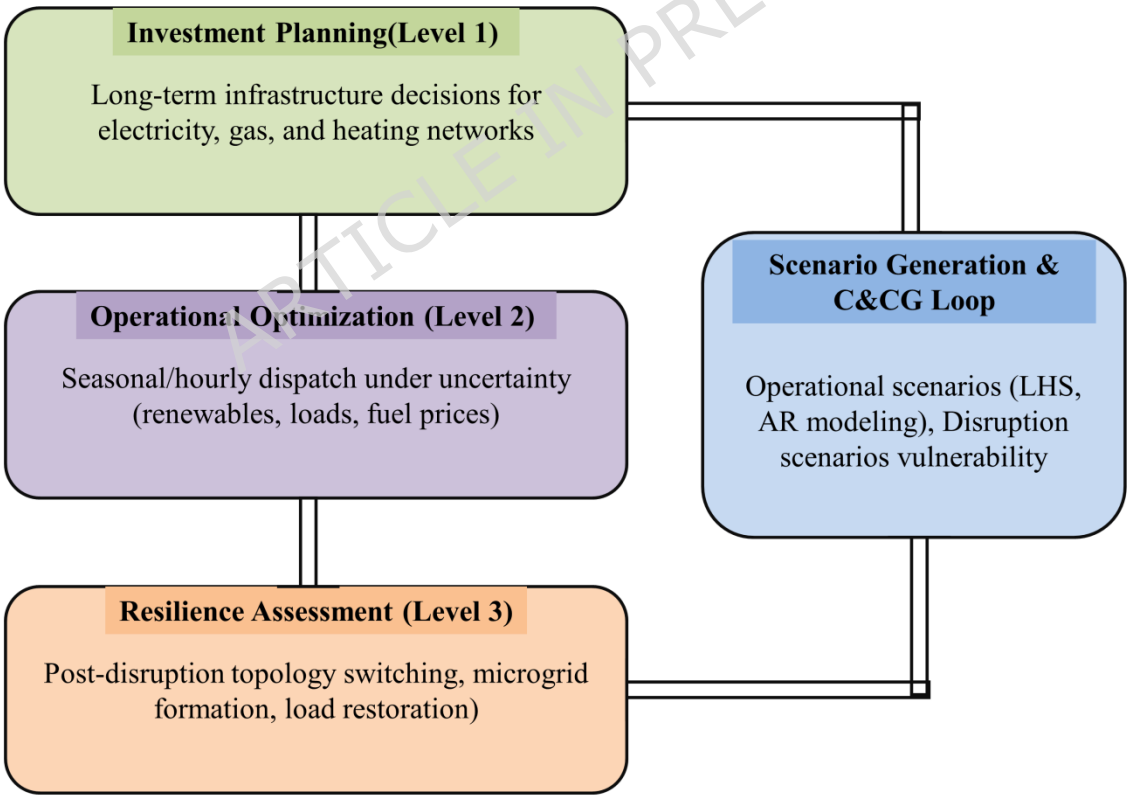

Fig. 2. Conceptual framework of the tri□level stochastic planning model for the integrated multi-carrier (electricity, gas, heat) system, showing the scenario generation and iterative C&CG solution process

Figure (2) demonstrates the conceptual representation of the tri level stochastic programming model in the presence of resilience for integrated electricity, gas, and district heating networks. The flow chart illustrates the hierarchy between the level three optimizations and the interaction with scenario generation and the iterative column and constraint generation (C&CG) process. The first level corresponds to investment planning, where long term decisions on network expansion and infrastructure hardening are taken. The results of this stage constitute the capacities and topologies that are feasible for a following operational analysis. The second level is the operational optimization problem that determines short term commitment of generating units, storages, and coupling devices over scenarios of renewable generation, load, and fuel price uncertainty. Results at this stage are employed to assess the daily routine operation of the system given the investment plan. The third level two analyzes resilience and reconfiguration against prospective disruptions, basing its evaluation on the system's capability to restore the supply through topology switching and microgrid formation; the third level then patches the network against severe outages and investigates microgrid operation. The block on the right captures the scenario generation and iterative refinement loop that builds operational and disruption scenarios, derives feasibility and optimality cuts, and sends them back to the higher levels. The iterative process of information exchange between the three levels guarantees a synchronized update of costs and constraints in the converged solution. Overall, the figure encapsulates the logical sequence of decisions and feedback mechanisms in the tri level optimization and solution scheme.

2-1-First Level: Investment Planning Model

The upper level of the proposed tri-level model is the stage of the investment planning, which represents the basis for long-term decisions affecting the integrated multi-carrier energy system. It aims at reducing the discounted sum of all the relevant costs over the planning horizon, subject to the adequacy, reliability, and resilience of the system. The overall objective function is given by (1a) and includes investment costs related to generation, transmission, gas and heating grids, and operation and resilience costs. The discount factor reflects the value of money in multiple years. The cost of operation is the expected cost of normal system operation over different scenarios, and the resilience cost is the expected cost of sustaining or recovering system performance during disruptive events. This consitutes a nice return to a principle of well-balanced trade-offs between economic efficiency and robustness against uncertainty and physical stress. Equation (1b) introduces an irreversibility constraint, which implies that each potential project is executed at most once in the entire planning horizon. This constraint avoids the repetition of decisions to invest in different years, and is what standing investment decisions are meant to represent in the real world of heavy infrastructure investments. Equation (1c) guarantees the temporal consistency across the investment years by imposing the constraint that the capacity built in a certain period will be used in the following years. It also enforces a logical ordering such that after an action is taken, the same action is taken at all subsequent stages. The sufficiency condition for electricity generation is given in (1d). The sum of the existing capacity and all the accumulated new capacity from conventional generators, wind farms and combined heat and power plants must be at least equal to peak electrical demand multiplied by a reserve margin. The impact of variability of wind generators is discounted through a capacity credit factor. This ensures that generation adequacy is equal to the peak load plus a reserve to cover for contingencies and unanticipated increments in the load. The adequacy condition for the gas network is expressed in (1e). The total quantity of gas supplied (produced and imported, including base supply and new developments) must be at least equal to the total gas required by all consumers, under the worst case in terms of peak consumption. This includes gas demand from direct consumption, gas in power generation and gas in heat production. A gas reserve margin is added to provide a adequate gas supply under the most severe operational conditions. Equation (1f) correspondingly defines a similar expression for the heat sector. The sum of available thermal generation from combined heat and power (CHP) units, gas boilers and heat pumps must be higher than the hourly thermal load of the year with the highest load, multiplied by a certain reserve margin. This additionally reserves capacity to accommodate sudden increases in heating demand and uphold thermal reliability during cold spells or fuel scarcity. The expansion of the electrical transmission/lines in (1g) and (1h). Equation (1g) caps the capacity expansion per line, bounded by technical constraints and right-of-way, and links the expansion quantity to a binary investment variable. Equation (1h) enforces an upper bound on the sum of incremental expansions invested in each line,

guaranteeing that the magnitude of total expansions does not exceed allowed physical or regulatory limits. Analogously, equations (1i) and (1j) enforce similar constraints for the gas pipeline system (both maximum allowed expansions per year and total long-run expansions). Equation (1k) restricts the amount of capacity addition for each generator to be within the technical limits of the minimum and maximum allowed expansion size. This results in more realistic unit installation decisions consistent with generator design options, available. Equation (1l) also limits the sum of existing and new capacity to each specific generating plant's ultimate technical potential to prevent overinvestment on a physical scale. Equation (1m) enforces renewable portfolio targets. This assures that the total capacity installed of renewable units (wind and solar) is greater than or equal to a certain percentage of the total capacity of conventional generation. This percentage, given by the minimum renewable penetration ratio, sets annual targets to steer system evolution towards decarbonization policies. Equation (1n) deals with storage element sizing. It enforces the energy-to-power ratio constraint to preserve a correct relationship between the energy storage capacity and rated power, implying a certain operational flexibility. This ratio also helps maintaining the storage system performance and avoiding unfeasible investments. Equation (1o) adds the annual budget constraint to make sure the total investment is less than the available income, since yearly outward investment must be bounded. It sums investment costs in generation, network, renewables and storage to ensure annual spending is financially feasible. Equation (1p) imposes the network connectivity constraints, where, for each bus, minimum number of outgoing connections is determined by predefined topological and reliability criteria. This prevents isolated nodes and guarantees stable grid form when expanding grid topologies. Equation (1q) restricts the power-to-gas capacity in terms of the maximal injection allowed to the gas network at every node. This injection limit is to observe the operational and safety regulations of the gas network, and the sum of the installed power-to-gas capacity of power-to-gas plants collocated at a node cannot be higher than the injection limit. Equation (1r) specifies the co-generation relation for combined heat and power investment in our model, by connecting the thermal and the electrical capacity expansions via the associated efficiency factors. This ensures that the technical heat to power production ratio for each CHP technology is maintained. Equation (1s) imposes geographic diversification constraints on generation expansion. It imposes a minimum amount of local generation at each zone with respect to its load to prevent too much spatial concentration of capacity which may cause problems in system reliability under regional contingencies. Equation (1t) defines a bulding investment threshold. A fixed portion of total investment must be invested in hardening or protective measures to increase the resiliency of the infrastructure in the face of disrupt events. This guarantees that resilience building will be rooted in the long term planning. Equation(1u) imposes the monotone increasing behavior of renewable energy capacity over the planning horizon time periods. Wind and solar IC in every year must be greater than or equal to the one in the previous year to reflect the realistic growing trend from policy in the study region. Equation (1v) guarantees an adequate gas storage capacity to generate the required strategic reserves. The total working volume of the base and incremental facilities must hold a quantity of gas consistent with a given reserve period over peak gas demand. This provides a hedge against a long-term interruption of fuel supply. Equation (1w) limits the growth of power-to-gas plants relative to wind generation capacity. It requires the overall power-to-gas capacity to be at least proportional to wind capacity, thus guaranteeing a compensatory growth of the electricity-to-gas conversion options with the renewable growth. Equation (1x) integrates vulnerability analyses within planning. It is for each critical network zone to have at least a certain number of hardened electric lines, proportional to their risk index and the number of lines they contain. This constraint directly couples system hardening to the vulnerability pattern in the spatial domain, which allows for an adaptive hardening design within the long-term planning. Together, these equations yield a holistic first-level investment planning model that guarantees economically," good, technical feasible, and resilient operation of integrated multi-carrier energy systems over the entire planning horizon.

$$\min_{x,y,\kappa} \Phi_1 \tag{1a}$$

$$= \sum_{t\in T} \delta_t \Big[\sum_{\iota\in C} C_{\iota}^{inv} x_{\iota,t} + \sum_{l^e\in L^e} C_{l^e,t}^{inv,e} \kappa_{l^e,t}^{cap,e} + \sum_{l^g\in L^g} C_{l^g,t}^{inv,g} \kappa_{l^g,t}^{cap,g} + \sum_{g\in G^{conv}} C_{g,t}^{inv,}$$

$$+ \Theta_t^{op} + Y_t^{resil} \Big]$$

$$\sum_{t\in T} x_{\iota,t} \le 1 \;\forall \iota \in C \tag{1b}$$

$$x_{\iota,t} \le x_{\iota,t+1} + \left(1 - \sum_{\tau=1}^{t+1} x_{\iota,\tau}\right) \forall \iota \in C, \forall t \in T \tag{1c}$$

$$\sum_{g\in G^{conv}} \left(\overline{P}_g + \sum_{\tau=1}^{t} \kappa_{g,t}^{cap,gen}\right) + \sum_{w\in G^{wind}} \left(\overline{P}_w^{wind} + \sum_{\tau=1}^{t} \kappa_{w,t}^{cap,wind}\right)\alpha^{wind} + \sum_{c\in G^{chp}} \left(\overline{P}_c^{chp} + \sum_{\tau=1}^{t} \kappa_{c,\tau}^{cap,chp}\right) \ge (1 + RM^e)\max_{s,h,\omega} \sum_{i\in N^e} P_{i,t,s,h,\omega}^{d,e} \;\forall t \in T \tag{1d}$$

$$\sum_{m\in M^{supply}} \left(Q_m^{supply,base} + \sum_{\tau=1}^{t} \kappa_{m,\tau}^{supply,g}\right) \ge (1 + RM^g)\max_{s,h,\omega}\left[\sum_{m\in N^g} Q_{m,t,s,h,\omega}^{d,g} + \sum_{g\in G^{gas}} \eta_g^{heat} p_{g,t,s,h,\omega}^{gen} + \sum_{b\in U^{boiler}} q_{b,t,s,h}^{boiler,} \right. \;\forall t \in T \tag{1e}$$

$$\sum_{c\in G^{chp}} \left(\overline{Q}_c^{chp} + \sum_{\tau=1}^{t} \kappa_{c,\tau}^{heat,chp}\right) + \sum_{b\in U^{boiler}} \left(\overline{Q}_b^{boiler} + \sum_{\tau=1}^{t} \kappa_{b,t}^{cap,boiler}\right) + \sum_{hp\in U^{hp}} \left(\overline{Q}_{hp}^{hp} + \sum_{\tau=1}^{t} \kappa_{hp,\tau}^{cap,hp}\right) \ge (1 + RM^h)\max_{s,h,\omega} \sum_{p\in N^h} H_{p,t,s,h,\omega}^{d,h} \;\forall t \in T \tag{1f}$$

$$\kappa_{i^e,t}^{cap,e} \le \overline{\kappa}_{i^e}^{max,e} y_{i^e,t}^{inv,e} \;\forall i^e \in L^e, \forall t \in T \tag{1g}$$

$$\sum_{\tau=1}^{t} \kappa_{i^e,\tau}^{cap,e} \le \overline{\kappa}_{i^e}^{total,e} \;\forall i^e \in L^e, \forall t \in T \tag{1h}$$

$$\kappa_{i^g,t}^{cap,g} \le \overline{\kappa}_{i^g}^{max,g} y_{i^g,t}^{inv,g} \;\forall i^g \in L^g, \forall t \in T \tag{1i}$$

$$\sum_{\tau=1}^{t} \kappa_{i^g,\tau}^{cap,g} \le \overline{\kappa}_{i^g}^{total,g} \;\forall i^g \in L^g, \forall t \in T \tag{1j}$$

$$\underline{\kappa}_g^{min,gen} y_{g,t}^{inv,gen} \le \kappa_{g,t}^{cap,gen} \le \overline{\kappa}_g^{max,gen} y_{g,t}^{inv,gen} \;\forall g \in G^{conv}, \forall t \in T \tag{1k}$$

$$\overline{P}_g + \sum_{\tau=1}^{t} \kappa_{g,t}^{cap,gen} \le \overline{P}_g^{total} \;\forall g \in G^{conv}, \forall t \in T \tag{1l}$$

$$\sum_{w\in G^{wind}} \left(\overline{P}_w^{wind} + \sum_{\tau=1}^{t} \kappa_{w,t}^{cap,wind}\right) + \sum_{pv\in G^{solar}} \left(\overline{P}_{pv}^{solar} + \sum_{\tau=1}^{t} \kappa_{pv,t}^{cap,solar}\right) \ge \beta_t^{RES} \sum_{g\in G^{conv}} \left(\overline{P}_g + \sum_{\tau=1}^{t} \kappa_{g,t}^{cap,gen}\right) \forall t \in T \tag{1m}$$

$$\sum_{\tau=1}^{t} \kappa_{es,\tau}^{energy,es} = \varrho_{es}^{E2P} \sum_{\tau=1}^{t} \kappa_{es,\tau}^{power,es} \;\forall es \in U^{storage,e}, \forall t \in T \tag{1n}$$

$$\sum_{\iota \in C} C_{\iota}^{inv} x_{\iota,t} + \sum_{l^e \in L^e} C_{l^e,t}^{inv,e} \kappa_{l^e,t}^{cap,e} + \sum_{l^g \in L^g} C_{l^g,t}^{inv,g} \kappa_{l^g,t}^{cap,g} + \sum_{g \in G^{conv}} C_{g,t}^{inv,gen} \kappa_{g,t}^{cap,gen} + \sum_{w \in G^{wind}} C_{w,t}^{inv,wind} \kappa_{w,t}^{cap,wind} + \sum_{pv \in G^{solar}} C_{pv,t}^{inv,solar} \kappa_{pv,t}^{cap,solar} \le B_t^{budget} \; \forall t \in T \quad (1o)$$

$$\sum_{l^e \in L^e : l^e \in L_i^{out}} y_{l^e,t}^{inv,e} \ge N_i^{min,connect} \; \forall i \in N^e, \forall t \in T \quad (1p)$$

$$\sum_{k \in U^{p2g} : k \in U_m^{p2g}} \left(\overline{Q}_k^{p2g} + \sum_{\tau=1}^{t} \kappa_{k,t}^{cap,p2g} \right) \le \overline{Q}_m^{inject,max} \; \forall m \in N^g, \forall t \in T \quad (1q)$$

$$\kappa_{c,t}^{heat,chp} = \frac{\eta_c^{heat}}{\eta_c^{elec}} \kappa_{c,t}^{elec,chp} \; \forall c \in G^{chp}, \forall t \in T \quad (1r)$$

$$\sum_{g \in G_z^{conv}} \left(\overline{P}_g + \sum_{\tau=1}^{t} \kappa_{g,t}^{cap,gen} \right) \ge \gamma_z^{gen} \sum_{i \in N_z^e} \max_{s,h,\omega} P_{i,t,s,h,\omega}^{d,e} \; \forall z \in Z, \forall t \in T \quad (1s)$$

$$\sum_{\iota \in C^{harden}} C_{\iota}^{inv} x_{\iota,t} \ge \chi_t^{harden,min} \sum_{\iota \in C} C_{\iota}^{inv} x_{\iota,t} \; \forall t \in T \quad (1t)$$

$$\sum_{w \in G^{wind}} \kappa_{w,t}^{cap,wind} + \sum_{pv \in G^{solar}} \kappa_{pv,t}^{cap,solar} \ge \sum_{w \in G^{wind}} \kappa_{w,t-1}^{cap,wind} + \sum_{pv \in G^{solar}} \kappa_{pv,t-1}^{cap,solar} \; \forall t \in T \quad (1u)$$

$$\sum_{gs \in U^{storage,g}} \left(\overline{V}_{gs} + \sum_{\tau=1}^{t} \kappa_{gs,\tau}^{cap,gs} \right) \ge \varsigma^{reserve,g} \max_{s,h,\omega} \sum_{m \in N^g} Q_{m,t,s,h,\omega}^{d,q} \; \forall t \in T \quad (1v)$$

$$\sum_{k \in U^{p2g}} \kappa_{k,t}^{cap,p2g} \ge \varepsilon^{p2g,min} \sum_{w \in G^{wind}} \kappa_{w,t}^{cap,wind} \; \forall t \in T \quad (1w)$$

$$\sum_{l^e \in L_z^e} y_{l^e,t}^{inv,e} \ge \lceil \Psi_z^{critical} \cdot N_z^{lines,total} \rceil \; \forall z \in Z^{critical}, \forall t \in T \quad (1x)$$

2-2-Second Level: Operational Optimization Model

The tri-level framework is detailed in the next section. the tri-level programming that is advanced so far. The second level of the tri-echelon framework is submitted to operational management including determination about the short-term operational operation strategy of the integrated multi-carrier energy system subject to its normal performance. It regards the investment decisions obtained in the first level as input parameters and optimizes generation dispatch, network flows, and storage at the operational stage in all the operational scenarios, seasons of the year and representative hours. At this stage it is based on minimization of the expected operational cost subject to operational constraints and to the coupling constrains among the electricity, gas and heat network. Equation (2a) is the objective function which is to minimize the expected total system cost of operation for all the years-seasons-hours-scenarios. It sums the fuel, start-up and shut-down and supply cost of thermal and co-generation units, the penalty cost of curtailment ofrenewable resources and the degradation cost or operation cost of electric and gas storage systems. Probability, season duration and hour weight are multiplied with each term in order to express the expected temporal and probabilistic effects. The resultant objective function reflects the economic tradeoff between dispatch efficiency and technology utilization in the presence of uncertain outputs. Equation (2b) is the nodal power balance equation for the electrical network. At each bus and under all scenarios the total power injected by thermal, wind, solar, and combined heat and power (CHP) units and discharging storages must be equal to the total power withdrawn by load, charging storages, power-to-gas (P2G) units, heat pumps, and net power transfers over the connected transmission lines. The formulation treats transmission

losses as a constant proportion of line flows, without losing the exact power balance at each node. The power production of any conventional generator is also limited by its capacity and commitment status in (2c). The lower limit corresponds to the minimum technical limit of the unit when it is on and the upper limit includes both the initial nominal capacity and any extension decisions made at the first stage. Equations (2d) and (2e) place restrictions from ramping-up and down, on the rate of change of the generation output from hour to hour. Start-up and shutdown are also considered to facilitate more rapid change when a unit is switched on or off. The binary start-up and shut-down variables are connected to the change of commitment status by Eq (2F) to guarantee the consistency of the operation sequencing and the logic structure of unit operation. Constraints (2g) and (2h) are the min up and min down time constraints. Upon a start-up a generating unit must stay on line for its minimum up time and after a shut-down, a unit is not allowed to be restarted within the minimum down time. Equation (2i) is the DC power flow equation which relates the active power flow and voltage angle difference on a transmission line, i. e. The D-C approximation of the power flow equations (linearized electrical flow equations) is used to represent network constraints in an efficient way which allows the problem to be solved for realistic system sizes. The maximum line flow is bounded in (2j) by the original design capacity fire together with any incremental capacity added at the investment stage. A reference bus condition is defined in (2k), where a bus angle is set to zero to serve as a phase reference. Equations (2l) and (2m) control the output of renewable energy. The real production of wind and solar units cannot exceed the available potential determined by or meteorological conditions, instruments, 54 or their installed capacities increased by expansion decisions. This is for consistency since renewable intermittency and the long-run capacity planning decisions should be linked. The nodal balance of the gas network is described by (2n). At each gas" node, the sum of total inflow from pipelines, imported supplies, storage withdrawals, and power to gas outputs must equal the total outflow to generation, boilers, and C the gas the demand side. Hence, with this equation we link the gas network to the electric and heat system, through conversion technologies and fuel requirements. The Weymouth equation is defined in (2o) and represents the relationship between gas flow and the pressure drop in a pipe. This nonlinear expression describes the physical properties of a gas flow. Since it is nonlinear, an approximation is usually made to keep the solution computationally tractable. Gas pressure at each node is subjected to the operation safety and performance requirements defined in (2p). Equation (2q) limits the supply of gas from external providers to its contracted capacity which could be increased in the first stage through investment decisions. Power-to-gas: The equation (2r) converts electrical input into gas output using the associated conversion efficiency. Then, in Equation (2s), the power consumption of the power-to-gas plants is limited by the available capacity. Equation (2t) ensures the balance of the heat network so the sum of the heat flows, including cogeneration units, boilers, heat pumps and thermal storage, corresponds to the heat demand at every nodal point to fulfill that the heat supply to the heat demand is guaranteed. Equation (2u) limits the permissible heat flowing in each district heating line by its technical capacity, a limit that can be increased by investments. Equation (2v) keeps the temperature at each heat node within comfort thresholds for a consistent quality-of-service. The relation of thermal generation for gas boilers is defined by Equation (2w), which relates heat output to gas consumption through efficiency in gas boilers. Equation (2x) imposes the existing and expanded capacities of the boilers as an upper limit to heat output of the boilers. Equations (2y, 2z) represent heat pumps: the coefficient of performance, COP, relates the heat output to the electricity input, and the electrical input is constrained by the available electricity capacity. These expressions give an explicit coupling between electric and thermal networks. Capacity constraints for the CHP units are introduced through (2ab) and (2ac), where we isolate relaxations for its heat an electrical outputs. Equations (2ad) and (2ae) impose restrictions on the feasible heat-to-power, which, in turn, restricts the set of possible operational points to the viable cogeneration region of each CHP technology and consequently keeps the thermodynamic consistency. The dynamic SoC evolution of ES, which tracks stored energy by integrating the effects of charging, discharging, and self-discharging over successive time slots, is expressed as (2af). The amount of energy stored is limited by the capacity of the installed, or upgraded, storage. The equations (2ah) and (2ai) are the upper limits on the charge and discharge rates of power determined by the installed, or expanded, power capacities. The gas storage level transition is defined in (2aj), which covers the net injections and withdrawals. (2ak) asserts the gas storage volume never falls outside of its allowable minimum and maximum limits, taking into consideration capacity expansions. The relevant injection and withdrawal rates in (2al) and (2am) are constrained, so that the flow is also constrained by compressor and valve

capacities. Equations (2an) and (2ao) require cyclicity for the rest, so that the storage states at the end of a season are equal to that at its beginning, thus implying operational periodicity, and energy neutrality, at seasonal interfaces. Spinning reserve constraints are imposed in Equations (2ap) and (2aq). The first one implies enough upward reserve, which means to have enough spare capacity (discharging or generating capacity) to respond to sudden increase of demand, the second one means enough downward reserve, which is to have enough absorbent capacity (absorbing or charging capacity) to receive excess of power. Both of these ensure that the frequency stability and the electrical system short-term reliability are met. Hence, the two-stage model characterizes the operation of linked energy carriers under realistic time and technical constraints. The model offers a detailed and physically consistent depiction souring long-term planning decisions and short-term operation, and is the means for connecting the investment and resilience layers in the tri-level optimization platform. Equalities (2ar) and (2as) define the electrical and thermal outputs as functions of the fuel input.

$$\min \Theta^{op} \tag{2a}$$
$$= \sum_{t\in T}\sum_{s\in S} D_s \sum_{h\in H} \eta_h \sum_{\omega\in\Omega} \pi_\omega \Bigg[\sum_{g\in G^{conv}} \left(C^{fuel}_{g,t}\eta^{heat}_g p^{gen}_{g,t,s,h,\omega} + C^{startup}_g v^{startup}_{g,t,s,h,\omega} + C^{shutdown}_g v^{shutdown}_{g,t,s,h,\omega}\right) + \sum_{m\in M^{supply}} C^{gas}_{m,t}$$
$$p^{supply}_{m,t,s,h,\omega} + \sum_{c\in G^{chp}} C^{fuel,chp}_{c,t} f^{chp,fuel}_{c,t,s,h,\omega} + \sum_{w\in G^{wind}} C^{curtail,wind}_{w}\left(p^{avail,wind}_{w,t,s,h,\omega} - p^{wind}_{w,t,s,h,\omega}\right)$$
$$+ \sum_{pv\in G^{solar}} C^{curtail,solar}_{pv}\left(p^{avail,solar}_{pv,t,s,h,\omega} - p^{solar}_{pv,t,s,h,\omega}\right) + \sum_{es\in U^{storage,e}} C^{degrade}_{es}\left(p^{ch}_{es,t,s,h}\right.$$
$$\left. + p^{dis}_{es,t,s,h,\omega}\right) + \sum_{gs\in U^{storage,g}} C^{operate}_{gs}\left(q^{inj}_{gs,t,s,h,\omega} + q^{with}_{gs,t,s,h,\omega}\right)\Bigg]$$

$$\sum_{g\in G^{conv}_i} p^{gen}_{g,t,s,h,\omega} + \sum_{w\in G^{wind}_i} p^{wind}_{w,t,s,h,\omega} + \sum_{pv\in G^{solar}_i} p^{solar}_{pv,t,s,h,\omega} + \sum_{c\in G^{chp}_i} p^{chp,e}_{c,t,s,h,\omega} + \sum_{es\in U^{storage,e}_i} \left(p^{dis}_{es,t,s,h,\omega} - p^{ch}_{es,t,s,h,\omega}\right) - \sum_{k\in U^{p2g}} p^{p2g}_{k,t,s,h,\omega} - \sum_{hp\in U^{hp}_i} p^{hp}_{hp,t,s,h,\omega} - \sum_{l^e\in L^{out,e}_i} f^{e}_{l^e,t,s,h,\omega}$$
$$+ \sum_{l^e\in L^{in,e}_i} f^{e}_{l^e,t,s,h,\omega}\left(1 - l^{loss}_{l^e}\right) = P^{d,e}_{i,t,s,h,\omega} \;\forall i \in N^e, \forall t,s,h,\omega \tag{2b}$$

$$u^{gen}_{g,t,s,h,\omega}\underline{P}_g \le p^{gen}_{g,t,s,h,\omega} \le u^{gen}_{g,t,s,h,\omega}\left(\overline{P}_g + \sum_{\tau=1}^{t} \kappa^{cap,gen}_{g,t}\right) \forall g \in G^{conv}, \forall t,s,h,\omega \tag{2c}$$

$$p^{gen}_{g,t,s,h,\omega} - p^{gen}_{g,t,s,h-1,\omega} \le R^{up}_g u^{gen}_{g,t,s,h-1,\omega} + \left(\overline{P}_g + \sum_{\tau=1}^{t} \kappa^{cap,gen}_{g,t}\right) v^{startup}_{g,t,s,h,\omega} \;\forall g \in G^{conv}, \forall t,s,h \in \tag{2d}$$

$$p^{gen}_{g,t,s,h-1,\omega} - p^{gen}_{g,t,s,h,\omega} \tag{2e}$$
$$\le R^{down}_g u^{gen}_{g,t,s,h,\omega} + \left(\overline{P}_g + \sum_{\tau=1}^{t} \kappa^{cap,gen}_{g,t}\right) v^{shutdown}_{g,t,s,h,\omega} \;\forall g \in G^{conv}, \forall t,s,h \in H, \omega$$

$$v^{startup}_{g,t,s,h,\omega} - v^{shutdown}_{g,t,s,h,\omega} = u^{gen}_{g,t,s,h,\omega} - u^{gen}_{g,t,s,h-1,\omega} \;\forall g \in G^{conv}, \forall t,s,h \in H, \omega \tag{2f}$$

$$\sum_{h'=h}^{\min\{h+T^{up}_g-1,|H|\}} u^{gen}_{g,t,s,h',\omega} \ge T^{up}_g v^{startup}_{g,t,s,h,\omega} \;\forall g \in G^{conv}, \forall t,s,h,\omega \tag{2g}$$

$$\sum_{h'=h}^{\min\{h+T^{down}_g-1,|H|\}} \left(1 - u^{gen}_{g,t,s,h',\omega}\right) \ge T^{down}_g v^{shutdown}_{g,t,s,h,\omega} \;\forall g \in G^{conv}, \forall t,s,h,\omega \tag{2h}$$

$$f^{e}_{l^{e},t,s,h,\omega} = \frac{1}{X_{l^{e}}}\left(\theta^{e}_{i(l^{e}),t,s,h,\omega} - \theta^{e}_{j(l^{e}),t,s,h,\omega}\right) \forall l^{e} \in L^{e}, \forall t,s,h,\omega \tag{2i}$$

$$-\left(\overline{F}_{l^{e}} + \sum_{\tau=1}^{t} \kappa^{cap,e}_{l^{e},\tau}\right) \leq f^{e}_{l^{e},t,s,h,\omega} \leq \left(\overline{F}_{l^{e}} + \sum_{\tau=1}^{t} \kappa^{cap,e}_{l^{e},\tau}\right) \forall l^{e} \in L^{e}, \forall t,s,h,\omega \tag{2j}$$

$$\theta^{e}_{1,t,s,h,\omega} = 0 \ \forall t,s,h,\omega \tag{2k}$$

$$p^{wind}_{w,t,s,h,\omega} \leq p^{avail,wind}_{w,t,s,h,\omega} \leq \left(\overline{P}^{wind}_{w} + \sum_{\tau=1}^{t} \kappa^{cap,wind}_{w,\tau}\right) \forall w \in G^{wind}, \forall t,s,h,\omega \tag{2l}$$

$$p^{solar}_{pv,t,s,h,\omega} \leq p^{avail,solar}_{pv,t,s,h,\omega} \leq \left(\overline{P}^{solar}_{pv} + \sum_{\tau=1}^{t} \kappa^{cap,solar}_{pv,\tau}\right) \forall pv \in G^{solar}, \forall t,s,h,\omega \tag{2m}$$

$$\sum_{l^{g} \in L^{in,g}_{m}} q^{g}_{l^{g},t,s,h,\omega} - \sum_{l^{g} \in L^{out,g}_{m}} q^{g}_{l^{g},t,s,h,\omega} + q^{supply}_{m,t,s,h,\omega} + \sum_{k \in U^{p2g}_{m}} q^{p2g,out}_{k,t,s,h,\omega} + \sum_{gs \in U^{storage,g}_{m}} \left(q^{with}_{gs,t,s,h,\omega} - q^{inj}_{gs,t,s,h,\omega}\right) - \sum_{g \in G^{gas}_{m}} \eta^{heat}_{g} p^{gen}_{g,t,s,h,\omega} - \sum_{b \in U^{boiler}_{m}} q^{boiler,in}_{b,t,s,h,\omega} - \sum_{c \in G^{chp}_{m}} f^{chp,fuel}_{c,t,s,h,\omega} = Q^{d,g}_{m,t,s,h,\omega} \ \forall m \in N^{g}, \forall t,s,h,\omega \tag{2n}$$

$$\left(q^{g}_{l^{g},t,s,h,\omega}\right)^{2} = K^{2}_{l^{g}}\left(\overline{Q}_{l^{g}} + \sum_{\tau=1}^{t} \kappa^{cap,g}_{l^{g},\tau}\right)^{2} \left(\left(pr^{g}_{m(l^{g}),t,s,h,\omega}\right)^{2} - \left(pr^{g}_{n(l^{g}),t,s,h,\omega}\right)^{2}\right) \forall l^{g} \in L^{g}, \forall t,s,h,\omega \tag{2o}$$

$$Pr^{g,min}_{m} \leq pr^{g}_{m,t,s,h,\omega} \leq Pr^{g,max}_{m} \ \forall m \in N^{g}, \forall t,s,h,\omega \tag{2p}$$

$$q^{supply}_{m,t,s,h,\omega} \leq Q^{supply,base}_{m} + \sum_{\tau=1}^{t} \kappa^{supply,g}_{m,\tau} \ \forall m \in M^{supply}, \forall t,s,h,\omega \tag{2q}$$

$$q^{p2g,out}_{k,t,s,h,\omega} = \eta^{p2g}_{k} p^{p2g}_{k,t,s,h,\omega} \ \forall k \in U^{p2g}, \forall t,s,h,\omega \tag{2r}$$

$$p^{p2g}_{k,t,s,h,\omega} \leq \overline{P}^{p2g}_{k} + \sum_{\tau=1}^{t} \kappa^{cap,p2g}_{k,\tau} \ \forall k \in U^{p2g}, \forall t,s,h,\omega \tag{2s}$$

$$\sum_{l^{h} \in L^{in,h}_{p}} h^{h}_{l^{h},t,s,h,\omega}(1 - \Lambda_{l^{h}}) - \sum_{l^{h} \in L^{out,h}_{p}} h^{h}_{l^{h},t,s,h,\omega} + \sum_{c \in G^{chp}_{p}} q^{chp,h}_{c,t,s,h,\omega} + \sum_{b \in U^{boiler}_{p}} q^{boiler,out}_{b,t,s,h,\omega} + \sum_{hp \in U^{hp}_{p}} q^{hp,out}_{hp,t,s,h,\omega} + \sum_{hs \in U^{storage,h}_{p}} \left(q^{dis,h}_{hs,t,s,h,\omega} - q^{ch,h}_{hs,t,s,h,\omega}\right) = H^{d,h}_{p,t,s,h,\omega} \ \forall p \in N^{h}, \forall t,s,h,\omega \tag{2t}$$

$$h^{h}_{l^{h},t,s,h,\omega} \leq \overline{H}_{l^{h}} + \sum_{\tau=1}^{t} \kappa^{cap,h}_{l^{h},\tau} \ \forall l^{h} \in L^{h}, \forall t,s,h,\omega \tag{2u}$$

$$T^{h,min}_{p} \leq \tau^{h}_{p,t,s,h,\omega} \leq T^{h,max}_{p} \ \forall p \in N^{h}, \forall t,s,h,\omega \tag{2v}$$

$$q^{boiler,out}_{b,t,s,h,\omega} = \eta^{boiler}_{b} q^{boiler,in}_{b,t,s,h,\omega} \ \forall b \in U^{boiler}, \forall t,s,h,\omega \tag{2w}$$

$$q^{boiler,out}_{b,t,s,h,\omega} \leq \overline{Q}^{boiler}_{b} + \sum_{\tau=1}^{t} \kappa^{cap,boiler}_{b,\tau} \ \forall b \in U^{boiler}, \forall t,s,h,\omega \tag{2x}$$

$$q^{hp,out}_{hp,t,s,h,\omega} = COP_{hp} p^{hp}_{hp,t,s,h,\omega} \ \forall hp \in U^{hp}, \forall t,s,h,\omega \tag{2y}$$

$$p^{hp}_{hp,t,s,h,\omega} \le \overline{P}^{hp}_{hp} + \sum_{\tau=1}^{t} \kappa^{cap,hp}_{hp,\tau} \; \forall hp \in U^{hp}, \forall t,s,h,\omega \tag{2z}$$

$$p^{chp,e}_{c,t,s,h,\omega} \le \overline{P}^{chp}_{c} + \sum_{\tau=1}^{t} \kappa^{elec,chp}_{c,\tau} \; \forall c \in G^{chp}, \forall t,s,h,\omega \tag{2ab}$$

$$q^{chp,h}_{c,t,s,h,\omega} \le \overline{Q}^{chp}_{c} + \sum_{\tau=1}^{t} \kappa^{heat,chp}_{c,\tau} \; \forall c \in G^{chp}, \forall t,s,h,\omega \tag{2ac}$$

$$\frac{q^{chp,h}_{c,t,s,h,\omega}}{p^{chp,e}_{c,t,s,h,\omega}} \le \overline{\Gamma}^{H2P}_{c} \; \forall c \in G^{chp}, \forall t,s,h,\omega : p^{chp,e}_{c,t,s,h,\omega} > 0 \tag{2ad}$$

$$\frac{q^{chp,h}_{c,t,s,h,\omega}}{p^{chp,e}_{c,t,s,h,\omega}} \ge \underline{\Gamma}^{H2P}_{c} \; \forall c \in G^{chp}, \forall t,s,h,\omega : p^{chp,e}_{c,t,s,h,\omega} > 0 \tag{2ae}$$

$$e^{soc}_{es,t,s,h,\omega} = e^{soc}_{es,t,s,h\text{-}1,\omega}\left(1 - \rho^{decay}_{es}\right) + \eta^{charge}_{es} p^{ch}_{es,t,s,h,\omega} - \frac{p^{dis}_{es,t,s,h,\omega}}{\eta^{discharge}_{es}} \; \forall es \in U^{storage,e}, \forall t,\omega \tag{2af}$$

$$e^{soc}_{es,t,s,h,\omega} \le \overline{E}_{es} + \sum_{\tau=1}^{t} \kappa^{energy,es}_{es,\tau} \; \forall es \in U^{storage,e}, \forall t,s,h,\omega \tag{2ag}$$

$$p^{ch}_{es,t,s,h,\omega} \le \overline{P}^{ch}_{es} + \sum_{\tau=1}^{t} \kappa^{power,es}_{es,\tau} \; \forall es \in U^{storage,e}, \forall t,s,h,\omega \tag{2ah}$$

$$p^{dis}_{es,t,s,h,\omega} \le \overline{P}^{dis}_{es} + \sum_{\tau=1}^{t} \kappa^{power,es}_{es,\tau} \; \forall es \in U^{storage,e}, \forall t,s,h,\omega \tag{2ai}$$

$$v^{level}_{gs,t,s,h,\omega} = v^{level}_{gs,t,s,h\text{-}1,\omega} + q^{inj}_{gs,t,s,h,\omega} - q^{with}_{gs,t,s,h,\omega} \; \forall gs \in U^{storage,g}, \forall t,s,h \in H, \omega \tag{2aj}$$

$$\underline{V}_{gs} \le v^{level}_{gs,t,s,h,\omega} \le \overline{V}_{gs} + \sum_{\tau=1}^{t} \kappa^{cap,gs}_{gs,\tau} \; \forall gs \in U^{storage,g}, \forall t,s,h,\omega \tag{2ak}$$

$$q^{inj}_{gs,t,s,h,\omega} \le \overline{Q}^{inj}_{gs} \; \forall gs \in U^{storage,g}, \forall t,s,h,\omega \tag{2al}$$

$$q^{with}_{gs,t,s,h,\omega} \le \overline{Q}^{with}_{gs} \; \forall gs \in U^{storage,g}, \forall t,s,h,\omega \tag{2am}$$

$$e^{soc}_{es,t,s,|H|,\omega} = e^{soc}_{es,t,s,1,\omega} \; \forall es \in U^{storage,e}, \forall t,s,\omega \tag{2an}$$

$$v^{level}_{gs,t,s,|H|,\omega} = v^{level}_{gs,t,s,1,\omega} \; \forall gs \in U^{storage,g}, \forall t,s,\omega \tag{2ao}$$

$$\sum_{g \in G^{conv}} u^{gen}_{g,t,s,h,\omega}\left(\overline{P}_{g} + \sum_{\tau=1}^{t} \kappa^{cap,gen}_{g,\tau}\right) - \sum_{g \in G^{conv}} p^{gen}_{g,t,s,h,\omega} + \sum_{es \in U^{storage,e}} \left(\overline{P}^{dis}_{es} - p^{dis}_{es,t,s,h,\omega}\right) \ge R^{spin,up}_{t,s,h} \; \forall t,s,h,\omega \tag{2ap}$$

$$\sum_{g \in G^{conv}} p^{gen}_{g,t,s,h,\omega} - \sum_{g \in G^{conv}} u^{gen}_{g,t,s,h,\omega} \underline{P}_{g} + \sum_{es \in U^{storage,e}} \left(\overline{P}^{ch}_{es} - p^{ch}_{es,t,s,h,\omega}\right) \ge R^{spin,down}_{t,s,h} \; \forall t,s,h,\omega \tag{2aq}$$

$$p^{chp,e}_{c,t,s,h,\omega} = \eta^{elec}_{c} f^{chp,fuel}_{c,t,s,h,\omega} \; \forall c \in G^{chp}, \forall t,s,h,\omega \tag{2ar}$$

$$q^{chp,h}_{c,t,s,h,\omega} = \eta^{heat}_{c} f^{chp,fuel}_{c,t,s,h,\omega} \; \forall c \in G^{chp}, \forall t,s,h,\omega \tag{2as}$$

2-3-Third Level: Resilience Assessment Model

The third-tier is the resilience evaluation and system adaptation level, which assesses middle of the system performance level during perturbation events. Following the investment planning (first level) and operational adjustment (second level) models, this level incorporates the decisions of the two preceding levels and finds the best post disturbance solution for network topology and resource dispatch. The goal is to reduce the expected cost of system disturbance (disrupted energy, switching and black start procedures, and the ability to recover critical areas). The function of the total cost minimization is defined in Equation (3a). It considers the expected cost for all seasons, hours, scenarios and cause disruption events weighted by occurrence probabilities of each scenario set. Key components of the solution are electrical, gas and heating load curtailment penalties, network switching and reconfiguration costs per energy carrier, black start costs for de energized islands and resilience penalties associated with critical zones left unserved. This multi-level formulation guarantees that the trade-off between service continuity and recovery cost following disruptions is optimally achieved. Subject to (3b)-(3d) are the permitted curtailed load limits of each energy carrier. These are for the most part electricity, gas and heating loads respecting system realism even in tightly constrained system disturbances. The power balance of a failure event is specified in Equation (3e). It takes into account the impact of component availability on generation, network flows and storage operation. For each electrical bus, it is imposing power conservation among generation, storage discharge, inflows along connected lines, local consumption, and demand curtailment. The availability factor is then applied to each of the components' contributions, providing a picture of the failures in each disruption scenario. The gas network balance at perturbed conditions is given by (3f). The equation accounts for the inflows and outflows of the pipeline, corrected by its availability, supplies from gas sources, injections and withdrawals from storage, consumption by gas fired generators, boilers and cogeneration units, together with curtailed demand. Each term is multiplied by the divergent scenario availability variable to capture the effect of partial or full loss of function. The corresponding heating network balance is given by Eq. (3g). For all heating nodes, the net heat inflow plus heat outflow is the heat demand after curtailment. The modelling captures the integrated operation of CHP thermal production, boilers, heat pumps and thermal storages, all subject to time dependent availability conditions as per scenario. Equation (3h) limits the generation after the disruption so that it is no more than the corresponding second-level pre disturbance generation. This ensures physical feasibility by ruling out unrealistic "power production gains" after equipment outages. Equation (3i) links the line switching status to its availability of component, so that the switch cannot be closed on an unavailable component. Equation (3j) enforces that flows over lines switched off due to an outage are forced to zero by employing a suitable big-M linearization term that connects the flow magnitude with the related binary switching variable. Equation (3k) adds the line flow limits for lines to be switched on: for the lines to be switched on, power flows cannot be greater than the total amount of capacity (existing and new built). Equation (3l) ensures that each bus is assigned to a unique island. This binary restriction avoids contradicting allocations and guarantees a uniform islanding configuration during system splitting. Equation (3m) states that island feasibility is related to the fact that the total generation accessible within the island must be above a certain least required level, in the form of the minimum island generation. Preventing this results in a complete lack of generation tightly coupled to electrically isolated areas. Equation (3n) defines a connection between buses, and indicates that two buses are connected only if a path of switched on lines provide a path connecting the two buses, which guarantees valid electrical topology during reconfiguration. Equation (3o) measures the restoration level of the zone based on the ratio of served load to the total pre disturbance load. The recovery ratio measures the portion of the load that is restored after a disturbance. Equation (3p) describes priority service to critical loads. It limits the curtailing of critical buses by bounding the ratio of this shedding process over the total demand by a priori given criticality weights. Equation (3q) generalizes resilience to the gas network. We also prove that the nodal gas pressures stay above a minimum allowable threshold that scales with the fraction of the demand that is being met, thus ensuring physical consistency

of the gas network operating under decreased service reliability. Equation (3r) restricts the total accumulated electric load curtailment during a disturbance so that continued curtailment shall not exceed the maximum tolerable load, reflecting operational recovery constraints in a long-term disturbance. The total resilience index for each time and disruption scenario is then derived as the weighted average of the restoration rate at zone level by using the zone criticality factors as the weighting scale. This index reflects the effectiveness of system-wide recovery in the post disturbance phases. Then, relation (3t) enforces a minimum resilience level, which guarantees that the overall resilience index of the system is never lower than some prescribed acceptable level in any disruption scenario. Equation (3u) expresses the cross carrier resilience constraint, in which the energy carriers are restored in a coordinated fashion. It restricts the disparity between normalized curtailed deliveries of electricity and gas at co located nodes so that the recovery mechanisms of multiple energy systems are physically and operationally consistent. Equation (3v) describes the impact of component hardening on availability. The equation establishes a relationship between increased line availability and its baseline value considering level-1 hardening selections. Hardened nodes are less vulnerable to failure in disruption scenarios, establishing a direct link between long term investments and real-time resilience . The role of microgrids in resilience enhancement is modeled by equation (3w). For zones with islanding capability, the total curtailed electrical load is decreased by the microgrid resilience enhancement factor in this is ensured. This formula quantifies the positive effect of local autonomous operation on disruption impact mitigation. Through these formulations level 3 coordinates post event recovery in terms of joint optimal network reconfiguration, load restoration, and resource utilization through third level acts as a coordinator for post event recovery that optimizes network reclosing, load restoration, and resource use jointly. It bridges infrastructure robustness and operational flexibility by measuring resilience as the system's capacity to sustain, or rapidly recover, electricity, gas, and heating services in the wake of disruptions.

$$\min Y^{resil} \tag{3a}$$
$$= \sum_{t\in T}\sum_{s\in S} D_s \sum_{h\in H} \eta_h \sum_{\omega\in\Omega} \pi_\omega \sum_{\xi\in\Xi} \pi_\xi \Big[\sum_{i\in N^e} C^{curtail,e}_{t,s,h} \lambda^{curtail,e}_{i,t,s,h,\omega,\xi} + \sum_{m\in N^g} C^{curtail,g}_{t,s,h} \lambda^{curtail,g}_{m,t,s,h,\omega,\xi} + \sum_{p\in N^h} C^{curtail,h}_{t,s,h} \lambda^{curtail,h}_{p,t,s,h,\omega,\xi} + \sum_{l^e\in L^e} C^{switch}_{l^e} \left|\sigma^{switch,e}_{l^e,t,s,h,\omega,\xi} - \sigma^{switch,e}_{l^e,t,s,h-1,\omega,\xi}\right|$$
$$+ \sum_{i\in N^e} C^{blackstart}_{i} (1 - \zeta^{island,e}_{i,t,\omega,\xi}) + \sum_{z\in Z} \Psi^{critical}_{z} C^{resilience}_{z} (1 - \mu^{restore}_{z,t,\omega,\xi}) \Big]$$

$$\lambda^{curtail,e}_{i,t,s,h,\omega,\xi} \le P^{d,e}_{i,t,s,h,\omega} \ \forall i \in N^e, \forall t,s,h,\omega,\xi \tag{3b}$$

$$\lambda^{curtail,g}_{m,t,s,h,\omega,\xi} \le Q^{d,g}_{m,t,s,h,\omega} \ \forall m \in N^g, \forall t,s,h,\omega,\xi \tag{3c}$$

$$\lambda^{curtail,h}_{p,t,s,h,\omega,\xi} \le H^{d,h}_{p,t,s,h,\omega} \ \forall p \in N^h, \forall t,s,h,\omega,\xi \tag{3d}$$

$$\sum_{g\in G^{conv}_i} A_{g,\xi} \grave{p}^{gen}_{g,t,s,h,\omega,\xi} + \sum_{w\in G^{wind}_i} A_{w,\xi} p^{wind}_{w,t,s,h,\omega} + \sum_{pv\in G^{solar}_i} A_{pv,\xi} p^{solar}_{pv,t,s,h,\omega} + \sum_{c\in G^{chp}_i} A_{c,\xi} p^{chp,e}_{c,t,s,} \tag{3e}$$
$$+ \sum_{es\in U^{storage,e}_i} A_{es,\xi} (p^{dis}_{es,t,s,h,\omega} - p^{ch}_{es,t,s,h,\omega}) - \sum_{k\in U^{p2g}_i} p^{p2g}_{k,t,s,h,\omega} - \sum_{hp\in U^{hp}_i} p^{hp}_{hp,t,s,h,\omega}$$
$$- \sum_{l^e\in L^{out,e}_i} A_{l^e,\xi} \sigma^{switch,e}_{l^e,t,s,h,\omega,\xi} \grave{f}^{e}_{l^e,t,s,h,\omega,\xi} + \sum_{l^e\in L^{in,e}_i} A_{l^e,\xi} \sigma^{switch,e}_{l^e,t,s,h,\omega,\xi} \grave{f}^{e}_{l^e,t,s,h,\omega,\xi} (1 - l^{loss}_{l^e})$$
$$= P^{d,e}_{i,t,s,h,\omega} - \lambda^{curtail,e}_{i,t,s,h,\omega,\xi} \ \forall i \in N^e, \forall t,s,h,\omega,\xi$$

$$\sum_{l^g \in L_m^{in,g}} A_{l^g,\xi}\sigma^{switch,g}_{l^g,t,s,h,\omega,\xi}\grave{q}^{g}_{l^g,t,s,h,\omega,\xi} - \sum_{l^g \in L_m^{out,g}} A_{l^g,\xi}\sigma^{switch,g}_{l^g,t,s,h,\omega,\xi}\grave{q}^{g}_{l^g,t,s,h,\omega,\xi} + A^{supply}_{m,\xi}q^{supply}_{m,t,s,h,\omega} + \sum_{k \in U_m^{p2g}} A_{k,\xi}q^{p2g,out}_{k,t,s,h,\omega} + \sum_{gs \in U_m^{storage,g}} A_{gs,\xi}(q^{with}_{gs,t,s,h,\omega} - q^{inj}_{gs,t,s,h,\omega}) - \sum_{g \in G_m^{gas}} A_{g,\xi}\eta^{heat}_{g}\grave{p}^{gen}_{g,t,s,h,\omega} - \sum_{b \in U_m^{boiler}} A_{b,\xi}q^{boiler,in}_{b,t,s,h,\omega} - \sum_{c \in G_m^{chp}} A_{c,\xi}f^{chp,fuel}_{c,t,s,h,\omega} = Q^{d,g}_{m,t,s,h,\omega} - \lambda^{curtail,g}_{m,t,s,h,\omega,\xi} \; \forall m \in N^g, \forall t,s,h,\omega,\xi \tag{3f}$$

$$\sum_{l^h \in L_p^{in,h}} A_{l^h,\xi}\sigma^{switch,h}_{l^h,t,s,h,\omega,\xi}\grave{h}^{h}_{l^h,t,s,h,\omega,\xi}(1 - \Lambda_{l^h}) - \sum_{l^h \in L_p^{out,h}} A_{l^h,\xi}\sigma^{switch,h}_{l^h,t,s,h,\omega,\xi}\grave{h}^{h}_{l^h,t,s,h,\omega,\xi} + \sum_{c \in G_p^{chp}} A_{c,\xi}q^{chp,}_{c,t,s} + \sum_{b \in U_p^{boiler}} A_{b,\xi}q^{boiler,out}_{b,t,s,h,\omega} + \sum_{hp \in U_p^{hp}} A_{hp,\xi}q^{hp,out}_{hp,t,s,h,\omega} + \sum_{hs \in U_p^{storage,h}} A_{hs,\xi}(q^{dis,h}_{hs,t,s,h,} - q^{ch,h}_{hs,t,s,h,\omega}) = H^{d,h}_{p,t,s,h,\omega} - \lambda^{curtail,h}_{p,t,s,h,\omega,\xi} \; \forall p \in N^h, \forall t,s,h,\omega,\xi \tag{3g}$$

$$\grave{p}^{gen}_{g,t,s,h,\omega,\xi} \le p^{gen}_{g,t,s,h,\omega} \; \forall g \in G^{conv}, \forall t,s,h,\omega,\xi \tag{3h}$$

$$\sigma^{switch,e}_{l^e,t,s,h,\omega,\xi} \le A_{l^e,\xi} \; \forall l^e \in L^e, \forall t,s,h,\omega,\xi \tag{3i}$$

$$- M^{big}\sigma^{switch,e}_{l^e,t,s,h,\omega,\xi} \le \grave{f}^{e}_{l^e,t,s,h,\omega,\xi} \le M^{big}\sigma^{switch,e}_{l^e,t,s,h,\omega,\xi} \; \forall l^e \in L^e, \forall t,s,h,\omega,\xi \tag{3j}$$

$$- \left(\bar{F}_{l^e} + \sum_{\tau=1}^{t} \kappa^{cap,e}_{l^e,\tau}\right)\sigma^{switch,e}_{l^e,t,s,h,\omega,\xi} \le \grave{f}^{e}_{l^e,t,s,h,\omega,\xi} \le \left(\bar{F}_{l^e} + \sum_{\tau=1}^{t} \kappa^{cap,e}_{l^e,\tau}\right)\sigma^{switch,e}_{l^e,t,s,h,\omega,\xi} \; \forall l^e \in L^e, \forall t,s,h, \tag{3k}$$

$$\sum_{z \in Z} \zeta^{island,e}_{i,z,t,\omega,\xi} \le 1 \; \forall i \in N^e, \forall t,\omega,\xi \tag{3l}$$

$$\sum_{i \in N_z^e} \sum_{g \in G_i^{conv}} A_{g,\xi}\grave{p}^{gen}_{g,t,s,h,\omega,\xi} \ge \sum_{i \in N_z^e} \zeta^{island,e}_{i,z,t,\omega,\xi} p^{min,island} \; \forall z \in Z, \forall t,s,h,\omega,\xi \tag{3m}$$

$$\nu^{connect,e}_{i,j,t,s,h,\omega,\xi} \le \sum_{l^e \in P^{path}_{i,j}} \sigma^{switch,e}_{l^e,t,s,h,\omega,\xi}/|P^{path}_{i,j}| \; \forall i,j \in N^e, \forall t,s,h,\omega,\xi \tag{3n}$$

$$\mu^{restore}_{z,t,\omega,\xi} \le \frac{\sum_{i \in N_z^e} (P^{d,e}_{i,t,s,h,\omega} - \lambda^{curtail,e}_{i,t,s,h,\omega,\xi})}{\sum_{i \in N_z^e} P^{d,e}_{i,t,s,h,\omega}} \; \forall z \in Z, \forall t,s,h,\omega,\xi \tag{3o}$$

$$\lambda^{curtail,e}_{i,t,s,h,\omega,\xi} \le (1 - \alpha^{critical}_{i})P^{d,e}_{i,t,s,h,\omega} \; \forall i \in N^{critical,e}, \forall t,s,h,\omega,\xi \tag{3p}$$

$$pr^{g}_{m,t,s,h,\omega,\xi} \ge Pr^{g,min}_{m}\frac{Q^{d,g}_{m,t,s,h,\omega} - \lambda^{curtail,g}_{m,t,s,h,\omega,\xi}}{Q^{d,g}_{m,t,s,h,\omega}} \; \forall m \in N^g, \forall t,s,h,\omega,\xi \tag{3q}$$

$$\sum_{h=1}^{\Gamma^{duration}_{\xi}} \lambda^{curtail,e}_{i,t,s,h,\omega,\xi} \le \Delta^{max,curtail}_{i} \; \forall i \in N^e, \forall t,s,\omega,\xi \tag{3r}$$

$$\phi^{resiliency}_{t,\omega,\xi} = \frac{\sum_{z \in Z} \Psi^{critical}_{z}\mu^{restore}_{z,t,\omega,\xi}}{\sum_{z \in Z} \Psi^{critical}_{z}} \; \forall t,\omega,\xi \tag{3s}$$

$$\phi^{resiliency}_{t,\omega,\xi} \ge \Phi^{min,resil} \; \forall t,\omega,\xi \tag{3t}$$

$$\frac{\lambda^{curtail,e}_{i,t,s,h,\omega,\xi}}{P^{d,e}_{i,t,s,h,\omega}} - \frac{\lambda^{curtail,g}_{m(i),t,s,h,\omega,\xi}}{Q^{d,g}_{m(i),t,s,h,\omega}} \leq \epsilon^{carrier,balance} \; \forall i \in N^{e}, \forall t,s,h,\omega,\xi \tag{3u}$$

$$A_{l^e,\xi} \geq 1 - \left(1 - A^{base}_{l^e,\xi}\right)\left(1 - \sum_{\tau=1}^{t} y^{harden}_{l^e,\tau}\right) \; \forall l^e \in L^{e}, \forall t,\xi \tag{3v}$$

$$\sum_{i \in N_z^{microgrid}} \lambda^{curtail,e}_{i,t,s,h,\omega,\xi} \leq \left(1 - \beta_z^{microgrid}\right) \sum_{i \in N_z^{microgrid}} P^{d,e}_{i,t,s,h,\omega} \; \forall z \in Z^{microgrid}, \forall t,s,h,\omega,\xi \tag{3w}$$

2-3-1 Duality-Based Reformulation of the Resilience Subproblem

The third-level resilience assessment model, at its core, represents a bi-level interdiction problem: a hypothetical attacker (inner level) seeks to maximize system damage by disabling components within a budget, while the system operator (outer level) reacts by minimizing the impact through optimal reconfiguration and dispatch. Formally, for a fixed investment plan (x,y,κ) and operational schedule from the upper levels, this can be expressed as:

$$\min_{\lambda,\sigma,\hat{p},\ldots} \; Y^{resil} \text{ (Eq. (3a))} \tag{3x}$$

$$\text{s.t. Operator's constraints: Eqs. (3b) - (3w)} \tag{3y}$$

$$A_{g,\xi}, A_{l^e,\xi}, \ldots = \arg \max_{A \in A_\xi \text{ (Attacker's Budget)}} I(A) \tag{3z}$$

where A_ξ is the set of component availability states defined by the disruption scenario ξ, and $I(A)$ is a metric of system impact (e.g., total load curtailment cost) induced by availability state A.

To solve this tri-level problem tractably, the inner bi-level structure must be resolved. We achieve this by reformulating the attacker's problem—a *maximization* over binary availability variables subject to a resource budget—into an equivalent *minimization* problem using strong duality.

Step 1: Attacker's Inner Problem Formulation. For a given disruption scenario type ξ, let binary variable $z_c \in \{0,1\}$ indicate whether component c (a generator, line, etc.) is disabled ($z_c = 1$). The attacker aims to maximize the system's operational cost (here approximated by the weighted sum of load curtailment) subject to a resource budget:

$$I^* = \max_{z} \sum_{i,t,s,h,\omega} C^{curtail,e}_{t,s,h} \grave{\lambda}^{curtail,e}_{i,t,s,h,\omega}(z) \tag{3za}$$

$$\text{s.t.} \sum_{c} C^{attack}_{c} z_c \leq B^{attack} \tag{3zb}$$

$$z_c \in \{0,1\}, \; \forall c \tag{3zc}$$

where $\grave{\lambda}^{curtail,e}(z)$ represents the resulting load curtailment from the operator's optimal response given the attack pattern z, and C^{attack}_{c} is the cost for the attacker to disable component c.

Step 2: Dual Transformation and Single-Level Reduction. The operator's response problem (minimizing Y^{resil} for a *fixed* z) is a linear program (LP) in the continuous variables (dispatch, flows, curtailment). Let $\pi(z)$ denote the optimal value of this LP. The attacker's problem becomes $\max_z \pi(z)$. By the strong duality theorem, the optimal value $\pi(z)$ of the operator's primal LP equals the optimal value of its dual LP. Therefore, $\max_z \pi(z)$ is equivalent to $\max_z \min_{\text{dual vars}} L(z,\text{dual})$, where L is the Lagrangian.

We can thus combine the two levels by: 1) writing the optimality condition of the operator's problem as its primal constraints, dual constraints, and a strong duality equality constraint that equates the primal and dual objective functions; and 2) treating the attacker's variables z_c and the operator's primal/dual variables as decision variables in a single, monolithic minimization problem.

Step 3: Final Single-Level MILP Formulation. The final reformulation yields a single-level problem that is mathematically equivalent to the original bi-level problem. This problem is a Mixed-Integer Linear Program (MILP) because:

- The strong duality equality is linear when the primal is an LP.
- The complementary slackness conditions, which are necessary for optimality, can be linearized using standard big-M techniques due to the binary nature of the attack variables z_c.
- The operator's reconfiguration variables (e.g., σ^{switch}, ζ^{island}) remain binary.

The resulting set of constraints is precisely what is presented in Section 2.3 (Eqs. 3a-3w), where the component availability parameters $A_{c,\xi}$ are now interpreted as $(1 - z_c)$ and the attacker's budget constraint (Eq. 7c) is included. The linearized complementary slackness conditions are embedded within the structure of the "big-M" constraints, such as Eqs. (3j) and (3k), which link the continuous flow variables $\hat{f}$ to the binary switching variables σ^{switch}.

This duality-based reformulation is crucial. It avoids the computational intractability of directly solving a nested bi-level optimization with integer variables in both levels, allowing the integrated tri-level model to be solved using the iterative C&CG algorithm described in Section 3.

2-4-Common Variables and Linking Constraints

The Coordination Section 4 describes the coordination terms that connect the investment, operational, and resilience layers in the tri-level optimization. These shared variables and coupling constraints maintain the hierarchical consistency and allow two-way interaction among the three models, which is the core structural of the integrated formulation. Expression (4a) presents the operational cost term within the first-level investment objective. It includes the fuel consumption, the startup and the gas supply costs, all derived from the second level operational optimization for all seasons, representative hours and operation scenarios. Each element of cost is multiplied by the duration of season, hourly weight and probability of scenario, so that the resulting value is expected operation cost in normal year for certain investment solution and specified year. Resilience cost part in the first-level objective is defined in (4b) and it is based on the third level reconfiguration model. It aggregates expected curtailment penalties for electricity, gas and heat, and these are multiplied with probabilities of operational and disruption scenarios. The second part of the sum represents for the critical unserved areas multiplied by their criticality and resilience restoral factors, considered as penalty. This cost quantifies the anticipated socio technical consequence of disturbances" in the current infrastructure design and operational policy. The non-anticipatively constraint between investment and operation is then given by Equation (4c). Investment capacity variables like transmission, generation, and pipeline expansions decided upon at the first level impose direct constraints on the operational quantity realizations in the second level. The functional relationship ensures that generation, renewable output and networks flows are less than or equal to installed capacities. Therefore, operational choices cannot infringe on the physical constraints defined by the previous stage's investments. Equation (4d) derives the connection between operational optimization and resilience assessment. The pre disruption operative conditions act as a boundary that separates post failure dispatch. Production in disruptive conditions cannot be greater than production before the disturbances, and flows on the network adjust in a dynamic manner through line availability and switching decisions. This guarantees that post event re configuration is physically realizable with respect baseline operations. Equations (4e) and (4f)

translate the hardening investment to component availability in the disruption scenarios. Each generator's and transmission line's availability parameter becomes a function of its baseline reliability and the aggregate hardening decisions made through that year. Hardened components also have greater survival probabilities in failure events, which provide a quantitative relation between preventive investment and performance of resilience. Equation (4g) introduces the multi carrier coupling of the electrical and gas system. The total consumption of gas by the gas fired generators and boilers cannot be greater than the available gas supply after fulfilling the direct demands. This condition guarantees interdependency coherence by realizing pair wise feasibility of gas supply to downstream electricity and heat generation. Power to gas conversion is defined by Equation (4h), where the amount of produced gas is a function of the amount of consumed electrical energy multiplied by the conversion efficiency. This commonality, found at both the second and third level, assures that cross carrier energy transformations are consistent in both normal and new cross carrier energy transformations are consistent in both normal and new conditions. Equation (4i) relates the thermal and electrical outputs of combined heat and power (CHP) plants. The heat to power generation ratio is now restricted to lie within the technology specific limits of the efficiency, ensuring that the (5h) is feasible in the specified heat to power region. The electricity use of heat pumps is also linked to their thermal output via the coefficient of performance, making a connection between the electrical and thermal systems. Equation (4k) ensures temporal consistency between planning periods. It leads to investment continuity so that infrastructure built in past years still exists in future periods, capturing the irreversible and accumulative nature of capacity expansion. Equation (4l) allows for the scenario linkage in the operational and disruption analyses. It imposes that the curtailment variables of the resilience evaluation are not greater than the demand realized in every operational scenario, in this way they coordinate the calculations of energy shortfalls in stochastic operation and post event evaluation. Equation (4m) correlates the storage state between seasons. The state at the beginning of each season is set equal to the final state of the previous one so to ensure a temporal consistency in the operation of storage. Equation (4n) adds an annual energy neutrality constraint, which states that the overall amount of charge and discharge over the year have to be equal, allowing a fair comparison of energy storage performance under different operating conditions. Finally, equation (4o) re-couples the resilience index calculated at the third level back to the investment decisions at the first level. It requires the expected (average) resilience over operational and disruption scenarios to be at least a target resilience level for each planning year. This representation reflects that strategic investments must not only meet economic and operational requirements but also that the system wide resilience level should steadily improve over time. Overall, the expression (4a)–(4o) establishes cross-level consistency and ensures that investment, operation and resilience decisions are consistent and hence enables the integration of economic efficiency, operational feasibility and reliability in the multi carrier energy system planning framework considering uncertainty. Equation (4p) is essentially a restatement of Eq. (2ar) to ensure the variable is consistent across the decomposed problem in the solution algorithm.

$$\Theta_t^{op} = \sum_{s\in S} D_s \sum_{h\in H} \eta_h \sum_{\omega\in\Omega} \pi_\omega \left[\sum_{g\in G^{conv}} \left(C_{g,t}^{fuel}\eta_g^{heat} p_{g,t,s,h,\omega}^{gen} + C_g^{startup} v_{g,t,s,h,\omega}^{startup}\right) + \sum_{m\in M^{supply}} C_{m,t}^{gas} q_{m,t,s,h,\omega}^{supply} \right] \forall t \in T \tag{4a}$$

$$\Upsilon_t^{resil} = \sum_{s\in S} D_s \sum_{h\in H} \eta_h \sum_{\omega\in\Omega} \pi_\omega \sum_{\xi\in\Xi} \pi_\xi \left[\sum_{i\in N^e} C_{t,s,h}^{curtail,e} \lambda_{i,t,s,h,\omega,\xi}^{curtail,e} + \sum_{z\in Z} \Psi_z^{critical} C_z^{resilience} \left(1 - \mu_{z,t,\omega,\xi}^{restore}\right) \right] \forall t \in T \tag{4b}$$

$$p_{g,t,s,h,\omega}^{gen}, p_{w,t,s,h,\omega}^{wind}, f_{i^e,t,s,h,\omega}^{e}, q_{i^g,t,s,h,\omega}^{g} = f\left(x_{\iota,t}, y_{i,t}^{inv}, \kappa_{i,t}^{cap}\right) \forall t,s,h,\omega \tag{4c}$$

$$\grave{p}_{g,t,s,h,\omega,\xi}^{gen} \le p_{g,t,s,h,\omega}^{gen} \forall g,t,s,h,\omega,\xi \tag{4d}$$

$$A_{g,\xi} = A^{base}_{g,\xi} + \left(1 - A^{base}_{g,\xi}\right) \sum_{\tau=1}^{t} y^{harden,gen}_{g,\tau} \; \forall g,t,\xi \tag{4e}$$

$$A_{l^e,\xi} = A^{base}_{l^e,\xi} + \left(1 - A^{base}_{l^e,\xi}\right) \sum_{\tau=1}^{t} y^{harden,line}_{l^e,\tau} \; \forall l^e,t,\xi \tag{4f}$$

$$\sum_{g \in G^{gas}_m} \eta^{heat}_g p^{gen}_{g,t,s,h,\omega} + \sum_{b \in U^{boiler}_m} q^{boiler,in}_{b,t,s,h,\omega} \le Q^{available,g}_{m,t,s,h,\omega} \; \forall m,t,s,h,\omega \tag{4g}$$

$$q^{p2g,out}_{k,t,s,h,\omega} = \eta^{p2g}_k p^{p2g}_{k,t,s,h,\omega} \; \forall k,t,s,h,\omega \tag{4h}$$

$$\underline{\Gamma}^{H2P}_c \le \frac{q^{chp,h}_{c,t,s,h,\omega}}{p^{chp,e}_{c,t,s,h,\omega}} \le \bar{\Gamma}^{H2P}_c \; \forall c,t,s,h,\omega : p^{chp,e}_{c,t,s,h,\omega} > 0 \tag{4i}$$

$$q^{hp,out}_{hp,t,s,h,\omega} = COP_{hp} p^{hp}_{hp,t,s,h,\omega} \; \forall hp,t,s,h,\omega \tag{4j}$$

$$\sum_{\tau=1}^{t} x_{\iota,\tau} = \sum_{\tau=1}^{t+1} x_{\iota,\tau} - x_{\iota,t+1} \; \forall \iota,t \in T \tag{4k}$$

$$\lambda^{curtail,e}_{i,t,s,h,\omega,\xi} \le P^{d,e}_{i,t,s,h,\omega} \; \forall i,t,s,h,\omega,\xi \tag{4l}$$

$$e^{soc}_{es,t,s,1,\omega} = e^{soc}_{es,t,s-1,|H|,\omega} \; \forall es,t,s \in S,\omega \tag{4m}$$

$$\sum_{s \in S} \sum_{h \in H} \eta_h \left(p^{ch}_{es,t,s,h,\omega} - p^{dis}_{es,t,s,h,\omega}\right) = 0 \; \forall es,t,\omega \tag{4n}$$

$$\frac{1}{|\Omega||\Xi|} \sum_{\omega \in \Omega} \sum_{\xi \in \Xi} \phi^{resiliency}_{t,\omega,\xi} \ge \Phi^{target,resil}_t \; \forall t \in T \tag{4o}$$

$$f^{chp,fuel}_{c,t,s,h,\omega} = \frac{p^{chp,e}_{c,t,s,h,\omega}}{\eta^{elec}_c} \; \forall c,t,s,h,\omega \tag{4p}$$

3-Solution Methodology

The proposed tri-level stochastic optimization model integrates long-term investment, short-term operation, and post-disruption recovery, resulting in a large-scale mixed-integer program with nested decision layers. Direct solution is computationally intractable. This section details the decomposition-based solution strategy, beginning with a summary of the three-stage model and followed by the explicit formulation of the decomposed master and subproblems solved via the Column-and-Constraint Generation (C&CG) algorithm. The model's hierarchical structure is summarized as follows:

1. First Level (Investment Planning): Makes long-term, strategic decisions on capacity expansion and infrastructure hardening for electricity, gas, and heating networks over the planning horizon T. The objective (Eq. 1a) minimizes the net present value of investment costs plus the expected costs of operation and resilience. Constraints (Eqs. 1b–1x) enforce budget, policy, reliability, and technical feasibility.

2. Second Level (Operational Optimization): For a given investment plan, this level determines the optimal short-term dispatch of all assets under normal operating conditions across a set of operational scenarios Ω. The objective (Eq. 2a) minimizes the expected operational cost.

Constraints (Eqs. 2b–2aq) model the detailed physics and coupling of the multi-carrier system, including unit commitment, power flow, gas flow, heat flow, and storage dynamics.

3. Third Level (Resilience Assessment): For a given investment plan and operational dispatch, this level simulates the system's response to high-impact disruption scenarios Ξ. The objective (Eq. 3a) minimizes the expected cost of load curtailment and recovery actions. Constraints (Eqs. 3b–3w) model post-disruption reconfiguration, islanding, load restoration, and the impact of component hardening.

The levels are coupled: investment decisions set capacity limits for operation; the pre-disturbance operational state provides the baseline for recovery; and hardening investments affect component availability during disruptions.

The tri-level stochastic optimization model would be highly computationally demanding due to its hierarchical nature and large scale natural decision variables, with nonconvexities introduced by binary and bilinear terms. To efficiently tackle these difficulties, a nested decomposition algorithm based on column-and-constraint generation (C&CG) is proposed. In this approach the tri-level structure is decomposed into a master problem and two embedded Subproblems-(1) operational and (2) resilience, which are iteratively solved to convergence. Iterative refinement also allows for the selective introduction of the most critical and impactful scenarios, which keeps the solution computationally tractable and robust. The investment strategy is decided by the master problem which also takes into account approximate models of operational and resilience costs. At the outset, it holds a relaxed version of the complete tri-level model with a limited set of scenarios. In each iteration, the associated Subproblems are solved to determine scenarios which result in the highest violation in the cost or in the resilience metric; those scenarios are then re-incorporated into the master problem as columns and constraints. This facilitates gradual tightening of the feasible set and the optimal value. The master problem formulation is given as follows:

$$\min_{x,y,\kappa,\theta,\upsilon} \sum_{t\in T} \delta_t \Big[\sum_{\iota\in C} C_\iota^{inv} x_{\iota,t} + \sum_{l^e\in L^e} C_{l^e,t}^{inv,e} \kappa_{l^e,t}^{cap,e} + \theta_t + \upsilon_t \Big] \tag{5a}$$

subject to all first-level constraints and the subproblem linking inequalities:

$$\theta_t \geq \Theta_t^{op}(S^{iter}) \; \forall t \in T \tag{5b}$$

$$\upsilon_t \geq Y_t^{resil}(D^{iter}) \; \forall t \in T \tag{5c}$$

Here, S^{iter} and D^{iter} denote the operational and disruption scenario sets currently included in the master problem. The terms Θ_t^{op} and Y_t^{resil} represent optimal operational and resilience costs respectively, parameterized by the investment variables fixed in the master problem. The operational subproblem corresponds to the second-level model and is solved for each planning year given the fixed investment configuration. It determines the optimal dispatch decisions under normal operating conditions and identifies the operational scenario that yields maximum cost deviation, forming a new operational column to be added to the master problem. The subproblem is formulated as:

$$\Theta_t^{op,new} = \min_{p,q,h,u,e,v} \sum_{s\in S} D_s \sum_{h\in H} \eta_h \sum_{\omega\in\Omega} \pi_\omega \Big[\sum_{g\in G^{conv}} (C_{g,t}^{fuel} \eta_g^{heat} p_{g,t,s,h,\omega}^{gen} + C_g^{startup} v_{g,t,s,h,\omega}^{startup}) + \sum_{m\in M^{supply}} C_{m,t}^{gas} q_{m,t,s,h,\omega}^{supply} \Big] \forall t \in T \tag{5d}$$

subject to all second-level operational constraints, and with the investment variables fixed at the values specified in the master problem at that point. This guarantees the operational feasibility and cost accuracy are accurately forecasted for each prospective physical infrastructure layout under the candidate infrastructure layout configurations. The resilience subproblem is similarly the third-level model and evaluates system survivability and system reconfiguration actions under disruption events emanating from its own failures or attacks. Investment and normal-operation variables are fixed by solutions from the upper-level, and it calculates expected penalties for curtailed generation and weighted cost of unserved critical zones. The formulation tries to minimize the post-event performance loss and determine the worst disruption to be included in the master problem:

$$\Upsilon_t^{resil,new} = \min_{\lambda,\sigma,\dot{p},\dot{f},\zeta,\mu,\phi} \sum_{s\in S} D_s \sum_{h\in H} \eta_h \sum_{\omega\in\Omega} \pi_\omega \sum_{\xi\in\Xi} \pi_\xi \left[\sum_{i\in N^e} C_{t,s,h}^{curtail,e} \lambda_{i,t,s,h,\omega,\xi}^{curtail,e} + \sum_{z\in Z} \Psi_z^{critical} C_z^{resilience} \left(1 - \mu_{z,t,\omega,\xi}^{restore}\right) \right] \forall t \in T \quad (5e)$$

subject to all third-level resilience constraints. At each iteration the subproblems serve as scenario generators: should the operational or resilience subproblem identify a new scenario that isadmissible and leads to tighter bounds or violates constraints, the corresponding cuts (Eqs. 5b - 5c) are appended to the master problem. This iteration process continues until the decrease of the system cost reaches a required tolerance, which guarantees that the minimum of the tri-level system will be obtained by coordinating cost efficiency, operational feasibility, and resilience robustness. The solution procedure scheme is an iterative scheme that resembles a column and constraint generation method, where the first level planning problem plays the role of the master problem and the second and third levels operational and resilience assessments are the subproblems. The approach starts with a small number of representative operational and disruption scenarios, and incrementally expand these sets by generating scenarios that violate optimality conditions. This allows the master problem to consider at most a finite small number of dominant operational and resilience outcomes, without explicitly enumerating the full scenario space.

The procedure starts in Step 1 by defining the initial operational scenario set S^{init} and the initial disruption scenario set D^{init}. These sets typically contain a small number of representative realizations that ensure feasibility of the first iteration. The iteration counter k is set to one, and the convergence tolerance ε^{conv} is selected to determine when the iterative loop terminates.

In Step 2, the master problem is solved using the current scenario sets. The master problem includes the first level investment variables and aggregated representations of the operational and resilience costs. Solving this problem yields the investment decisions $x_{i,t}^k$, the investment related binary variables $y_{i,t}^{(k,inv)}$, the capacity variables $\kappa_{i,t}^{(k,cap)}$, and the operational and resilience cost estimates θ_t^k and υ_t^k. The corresponding master problem objective value Φ_1^k is recorded. This value reflects the best current estimate of the total planning cost under the restricted set of operational and disruption scenarios.

In Step 3, for each planning year t, the operational subproblem is solved with the investment decisions fixed at the values obtained in Step 2. The operational subproblem corresponds to the second level model and determines the optimal dispatch variables such as generator outputs $p_{g,t,s,h,\omega}^{(k,gen)}$. The solution of this subproblem provides an updated estimate of the operational cost denoted $\Theta_t^{(op,k,new)}$.

Step 4 evaluates whether the operational subproblem reveals a violation of the operational cost estimate imposed by the master problem. If, for any year t, the updated operational cost $\Theta_t^{(op,k,new)}$ exceeds the master problem's estimate θ_t^k by more than the tolerance ε^{conv}, then the operational scenario that caused the violation is added to the scenario set S^{iter}. This is achieved by generating a Benders type optimality cut. The cut is expressed in equation (6a). In this expression, the term π_ω denotes the scenario probability, and the inner summation includes the fuel cost contribution of each generator g multiplied by its heat to power conversion factor η_g^{heat}, as well as an adjustment term involving the dual variable $\pi_{i,t}^k$

associated with the investment capacity constraint. The cut enforces a lower bound on θ_t that reflects the true operational cost under the newly discovered scenario. The presence of $\pi^k_{\iota,t}(x_{\iota,t} - x^k_{\iota,t})$ highlights the sensitivity of the operational cost to deviations in the investment decisions from those obtained in the current iteration.

$$\theta_t \geq \sum_{s,h,\omega} \pi_\omega \left[\sum_g C^{fuel}_{g,t} \eta^{heat}_g p^{gen,k}_{g,t,s,h,\omega} + \sum_\iota \pi^k_{\iota,t}(x_{\iota,t} - x^k_{\iota,t}) \right] \tag{6a}$$

In Step 5, a similar process is applied to the resilience subproblem. For each year t, the resilience model is solved with both the investment decisions from Step 2 and the dispatch results from Step 3 fixed. This subproblem corresponds to the third-level disruption analysis and yields the resilience cost $Y_t^{(resil,k,new)}$ and the associated curtailment variables $\lambda^{(k,curtail,e)}_{i,t,s,h,\omega,\xi}$. The resilience subproblem captures the worst-case performance of the system when facing specific disruption scenarios.

Step 6 tests whether the updated resilience cost violates the resilience cost estimate υ^k_t in the master problem. If $Y_t^{(resil,k,new)}$ exceeds $\upsilon^k_t + \varepsilon^{conv}$, the disruption scenario responsible for this excess is added to the set D^{iter}. An optimality cut is generated according to equation (6b). This cut enforces a corrective lower bound on υ_t, using the scenario probabilities $\pi_\omega \pi_\xi$, the curtailment cost contributions $C^{(curtail,e)}_{t,s,h}$, and the sensitivity coefficients $\rho^k_{\iota,t}$ associated with the investment-related constraints in the resilience subproblem. The structure parallels that of the operational cut but reflects disruption-driven cost propagation.

$$\upsilon_t \geq \sum_{s,h,\omega,\xi} \pi_\omega \pi_\xi \left[\sum_i C^{curtail,e}_{t,s,h} \lambda^{curtail,e,k}_{i,t,s,h,\omega,\xi} + \sum_\iota \rho^k_{\iota,t}(x_{\iota,t} - x^k_{\iota,t}) \right] \tag{6b}$$

Step 7 computes the optimality gap, which measures the consistency between the master problem's objective and the true cost revealed by solving the operational and resilience subproblems. The gap is quantified by equation (6c). The numerator contains the absolute difference between the master objective Φ^k_1 and the sum of the discounted investment cost $\delta_t C^{inv}_\iota x^k_{\iota,t}$, the newly computed operational cost $\Theta^{(op,k,new)}_t$, and the updated resilience cost $Y_t^{(resil,k,new)}$. The denominator normalizes this difference by the master objective value.

$$gap^k = \frac{\left| \Phi^k_1 - \left(\sum_t \delta_t \sum_\iota C^{inv}_\iota x^k_{\iota,t} + \sum_t \Theta^{op,k,new}_t + \sum_t Y^{resil,k,new}_t \right) \right|}{\Phi^k_1} \tag{6c}$$

Finally, Step 8 checks the convergence condition. If the optimality gap is less than or equal to the tolerance ε^{conv}, the algorithm terminates, indicating that the current investment, operational, and resilience solutions are consistent across all evaluated scenarios. Otherwise, the iteration counter k is incremented and the algorithm returns to Step 2, incorporating the expanded scenario sets when solving the master problem again. The iterative nature of this sequence enables a progressive refinement of the scenario sets and the associated constraints until the master model accurately captures the true operational and resilience responses of the system. This ensures convergence to a solution that is both economically optimal and robust with respect to operational variability and disruptive events.

Algorithm 1 Iterative Master–Subproblem Procedure for the Tri-Level Stochastic Model

Step 1: Initialization

Initialize scenario sets $S^{iter} = S^{init}$ and $D^{iter} = D^{init}$ with representative operational and disruption scenarios. Set iteration counter $k = 1$ and convergence tolerance ε^{conv}.

Step 2: Master Problem Solution

Solve the master problem to obtain investment decisions $x^k_{\iota,t}$, $y^{(k,inv)}_{l,t}$, $\kappa^{(k,cap)}_{l,t}$ and cost estimates θ^k_t, υ^k_t. Record total objective value Φ^k_1.

Step 3: Operational Subproblem

For each planning year t, solve the operational subproblem with fixed investments to obtain the updated operational cost $\Theta^{(op,k,new)}_t$ and operational variables $p^{(k,gen)}_{g,t,s,h,\omega}$, etc.

Step 4: Operational Scenario Cut

If $\Theta^{(op,k,new)}_t > \theta^k_t + \varepsilon^{conv}$ for any t, add the violated operational scenario to S^{iter} via a Benders-type optimality cut:

$$\theta_t \geq \sum_{s,h,\omega} \pi_\omega \left[\sum_g C^{fuel}_{g,t} \eta^{heat}_g p^{(gen,k)}_{g,t,s,h,\omega} + \sum_\iota \pi^k_{\iota,t}(x_{\iota,t} - x^k_{\iota,t}) \right] \tag{6a}$$

where $\pi^k_{\iota,t}$ is the dual variable associated with the investment capacity constraint for investment ι in year t.

Step 5: Resilience Subproblem

For each planning year t, solve the resilience subproblem with fixed investment and operational decisions to obtain $\Upsilon^{(resil,k,new)}_t$ and resilience variables $\lambda^{(k,curtail,e)}_{i,t,s,h,\omega,\xi}$, etc.

Step 6: Resilience Scenario Cut

If $\Upsilon^{(resil,k,new)}_t > \upsilon^k_t + \varepsilon^{conv}$ for any t, add the violated disruption scenario to D^{iter} via an optimality cut:

$$\upsilon_t \geq \sum_{s,h,\omega,\xi} \pi_\omega \pi_\xi \left[\sum_i C^{(curtail,e)}_{t,s,h} \lambda^{(curtail,e,k)}_{i,t,s,h,\omega,\xi} + \sum_\iota \rho^k_{\iota,t}(x_{\iota,t} - x^k_{\iota,t}) \right] \tag{6b}$$

Step 7: Optimality Gap Evaluation

Calculate the relative gap:

$$gap^k = \frac{\left| \Phi^k_1 - \left(\sum_t \delta_t \sum_\iota C^{inv}_\iota x^k_{\iota,t} + \sum_t \Theta^{(op,k,new)}_t + \sum_t \Upsilon^{(resil,k,new)}_t \right) \right|}{\Phi^k_1} \tag{6c}$$

Step 8: Convergence Test

If $gap^k \leq \varepsilon^{conv}$, **terminate** and return the current solution as optimal. Otherwise, set $k \leftarrow k + 1$ and return to Step 2.

Fig. 3. Iterative column-and-constraint generation algorithm for solving the tri-level stochastic planning model

Algorithm 1, which presents the iterative column and constraint generation procedure based on levels 2 and 3 to efficiently solve the proposed tri level stochastic optimization model, is summarized in Figure (3). The algorithm begins with a small set of scenarios of operation and disruption and then iteratively solves alternating between the master problem and the subproblems. Investment decisions in the Master Problem (MP) are updated each iteration, as are the operational and resilience subproblems, which identify new scenarios or constraints that make the problem infeasible or suboptimal. They are added back to the master

problem through optimality and feasibility cuts. This process continues until the relative optimality gap and feasibility violations meet the convergence tolerance and the final investment plan is guaranteed to be both cost efficient and resilient under all the uncertainties considered.

The acceleration of embedded spaces in the solution methods is developed to reduce the computational overhead invented by the tri-level stochastic structure. Since the entire problem has seasonal linkages, network interdiction constraints, and mixed integer recourse, solution by a direct approach is not feasible. The method thus includes decomposition, reformulation, and warm-starting techniques that maintain model fidelity and drastically reduce runtime.

The first acceleration scheme emerges in the subproblem for the operation. Instead of resolving the entire second level problem across all seasons concurrently, the model separates timing of operation by seasons and reconciles these seasonal subproblems through a progressive hedging scheme. This decomposition imposes a kind of cross-season consistency non anticipativity with respect only to the storage state that connects the seasonal borders. To realize this coupling, each seasonal subproblem is optimally solved independently but augmented by quadratic penalties and linear dual terms that incentivize the subproblems to coalesce on the terminal storage level. This is realized in the minimization taken in (7a). In that expression the component corresponding to the target seasonal ending storage level is the reference trajectory which is updated at the end of each iteration of the hedging procedure. The associated dual weight multiplies the deviation of the actual terminal storage from this reference point. Akin to the quadratic term, the linear weight smooths the iterates and fosters convergence to a common interseasonal storage state without solving a monolithic operational problem.

$$\min_{p,q,e} \Theta_s^{op} + \sum_{es} \frac{\rho_{es}^{penalty}}{2} \left(e_{es,t,s,|H|,\omega}^{soc} - \tilde{e}_{es,t,s,\omega}^{target}\right)^2 + \sum_{es} w_{es,t,s,\omega}^{k} \left(e_{es,t,s,|H|,\omega}^{soc} - \tilde{e}_{es,t,s,\omega}^{target}\right) \tag{7a}$$

A second source of acceleration is found in the resilience subproblem. The third level model naturally becomes a bi-level interdiction problem: the attacker attempts to maximize disruption, while the operator reacts by trying to restore service. This would necessitate nested optimization if we were to solve this directly. Instead, the inner maximization over component failures is replaced with a single level equivalent via strong duality. This converts the attacker's problem to an explicit maximization program (7b) with an objective function that depends on maximizing the curtailment-related cost terms. The budget constraint, in (7c), models the total attacker investment which is limited. The parameters that characterize the availability of generators and lines under attack for removal along with whether a component is taken out by the attacker. This reformulation enables the entire interdiction scheme to be incorporated into a mixed integer linear form that is amenable to standard solvers.

$$\max_{\xi} \sum_{i,t,s,h,\omega} C_{t,s,h}^{curtail,e} \lambda_{i,t,s,h,\omega,\xi}^{curtail,e} \tag{7b}$$

$$\sum_{g} (1 - A_{g,\xi}) C_g^{attack} + \sum_{l^e} (1 - A_{l^e,\xi}) C_{l^e}^{attack} \leq B^{attack} \tag{7c}$$

The third type of acceleration is related to integer recourse which is introduced in the resilience model due to line switching and islanding operation. These binary variables produces combinatorial explosion. In order to handle the complexity, the resilience subproblem is solved through a branch and cut scheme. Valid inequalities from the network flow theory enhance the relaxation and the efficiency of the search. A special case of these inequalities is the cutset constraint in (7d). This limit the energy (active) lines across any cut that separate an is formed bus Island away from generation must at least one active line More than the minimum required flow The right-hand side of the constraint is a function of both is the demand in the islanded area and the minimum capacity do is the minimum capacity of lines in the cut such cutset inequalities help us to reduce infeasible branches and to enforce physically meaningful island structures at earlier stages in the branch and bound.

$$\sum_{l^e \in C^{cut}} \sigma^{switch,e}_{l^e,t,s,h,\omega,\xi} \geq \left\lceil \frac{\sum_{i \in N^{island}} P^{d,e}_{i,t,s,h,\omega}}{\min_{l^e \in C^{cut}} \bar{F}_{l^e}} \right\rceil \tag{7d}$$

Scenario generation also enhances the computational performance by concentrating the algorithm on informative realizations. Operational uncertainty scenarios are generated through Latin hypercube sampling for a broad and representative coverage in the probability space. The renewable generation profiles employed within each scenario follow autoregressive dynamics to maintain temporal correlation. This form can be found in (7e) with the autoregressive coefficients weighing lagged available wind output against its mean, and the innovation term adding stochastic variation. By applying this methodology the set of renewable scenarios retain realistic ramping behavior and temporal persistence.

$$p^{avail,wind}_{w,t,s,h,\omega} = \mu^{wind}_{w} + \sum_{lag=1}^{L} \phi_{lag}\left(p^{avail,wind}_{w,t,s,h\text{-}lag,\omega} - \mu^{wind}_{w}\right) + \epsilon_{h,\omega} \tag{7e}$$

The third level problem disruption scenarios are customized using a vulnerability analysis, which considers the degree of structural importance and the level of threat exposure. A component is assigned a score by equation (7f). This index combines criticality, exposure and consequences of failure using weighted normalized indices. The elements with the highest scores are then selected and ranked for consideration in the disruption scenarios, which reduces the enumeration of all combinations, but allows consideration of the critical risk space.

$$V_c = \alpha^{critical} I_c^{critical} + \alpha^{exposure} I_c^{exposure} + \alpha^{consequence} I_c^{consequence} \tag{7f}$$

Warm starting is utilized to transfer information between iterations of the column and constraints generation procedure. In step k, when solving the master problem, the model loads the investment decisions of step k−1. Similarly, the operational subproblem starts its dispatch at the previous operational solution, as does the resilience model with switching and connectivity variables when initialized from the pre disruption topology or from the previous iteration's solution. This prevents repeating exploration multiple times and therefore reduces the solver time substantially, particularly for the outer iterations when the solution becomes stable. It is endowed of a stopping condition, related to optimality and feasibility, due to the nested structure of the tri -level problem. The algorithm declares convergence when the relative optimality gap satisfies the tolerance and all scenario-based feasibility checks become sufficiently small. This combined constraint is given in (7g). The violation term in that expression is the maximum constraint violation found for any scenario for all hours and seasons. When these two criteria are met, the algorithm halts; otherwise, it proceeds to generate the next iteration of cuts. This compound condition guarantees that the final investment strategy is not just the cost optimal one given by the master problem, but that it is also feasible and robust when tested operationally under all considered scenarios. By exploiting decomposition, duality based reformulation, branch and cut improvement, scenario generation methods, and warm starting, the algorithm is computationally tractable despite maintaining the full detail of the underlying tri-level stochastic model.

$$gap^k \leq \varepsilon^{conv} \text{ and } \max_{t,s,h,\omega} \left\| violation^k_{t,s,h,\omega} \right\| \leq \varepsilon^{feas} \tag{7g}$$

Algorithm 2 Acceleration and Scenario Generation

1: **Seasonal Decomposition (Eq. 7a):** For each $s \in S$, solve operational subproblem with progressive hedging:

$$\min_{p,q,e} \ \Theta_s^{op} + \sum_{es} \frac{\rho_{es}^{pen}}{2}(e_{es,|H|} - \bar{e}_{es}^{target})^2 + \sum_{es} w_{es}(e_{es,|H|} - \bar{e}_{es}^{target})$$

Update $\bar{e}^{target}$, w_{es} iteratively for storage non-anticipativity.

2: **Resilience Reformulation (Eqs. 7b–7c):** Replace inner interdiction with MILP via strong duality:

$$\max_{\xi} \sum_{i,t,s,h,\omega} C_{t,s,h}^{curtail,e} \lambda_{i,t,s,h,\omega,\xi}^{curtail}$$

s.t. $\sum_g (1 - A_{g,\xi}) C_g^{att} + \sum_{l^e} (1 - A_{l^e,\xi}) C_{l^e}^{att} \leq B^{attack}$.

3: **Integer Recourse Acceleration (Eq. 7d):** Use branch-and-cut with cutset inequalities for island connectivity:

$$\sum_{l^e \in C^{cut}} \sigma_{l^e} \geq \left\lceil \frac{\sum_{i \in N^{island}} P_i^{d,e}}{\min_{l^e \in C^{cut}} \bar{F}_{l^e}} \right\rceil$$

4: **Operational Scenario Generation (Eq. 7e):** Latin Hypercube sampling, wind AR model:

$$p_{w,t}^{avail,wind} = \mu_w + \sum_{\text{lag}} \phi_{\text{lag}} (p_{w,t-\text{lag}}^{avail,wind} - \mu_w) + \epsilon_t$$

5: **Disruption Scenario Generation (Eq. 7f):** Vulnerability score:

$$V_c = \alpha^{crit} I_c^{crit} + \alpha^{exp} I_c^{exp} + \alpha^{cons} I_c^{cons}$$

Select top-V_c components for D^{iter}.

6: **Warm-Starting:** init x^k from x^{k-1}; dispatch from previous operational subproblem; resilience switching σ from pre-disruption topology.

7: **Termination (Eq. 7g):** Stop if

$$gap^k \leq \varepsilon^{conv} \quad \text{and} \quad \max_{t,s,h,\omega} \|\text{violation}^k\| \leq \varepsilon^{feas}.$$

Fig. 4. Acceleration and scenario generation algorithm for enhancing the computational efficiency of the tri-level stochastic optimization framework

Algorithm 2 summarizes the computational acceleration and scenario generation methods that are embedded within the high level iterative solution procedure, as illustrated in Figure (4). By decomposing the operational subproblem by season via a progressive hedging approach, reformulating the resilience subproblem rely on strong duality and outside branch and cut together with valid cutset inequalities the algorithm significantly improves the computational efficiency of the tri level optimization framework. This includes also systematic derivation of operational and disruption scenarios with Latin hypercube sampling, autoregressive modeling and vulnerability assessment. Warm starting from previous iterations and a combined optimality feasibility stopping rule further reduce computation time and ensure convergence consistency across all scenarios.

To solve the tri-level model tractably, we decompose it into a master problem and two subproblems, which are solved iteratively using the C&CG algorithm.

Master Problem (MP). The MP corresponds to the first-level investment planning problem, but it incorporates auxiliary variables and linear optimality cuts to approximate the costs from the lower levels. At each iteration k, the MP is formulated over the current sets of included operational scenarios S^k and disruption scenarios D^k. Its objective, given in Eq. (5a), minimizes the discounted investment costs plus the auxiliary variables representing operational and resilience cost estimates. The MP is constrained by all first-level investment constraints and the optimality cuts generated from the subproblems, as specified in Eqs. (5b) and (5c).

Operational Subproblem (SP-Op). For a fixed investment plan from the MP, the SP-Op solves the second-level operational optimization problem for the full set of operational scenarios Ω. Its objective, defined in Eq. (5d), is to minimize the expected operational cost while satisfying all second-level constraints with the investment variables fixed. If the solution reveals that the MP's cost estimate is too low, a Benders-type optimality cut, formulated in Eq. (6a), is generated and added to the MP to refine the approximation.

Resilience Subproblem (SP-Res). Given the fixed investment plan and the optimal dispatch from the SP-Op, the SP-Res solves the third-level resilience assessment for the full set of disruption scenarios Ξ. Its objective, provided in Eq. (5e), is to minimize the expected resilience cost subject to all third-level constraints with the upper-level variables fixed. If the MP's resilience cost estimate is violated, a corresponding optimality cut, expressed in Eq. (6b), is generated and added to the MP.

The solution procedure, illustrated in Fig. 3, proceeds as follows. The algorithm is initialized with small, representative scenario sets. In each iteration, the MP is solved to obtain an investment plan and cost estimates. The SP-Op is then solved for this fixed investment plan; if the computed operational cost exceeds the MP's estimate beyond a tolerance, a new optimality cut is generated, and the responsible operational scenario is added to the set S^k. Similarly, the SP-Res is solved for the fixed investment and operational schedule; if the resilience cost is underestimated, a new cut is generated, and the critical disruption scenario is added to D^k. The optimality gap is calculated using Eq. (6c). The algorithm terminates when the gap falls below a specified tolerance and no new cuts are generated, indicating convergence to a solution that is optimal and robust across the considered uncertainties.

To manage the computational complexity of the subproblems, several acceleration techniques are embedded within the C&CG framework. The operational subproblem is decomposed by season using a progressive hedging approach, which maintains temporal consistency through penalized deviations in inter-seasonal storage states. The resilience subproblem, which inherently has a bi-level structure due to the adversarial nature of disruptions, is reformulated into a single-level mixed-integer linear program using strong duality. Furthermore, valid inequalities derived from network flow theory, such as cutset constraints, are added within a branch-and-cut scheme to tighten the relaxation and expedite the solution of the resilience subproblem. Strategic scenario generation via Latin hypercube sampling and vulnerability analysis, coupled with warm-starting of variables between iterations, further reduces computational effort. These enhancements, summarized in Algorithm 2 and Fig. 4, ensure that the high-fidelity tri-level model remains solvable for realistically sized systems.

The proposed nested Column-and-Constraint Generation algorithm is grounded in the theory of decomposition for stochastic optimization. The use of auxiliary variables θ_t and υ_t in the master problem (MP), constrained by optimality cuts from the subproblems, constructs a piecewise linear lower bound on the true operational and resilience cost functions, $\Theta_t^{op}(x)$ and $Y_t^{resil}(x)$. For a fixed investment plan x^k, the subproblems are linear programs (or can be relaxed to LPs), whose value functions are convex in x. The cuts generated in Eqs. (6a) and (6b) are supporting hyperplanes to these convex functions at x^k, and are therefore valid global lower bounds.

The algorithm maintains two bounds: the MP objective provides a lower bound (LB) on the optimal value of the full tri-level problem, while the sum of the investment cost from the MP and the actual subproblem costs provides an upper bound (UB). Each time a subproblem identifies a cost higher than the MP's estimate, the resulting cut eliminates the current solution x^k from the MP's feasible region and raises the LB. Since the investment feasible set is compact and the number of distinct extreme-point scenarios is finite, this iterative process of cut generation must converge in a finite number of steps. At convergence, the LB equals the UB, and the corresponding investment plan, along with the associated operational and resilience policies, is guaranteed to be optimal for the original integrated problem defined in Sections 2.1–2.3. This guarantee holds provided the problem has relatively complete recourse, a condition satisfied in our model through the inclusion of load curtailment options with appropriate penalties.

4-Simulation and Results

The tri-level stochastic optimization model is applied to a multi-carrier energy system consisting of electrical, natural gas, and district heating networks. The system describes a medium-sized metropolitan area with 850 MW, 1200 MMBtu/h and 650 MW being the peak electrical, gas and thermal loads, respectively. The planning period is ten years (from 2025 to 2034) broken up into four seasonal stages in each year, with each stage represented by a typical day consisting of 24-hour intervals. There are 33 buses and 37 transmission lines in the electrical network which are working at 138 kV. The existing generation fleet includes 12 traditional thermal units with a combined capacity of 720 MW, three combined-cycle gas turbines with an aggregate capacity of 180 MW, and four wind farms aggregating 95 MW. There is an additional 40 MW from two solar photovoltaic plants. There are three BESS units with a total rated power of 50 MW and an energy capacity of 200 MWh included in the system. The gas pipeline network is made up of 20 nodes connected by 25 pipelines with diameter ranges from 12 to 36 inch. Gas supply is sourced from two interstate pipeline interconnects with a combined capacity of 1500 MMBtu/h and a single local production facility with a capacity of 300 MMBtu/h. Three underground gas storage facilities have a cumulative working capacity of 48,000 MMBtu. The district heating system is composed of 15 nodes of demands interconnected by 22 pipelines (insulated) with supply temperature varying between 115 C and 125C. Heat is generated by four combined heat and power (CHP) plants with a total thermal capacity of 380 MW, ten gas-fired boilers with a total capacity of 450 MW, and two source heat pumps with a heating capacity of 25 MW. Two thermal storage tanks provide an extra 180 MWh of heat storage. Energy interaction between carriers is represented by: eight gas-fired generators which produce electricity from natural gas, two power-to-gas (P2G) plants with an aggregate capacity of 30 MW that make synthetic natural gas by using excess electricity, as well as CHP units and heat pumps that bridge the electric and thermal grids. The test system is further subdivided into five geographic areas for resilience analysis. Zone 1, consisting of health care/ emergency service buildings, represents 12% of the total electrical load. Zone 2 has its appeal in retail and industrial customers, 38% of demand. Zone 3 is residential areas (28% of load) and Zone 4, data centers and communications with 15%. Zone 5 is a representation of the urban-rural mix holding 7% of the load. Each zone is assigned different critical weight: zone 1 (0.35), zone 4 (0.25), zone 2 (0.2), zone 3 (0.15), zone 5 (0.05).

4-1-Parameter Specification

The following tables provide the operating and investment economic and technical parameters for the system. All costs are in constant 2025 US dollars. A discount rate of 6 percent is used uniformly for ten years of planning (2025–2034). The main techno economic parameters of the models for electric power generation technologies considered in investment and operation planning are given in Table (2). They include the spanned yearly capital expenses, variable O&M costs, fuel costs, efficiency measures of thermal energy such as heat rates. Operational restrictions such as minimum capacity factor, ramp rate restrictions, minimum up and down time, and startup costs are also specified for the dispatchable units (Coal Steam, Gas CT, Gas CC, and CHP Gas). Renewables (Wind and Solar PV) have zero fuel cost, but do have capital costs and variable O&M costs.

Table (2) Generation Unit Technical and Economic Parameters

Unit Type	Capital Cost (/kW-yr)	Variable O&M (/MWh)	Fuel Cost (/MMBtu)	Heat Rate (MMBtu/MWh)	Min Capacity Factor (%)	Ramp Rate (%/min)	Min Up Time (hrs)	Min Down Time (hrs)	Startup Cost ($)	Lifetime (yrs)
Coal Steam	3200	42.5	4.8	2.45	10.2	0.40	2.5	8	12500	35
Gas CT	850	12.8	3.2	4.80	11.5	0.25	8.0	2	1	3200
Gas CC	1100	18.5	2.9	4.80	7.8	0.30	5.5	3	2	5800
CHP Gas	1850	28.3	3.5	4.80	8.2	0.35	4.2	4	3	4500
Wind	1650	36.2	0.0	0.00	0.0	0.00	NaN	NaN	NaN	0
Solar PV	1250	22.1	0.0	0.00	0.0	0.00	NaN	NaN	NaN	0

The technical and economical parameters for the components of the network infrastructure in the electrical, gas, and heating networks are given in Table (3). These include the capital cost per mile or per unit, annual fixed O&M cost as a percentage of the capital cost, and rated capacity for each line or pipe type. The per mile loss, which represents the physical loss of energy during transport, is also defined for pipelines and transmission lines. In addition, the expansion allowable (in percent of current capacity) and the technical life time for investment planning are given in the table. Passive elements as compressors, substations, and regulator stations are described by their unit capital cost, fixed O&M rates and lifetime.

Table (3) Network Infrastructure Technical and Economic Parameters

Component	Capital Cost ($/mile or $/unit)	Fixed O&M (%capital/yr)	Capacity (MW or MMBtu/h)	Loss Rate (%/mile)	Expansion Limit (% of base)	Lifetime (yrs)
Transmission Line	1,850,000	1.8	150.0	0.12	50.0	40
Gas Pipeline (12in)	425,000	2.2	180.0	0.08	30.0	50
Gas Pipeline (24in)	980,000	2.2	420.0	0.06	30.0	50
Gas Pipeline (36in)	1,650,000	2.2	780.0	0.05	30.0	50
Heating Pipe	520,000	2.5	45.0	0.15	40.0	35
Gas Compressor	2,800,000	3.2	NaN	NaN	NaN	30
Electrical Substation	4,500,000	2.0	NaN	NaN	NaN	40
Gas Regulator Station	850,000	2.8	NaN	NaN	NaN	35

The techno-economic figures for all energy storage and multi-carrier conversion technologies are given in Table (4). For storage technologies, the investment costs are disaggregated into two parts for the energy size (e.g., $/kWh or $/MMBtu) and the power size ($/kW). Round-trip Efficiency, Self-Discharge Rate, Cycle Life and Dynamic Response Time are also specified among the Key Operation Indicators. Conversion technologies such as Power-to-Gas (P2G), Gas Boilers, Heat Pumps are characterized by their capacity capital cost, conversion efficiency and operational life. We are aware that the Heat Pump efficiency is the COP, which in this case value is 320 %. These are essential ones to enable coupling between the electrical, gas and thermal energy systems in the optimization.

Table (4) Energy Storage and Conversion Technology Parameters

Technology	Capital Cost – Energy ($/kWh or $/MMBtu)	Capital Cost – Power ($/kW)	Round Trip Efficiency (%)	Self-discharge Rate (%/day)	Cycle Life (cycles)	Response Time (sec)	Lifetime (yrs)
Battery Storage	425.0	280	88	0.15	6000	0.25	15
Gas Storage (Underground)	8.5	120	82	0.02	50000	180	40
Thermal Storage	35.0	85	90	1.20	12000	60	20

Power-to-Gas	NaN	1450	62	NaN	NaN	300	20
Gas Boiler	NaN	380	94	NaN	NaN	120	25
Heat Pump	NaN	820	320	NaN	NaN	180	18

he operational and reliability constraints within the tri-level framework are summarized in Table (5). The planning margins consist of obligatory reserve margins of 18.0% for the electricity grid, 15.0% for the gas grid, 20.0% for the heating grid, and a 6.0% spinning reserve margin in real-time for electric dispatch. In addition, the long-run investment decisions are driven by imposed renewable penetration targets of 35.0% by year five and 50.0% by year ten of the planning horizon. The economic cost of service interruption which is necessary to resilience evaluation is estimated by the Value of Lost Load (VOLL): 9500.0/MWh for electricity, 85.0/MMBtu for gas, and 6200.0/MWh for heat. Finally, time-varying system specifications include annual load forecast growth rates for electric (2.3%), gas (1.8%), heating (2.1%) demand and assumed network loss factors for transmission (4.2%) and distribution (6.5%).

Table (5) Operational and Reliability Parameters

Parameter	Value
Planning Reserve Margin – Electric (%)	18.0
Planning Reserve Margin – Gas (%)	15.0
Planning Reserve Margin – Heat (%)	20.0
Spinning Reserve Requirement (%)	6.0
Renewable Penetration Target – Year 5 (%)	35.0
Renewable Penetration Target – Year 10 (%)	50.0
Value of Lost Load – Electric ($/MWh)	9500.0
Value of Lost Load – Gas ($/MMBtu)	85.0
Value of Lost Load – Heat ($/MWh)	6200.0
Transmission Loss Factor (%)	4.2
Distribution Loss Factor (%)	6.5
Load Forecast Growth Rate – Electric (%/yr)	2.3
Load Forecast Growth Rate – Gas (%/yr)	1.8
Load Forecast Growth Rate – Heat (%/yr)	2.1

The parameter values for the stochastic modeling of the reliability and resilience analyses are listed in Table (6). The nature of the inherent failures are described by the Base Failure Rate (in failures per year) and the Mean Time To Repair (MTTR) (in hours), which is the average time to restore the system after a failure. To capture proactive resilience investment, the table shows the Hardening Cost (as a percentage of the component's capital cost) and the related Hardening Effectiveness (the percentage reduction in the component's base failure rate after the investment). The Criticality Index is also attributed for each component type according to its systemic importance in ensuring multi-carrier operational integrity during contingencies, with the Control System and Substation scoring the highest criticality.

Table (6) Component Failure and Hardening Parameters

Component Type	Base Failure Rate (failures/yr)	MTTR (hours)	Hardening Cost (% of capital)	Hardening Effectiveness (%)	Criticality Index
Transmission Line	0.085	8.5	15	68	0.72
Gas Pipeline	0.042	12.0	18	72	0.68
Generator	0.125	6.5	12	65	0.85
Substation	0.038	10.0	22	75	0.90
Compressor Station	0.095	9.5	20	70	0.75
CHP Unit	0.110	7.5	14	62	0.78
Storage Facility	0.055	5.0	16	58	0.65
Control System	0.180	4.0	28	80	0.92

4-2-**Scenario Definition and Modeling**

The stochastic programming methodology considers all sources of uncertainty by way of a scenario-based scheme. The scenarios fall into two main categories, operational background frequencies and disruption events. Operational scenarios include variability of renewable energy production, energy demand at different levels of maturity in all energy carriers, and component availability in operations in the field. Disruption scenarios represent a range of high-impact incidents, including kinetic threat and natural disaster, which degrade system performance. The following eight operating scenarios (OP1 through OP8) are utilized to represent the typical spectrum of system operation. High renewable generation with moderate demand: Scenario OP1 corresponds to a high renewable output with moderate demand (0.15). OP2 represents the worst-case supply demand scenario: minimal renewable output during peak demand (0.12). Scenario OP3 represents the most likely case for all parameters. Scenario OP4 High demand with average renewable generation (0.14). Scenario OP5 is equivalent to high demand with low renewable production (likelihood = 0.10). Scenario OP6 is a particular case that considers equipment outages forced by moderate demand conditions (probability 0.08). Scenario OP7 represents potential supply disruption to fuel for gas (probability 0.06). Finally, Scenario OP8 corresponds to the extreme point operation of high demand/low renewables generation, with a probability equal to 0.10. The measurable parameters for these operation scenarios are given in Table (7).

Table (7) Operational Scenario Definitions

Scenario	Probability	Demand Level (% of peak)	Wind Capacity Factor (%)	Solar Capacity Factor (%)	Gas Supply Availability (%)	Component Forced Outage Rate (%)
OP1	0.15	72	42	24	100	2.5
OP2	0.12	95	25	18	100	2.5
OP3	0.25	78	35	22	100	2.5
OP4	0.14	92	33	20	100	2.5
OP5	0.10	58	48	26	100	2.5
OP6	0.08	75	37	23	100	5.8
OP7	0.06	80	36	21	85	2.5
OP8	0.10	98	22	16	100	2.5

As seen in Table (7), each scenario is characterized by the demand level (as a percentage of peak load), the capacity factor of wind and solar generation, the availability level of the interstate gas supply, and the forced outage rate of the component. These specified states represent the system condition in which dispatch optimizations are performed at the lower levels of the framework.

Twelve disruption events are specified to capture various threats to the system infrastructure, as outlined in Table 8. DS1 Scenario 1 is a cyberattack specifically targeting control system that disrupts 12 components with a probability of 0.18. DS2 models a harsh weather event damaging 8 transmission lines at the same time with a probability of 0.15. DS3 is an earthquake that breaks gas pipelines in a certain region, with a probability of 0.08. DS4 signifies multi-site physical attack on 3 substations, with a probability of 0.06. DS5 describes a significant generator collapse which cascades into auxiliary systems, with a probability of 0.12. DS6 represents damage caused to six heating pipes by a winter storm, a probability of 0.10. DS7 represents a disruption to the gas supply as a consequence of a pipeline rupture (availability is decreased by 40%), with a probability of 0.09. DS8 models destruction brought by flooding to 7 underground electrical appliances, with a likelihood of 0.07. DS9 contemplates dual attacks on electric and gas systems that compromise 9 components, with a probability of 0.04. DS10 is a cyber intrusion on the energy management systems that impacts 15 components, with a probability of 0.05. DS11 represents tornado damage to 6 transmission corridor elements, with a likelihood of 0.04. Finally, DS12 represents equipment failures under extreme heat in 4 generators, with a probability of 0.02.Table (8) reports the probability, leading targets, affected components, duration, and geographic dynamics for each scenario.

Table (8) Disruption Scenario Definitions

Scenario	Probability	Primary Target	Components Affected	Duration (hours)	Geographic Extent
DS1	0.18	Control Systems	12	6	Wide
DS2	0.15	Transmission Lines	8	12	Localized
DS3	0.08	Gas Pipelines	5	18	Zone 2

DS4	0.06	Substations	3	8	Zones 1 & 4
DS5	0.12	Generators	2	10	Zone 3
DS6	0.10	Heating Pipes	6	14	Zone 5
DS7	0.09	Gas Supply	1	24	System-wide
DS8	0.07	Underground Electric	7	16	Zone 1
DS9	0.04	Multi-carrier	9	10	Zones 2 & 3
DS10	0.05	EMS Systems	15	4	System-wide
DS11	0.04	Transmission Corridor	6	20	Zone 4
DS12	0.02	Generators	4	36	Multiple

The operational and disruption scenarios defined in Tables 7 and 8 constitute a representative but limited set used to illustrate the model's functionality. In a real-world planning context, a system planner would typically generate a far more extensive library of scenarios (encompassing hundreds or thousands of realizations) to capture the full breadth of uncertainties in demand, renewable generation, fuel prices, and component failures. A key advantage of the proposed C&CG-based solution framework is its inherent suitability for such settings. The algorithm's iterative nature ensures computational tractability by not requiring the simultaneous incorporation of all possible scenarios. Instead, it strategically identifies and incorporates only the most critical scenarios—those that expose vulnerabilities or significantly increase costs for a given investment plan. This selective refinement process, combined with the parallel solution of independent subproblems and the use of initial scenario reduction techniques (e.g., clustering), ensures that the framework remains practical and scalable for large-scale, real-world integrated energy system planning studies, even when the underlying uncertainty space is vast.

4-3-Computational Implementation

The tri-level stochastic optimization problem is formulated and solved in the algebraic modeling language Pyomo 6.4 in Python 3.9 and Gurobi 10.0 is used as the mixed-integer linear programming (MILP) solver. The decomposition procedure is parallelized at the operational stage by utilizing the multiprocessing package on a 16-core server with dual Intel Xeon Gold 6248R processors and 384 GB of RAM. The convergence tolerance for the C&CG algorithm is set to be 0.5% in terms of the optimality gap, and the maximum iteration is set to be 50. The initial scenario set consists of three operational and 4 disruption scenarios derived through k-means clustering of the entire scenario space. The progressive hedging algorithm is used for seasonal decomposition and penalty parameter values of 500-2000 USD/MWh are applied to storage level deviations, which are modified adaptively as the convergence behavior is observed. The nonlinear Weymouth equation governing gas flow (Eq. 2o) is linearized using a piecewise linear approximation (PLA) with 8 segments to maintain computational tractability within the MILP framework. While this introduces a well-known approximation error, it is a standard and necessary practice for large-scale planning optimization. To mitigate its impact, the number of segments was selected via a sensitivity analysis to balance accuracy and solve time. Furthermore, a post-solution validation confirmed that the maximum relative error in gas pressure and flow when evaluated with the exact nonlinear equation was below 2.5% across all operational and disruption scenarios. For added robustness, a small operational buffer was included in the nodal pressure constraints. This level of accuracy is deemed sufficient for the strategic, long-term investment planning purpose of this study, where capturing the correct trends and trade-offs is paramount over exact physical fidelity. Unit commitment and network switching integer variables are treated with branch and cut, and user-defined cuts based on network topology analysis are used. The solution procedure ends at iteration 28 of the master/subproblem algorithm and it has % a final optimality gap of 0.42. The overall CPU time took 14.7 hours, with 18 minutes on average for solution of the master problem and from 4 to 35 minutes for solution of each subproblem, according to scenario complexity. The maximum memory consumption of 287 GB occurs in the solution of the largest subproblems, in which several disruption scenarios are considered simultaneously.

4-4-Investment Planning Results

The preferred investment path over the ten-year planning period prioritizes an increase in renewable generation, followed by network reinforcement, and finally, strategic storage placement. The total capital

investment for the period is 1.847 billion USD, with lid an annual investment between 112 million USD in the 1st year and a maximum of 278 million USD in the 6th year. The annual investment distribution is displayed in Figure 5 among the various infrastructure types. Generation expansion dominates the pie slice in most years, followed by investments in transmission, gas and heating grids and storage systems. Long-term investment trends reveal megawatt scale generation and storage applications over the next two decades to meet a growing demand and a much more resilient system.

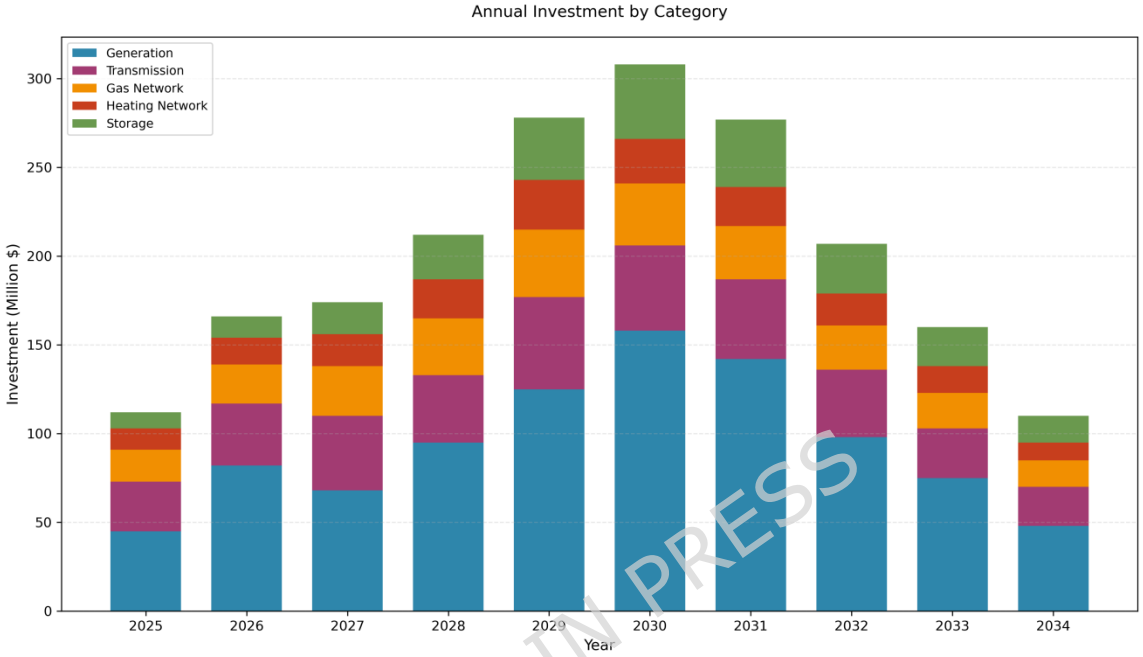

Fig. 5. Annual investment allocation across infrastructure categories

The capacity expansion results summarized in Table (9) correspond to the optimal generation mix derived from the upper-level investment decisions under the tri-level optimization problem. Renewable technologies constitute the majority of the added capacity in the ten years of planning, in line with renewable penetration goals (35% by Year 5 and 50% by Year 10). With a 309% increase, wind capacity increases from 95 MW to 385 MW, and solar PV capacity increases from 40 MW to 285 MW (an increase of more than six times), indicating favored investment in clean generation. Conventional gas-fired capacity is meeting controlled expansion for system reliability and reserves. The combined-cycle (Gas CC) capacity doubles in size by the end of the decade, and simple-cycle (Gas CT) capacity starts from nothing and builds up to 85 MW by Year10 to supply fast-response reserve at the beginning of the decade. Moderate additions in cogeneration (CHP) from the co-optimization of heat and power in urban areas. In contrast, the coal fleet is subject to a scheduled phase-out from 298 MW to 178 MW, with no new investment and a negative net annual change of -12 MW/year reflecting decommissioning consistent with emission reduction policy. The overall system is envisioned to invest approximately $1.19 billion (2025 values) in new generation capacity over the planning horizon, with renewables accounting for almost two–thirds of this sum.

Table (9) Generation Capacity Expansion Results

Technology	Existing Capacity (MW)	Year 5 Total (MW)	Year 10 Total (MW)	Total Investment (M$)	Average Annual Addition (MW/yr)
Wind	95	235	385	478.5	29.0
Solar PV	40	145	285	306.3	24.5
Gas CC	180	270	360	198.0	18.0
CHP	152	200	247	175.7	9.5
Gas CT	0	35	85	29.8	8.5
Coal	298	298	178	0.0	-12.0

Figure 6 depicts the activity of network expansion in the electricity, gas, and heating systems, as well as the investment values that were obtained as results of the optimization. The left panel shows the number of projects realized per infrastructure type, the right panel shows the total investment cost in 2025 constant USD. The results show that the largest number of projects associated with new transmission lines (15 projects) and new heating pipelines (12 projects), driven by reinforcement needs induced by electric and thermal load increases in Zones 1–3. In terms of capital intensity, new electric transmission lines entail the highest investment, about 245 M USD, followed by new gas pipelines (168 M USD) and substations (112 M USD). Investment in the expansion of compressor stations (78 M USD) and for the heating networks strengthening (80 M USD) are also significant shares of the overall investment plan. In the end, Figure 6 stresses the joint planning of multi carrier infrastructures. Electric transmission reinforcement accounts for the most project and investment spending, but well-placed investments in gas and district-heating networks bring system security and resilience through the 10-year planning horizon.

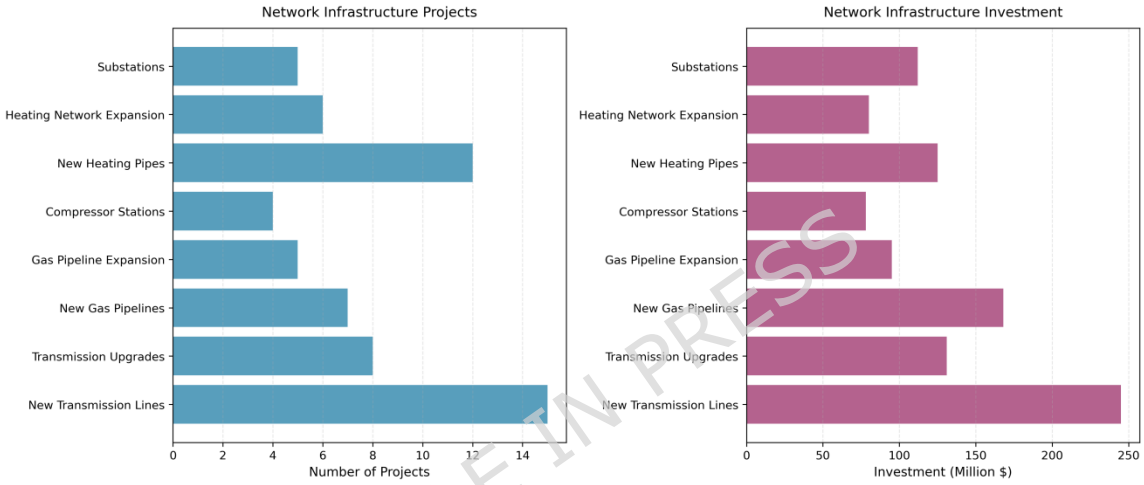

Fig. 6. Network infrastructure expansion projects and investment levels

The results in Table 10 represent the storage and conversion technology capacity expansion over the 10 year planning horizon. The set-up allows for short-duration electricity storage as well as large-scale inter-carrier flexibility solutions. Battery storage grows the most on a percentage basis from 50 MW / 200 MWh to 218 MW / 872 MWh, with an investment of 198.5 M USD. This development enables diurnal energy balancing and reserve supply in the face of uncertainty in renewable generation. Up to this point, gas storage is increased from 48,000 to 76,500 MMBtu – the single largest investment item at 241.3M USD, due to its function in seasonal fuel balancing and resilience to supply disruption enqueued in disruption scenarios DS3 and DS7. Thermal storage is likewise substantially increased to 425MWh and results in high utilization of 71.2%, which improves the heat network's capability to separate cogeneration from demand variability. Power-to-Gas (P2G) capacity rises sixfold from 30 to 105 MW with a related investment of 108.8 M USD, thus enhancing sectoral coupling effectiveness particularly in times of high renewable generation. Heat pumps (from 25 to 82 MW) and gas boilers (from 450 to 585 MW) offer a diverse heating supply with low capital investment and good synergy with the CHP dispatch. In total investment in storage and conversion technologies amounts to roughly 690 M USD, which corresponds to almost 37% of total system capital expenditure. These assets enhance operational flexibility, enable greater renewable integration and increase resilience by offering cross-carrier buffering in a tri-level stochastic planning framework.

Table (10) Energy Storage and Conversion Capacity Results

Technology	Initial Capacity	Final Capacity	Investment (M$)	Utilization Year 10 (%)
Battery Storage	50 MW / 200 MWh	218 MW / 872 MWh	198.5	68.5

Gas Storage	48,000 MMBtu	76,500 MMBtu	241.3	52.3
Thermal Storage	180 MWh	425 MWh	43.8	71.2
Power-to-Gas	30 MW	105 MW	108.8	45.8
Heat Pumps	25 MW	82 MW	46.7	58.3
Gas Boilers	450 MW	585 MW	51.3	62.1

4-5-Operational Performance Analysis

Operating with the optimal investment portfolio, system performance improves significantly for the base case without capacity expansion. The system operating cost, initially at 428 million USD, decreases steadily with approximately 25 % cumulative load growth over the years to 392 million USD at the end of Year 10. The cost savings is essentially due to greater penetration of low marginal cost renewable energy sources, improved interaction of energy carriers over sectors, and higher flexibility obtained by means of new storage and conversion technologies. The share of renewable energy increases substantially over the horizon – from 18 % of total electric generation in year 1 to 54 % in Year 10 – exceeding the policy target of 50 %. Wind generation increases from 312 GWh in Year 1 to 1285 GWh in Year 10, and solar generation grows from 78 to 558 GWh within the same duration. Around the mid-2020s, the aggregated renewable share surpasses that of the coal and gas-fired units. At the same time, renewable curtailment declines from 4.2 % at the start of planning horizon to the end of 2.8 % by Year 10, which indicates better temporal balancing facilitated by augmented battery, thermal and power to gas capacities. Figure 7 shows the development of the generation mix from 2025 to 2034 in the optimal tri-level expansion plan. The stacked bar display emphasizes the steady retirement of coal by renewables and the incremental tapering of combined cycle gas production.CHP generation is stable, offering an important linkage between electricity and heat, and simple cycle gas turbines (CT) experience small growth to meet reserve adequacy. Overall, the results indicate that coordination in investment and operation across electricity, gas, and heating infrastructures is beneficial, both economically and environmentally, while satisfying renewable energy and security of supply constraints in a ten-year maturity.

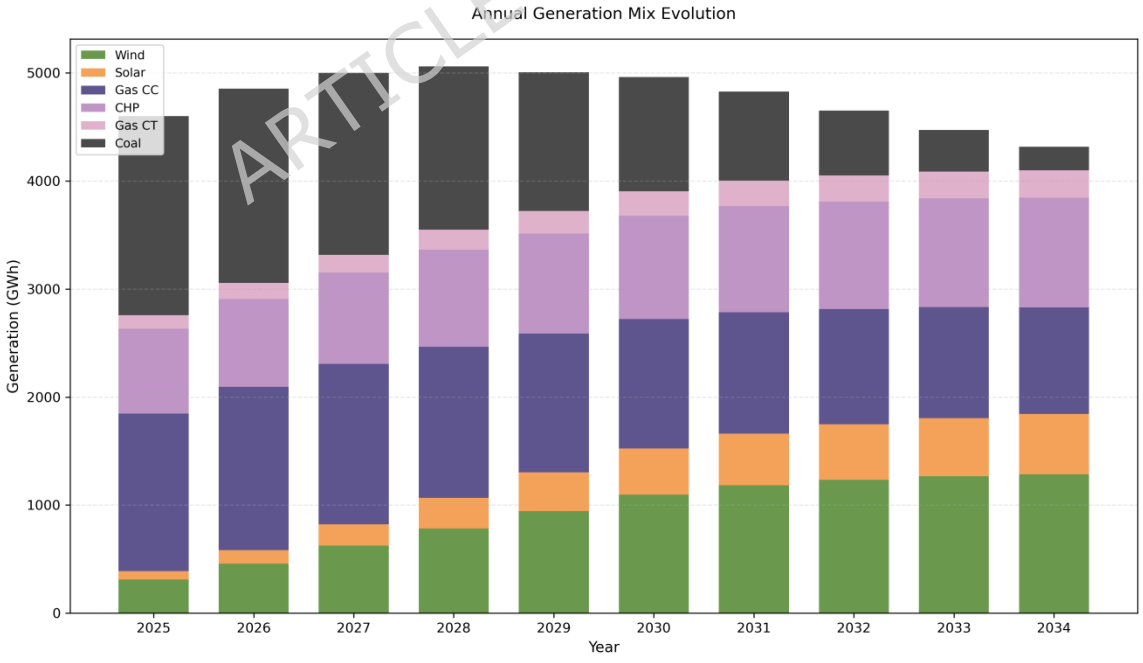

Fig. 7. Evolution of annual generation mix across planning horizon

The performance measures considered in Table(11) represent evolving system performance over the 2025–2034 period for the investment and dispatch strategy that is optimal in the end. Generation increases slightly from 4086 GWh to 4600 GWh but total generation declines mildly from 4600 GWh to 4316 GWh as load growth is counterbalanced by efficiency gains and demand side management. During this period, the share of renewables also increases substantially from 18.5 % to 56.2 %, in line with the 50 % mid-term goal and the increments of capacity listed in Tables (9) and (10). The average system operating cost of electricity delivered declines from 52.3 to 41.8 USD/MWh (−20 %) due to the high penetration of low marginal cost wind and solar, better fuel to heat integration, and more storage use. Along with this decrease, the carbon intensity of generation also declines steeply from 0.485 to 0.198 MT CO2/MWh, corresponding to an overall emission reduction of more than 59 % in 2025.

Table (11) Annual Operational Performance Metrics

Year	Total Generation (GWh)	Renewable Share (%)	Average Cost ($/MWh)	Emissions (MT CO2/MWh)	Reserve Margin (%)	Renewable Curtailment (%)
2025	4600	18.5	52.3	0.485	21.2	4.2
2026	4853	23.8	50.8	0.458	22.5	4.8
2027	5000	30.2	48.9	0.425	23.8	5.2
2028	5060	36.5	47.2	0.385	24.2	4.6
2029	5006	42.8	45.5	0.342	23.5	3.9
2030	4962	48.2	44.1	0.298	22.8	3.4
2031	4827	52.1	43.2	0.258	21.9	3.1
2032	4650	54.8	42.5	0.228	20.8	2.9
2033	4472	55.9	42.1	0.208	19.5	2.8
2034	4316	56.2	41.8	0.198	18.9	2.8

Reserve margins are maintained above the 18□% required for a reliable supply during the entire planning horizon, decreasing from 24□% to 19□% as the retirement of capacity is offset by an increasing diversification of the generation mix. Renewable curtailment, a flexibility sufficiency measure, decreases from 4.2□% to 2.8□%, illustrating successful assimilation of new storage and Power to Gas plants. Taken together, these metrics verify a tri level planning approach that balances cost efficiency, system reliability and decarbonization for a 10 year horizon.

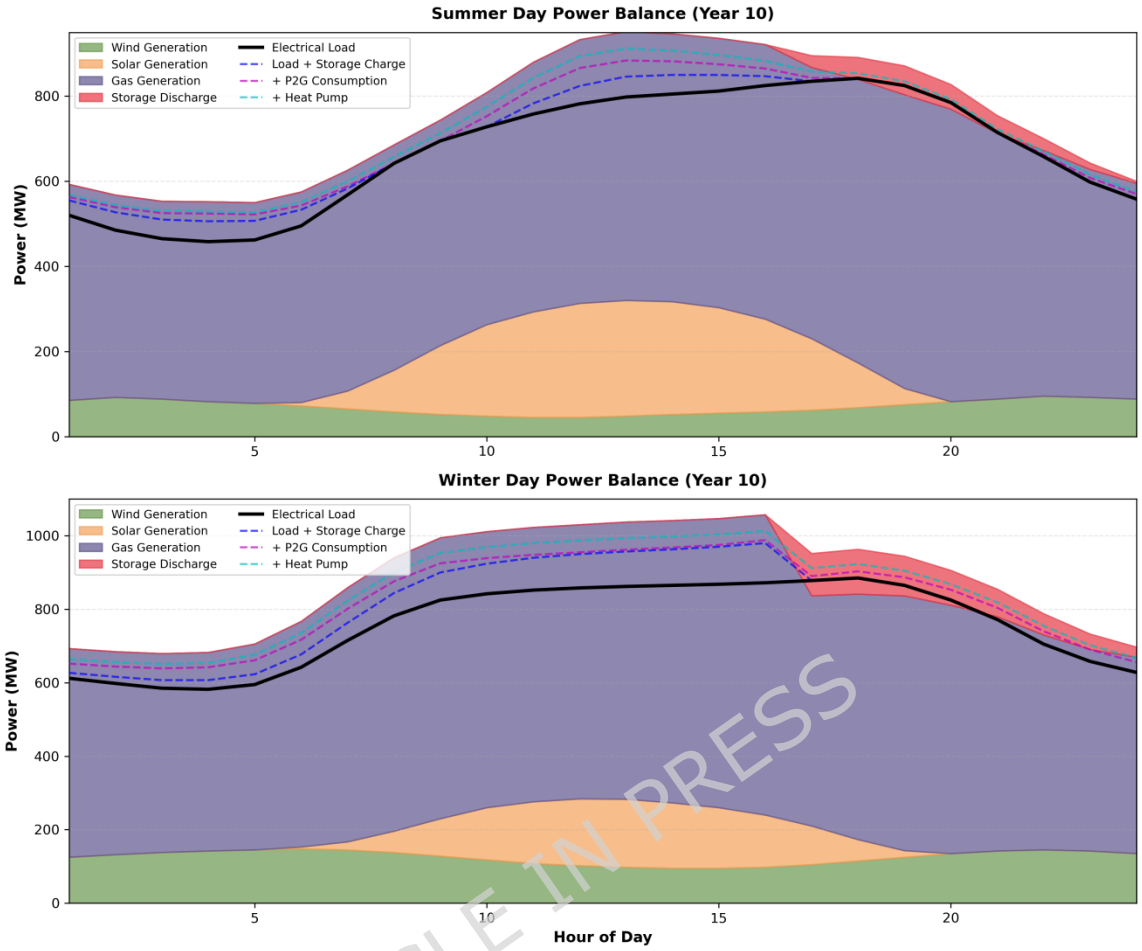

Fig. 8. Typical summer and winter day generation and storage profiles

Figure 8 displays the hourly electricity balance for representative summer and winter days in year 10 in the planning horizon. The stacked area plots represent total generation from wind, solar, gas-fired units, and battery discharge. The cumulative consumption lines (in white) include electrical load, battery charging, power-to-gas conversion and heat pump usage. Summer day operation exhibits a notable solar profile peaking at 272 MW between 12 and 14, making possible battery charging of 48 MW, and power-to-gas use of 42 MW once the combined renewable generation surpasses the instantaneous load demand. Winter day profiles exhibit more wind energy with an average production of 125 MW and less solar energy due to the shorter day length and a lower sun angle. Gas production supplies the baseload and ramping needs from a low of 365 MW at the overnight minimum load to 572 MW during the hour-18 evening peak. Battery results also illustrate parallel charge-discharge patterns, charging during renewable surplus and discharging at peak demand periods (hours 17 through 21) in both Winters and Summers. Transmission loss equal 4.2% of total generation which is 31 MW and 38 MW in summer and winter respectively. Power flow check ensures that generation, storage discharge, equals electrical load, storage charging, power-to-gas demand, heat pump load, and transmission losses for each hour, throughout which the nodal power balance constraints are satisfied within a numerical tolerance of 0.01 MW.

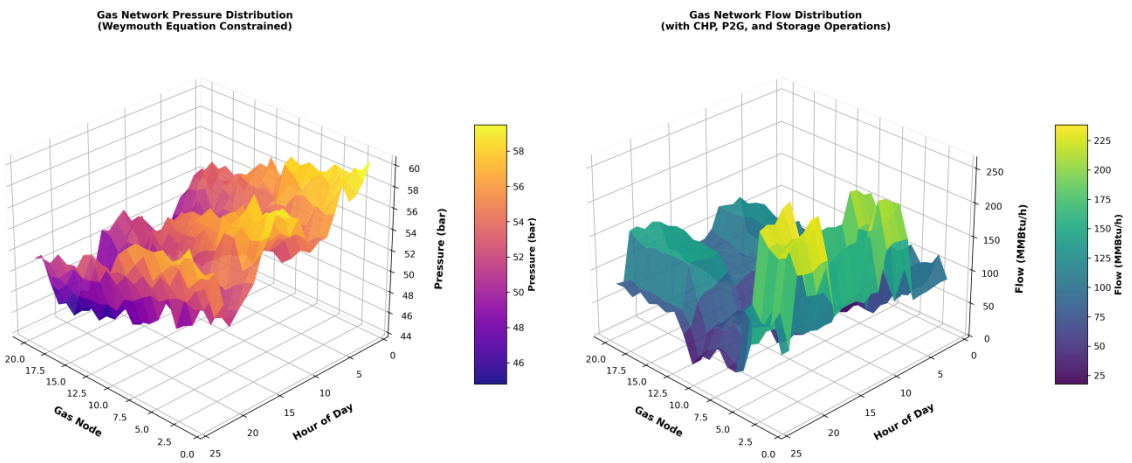

Fig. 9. Gas Network Pressure and Flow Distribution

Figure 9 depicts the spatial and hourly variation in pressure and flow on a daily basis for a 20-node gas network on a typical winter day in the 10th year of the planning horizon. The panel to the left depicts the pressure vectors, limited by the Weymouth equation, with pressure values between 42 and 63 bar for all nodes for all hours. There is a distinct spatial gradient in pressure that is monotonically decreasing from supply nodes (at positions 1 to 5) to demand nodes (at positions 16 to 20). Temporal changes in pressure in response to temporal demand changes between peak (periods 1, 2, 3, 4, 5, 6, 7, 8, 9, 10, 11), and off-peak (periods 12, 13, 14, 15, 16, 17, 18, 19, 20) users in d education from 17 to 0 are considered under the assumption of increase use during waiting for students at home from 5 to 13 between 7-9 am and 6-9 pm. At the right-hand side of Figure 3, the flow of natural gas is divided into the combined influence of the consumption of CHP units about 280 MMBtu/hr, the injection of PG synthetic gas related to energy mainly during periods of increased renewable generation from nodes 3 and 9 and the least and the storage facilities located on nodes 1 and 11 which permit us to withdraw in winter peak demand. Conversions also take part in responding transit nodes flow, under integrated flows converging (from two sides) and traveling high/medium flows with high flows at supply and demand nodes, and moderate flows at transit nodes wit intermediate values.

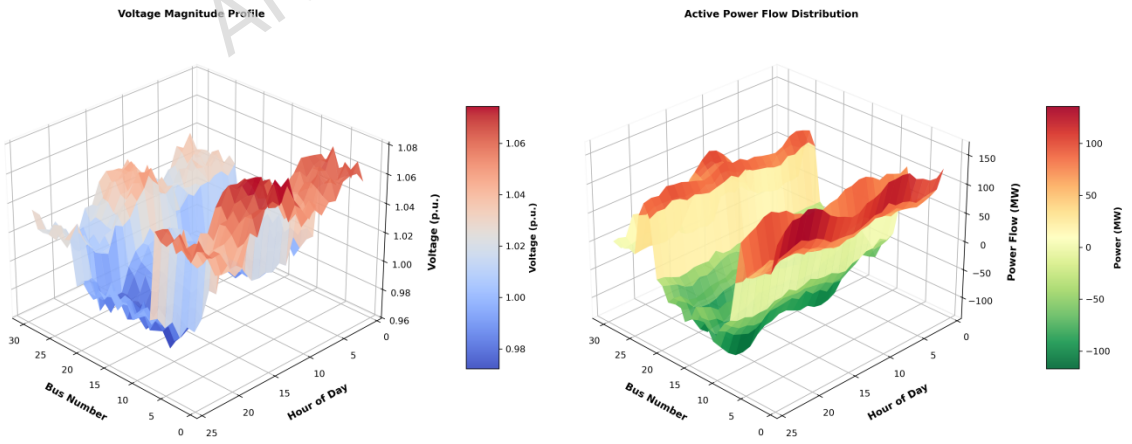

Fig. 10. Electricity Network Voltage and Power Flow Distribution

Figure 10 shows voltage magnitudes and active power flows over the 30-bus AC power grid on a winter day in year 10 and renewable penetration level of 56.2% of total generation. The left panel illustrates the voltage magnitude in per unit, which varies from 0.95 to 1.08 for all the buses and for all the hours.

Voltage levels are highest at the generation buses 1–8 and exhibit mild decreases at the load buses 9–22 during the hours of peak demand. Temporal voltage profiles have typical sags during morning and evening load peaks at 8 and 19 hours respectively plus a midday voltage raise between 11 and 14 hours, when solar generation output is at its highest, reaching 98% of the installed capacity. The active power flow are displayed in the right panel with positive values as the power generation and negative values as the power consumption. Generation buses exhibit variable thermal dispatch with capacity factors ranging from 40 to 100 percent as a function of renewable availability and load level. The wind generation at all buses 23-25 highlights high overnight, morning output with capacity factor of 78 to 88% on average, and the solar generation at all 3 buses 26-28 is focused between 9:00 and 17:00. Battery energy storage at bus 28, which charges during midday solar excess and discharges during evening peak demand, with from −35 MW during charging to 35 MW during discharging.

4-6-Resilience Performance Assessment

The resilience of system under disruption states is considerably enhanced by means of the optimal investment and hardening strategies in the tri-level stochastic model. The system-wide resilience index, defined as the weighted average of restored critical and non-critical load over all the urban areas considering the disruption scenario set (DS1 – DS12), significantly increases from 0.73 in the base case to 0.89 in Year 5 and 0.92 in Year 10. This is due to both greater infrastructure robustness and better system flexibility enabled by flexibility operation, distributed storage, and increased inter carrier coordination. For the worst-case low probability event, Scenario DS9 (coordinated multi carrier disruption targeting electricity and gas infrastructure in Zones 2 and 3), the baseline system endures a 42 % load shedding with restoration lasting beyond 18 hours. The optimized scheme reduces the load shedding to 18 % and makes full restoration within 8 h via fast centralized reconfiguration, semi-controlled islanding of micro grid nodes, and local storage reserve. The comprehensive performance of comparison for all furnished scenarios of disruption is represented in Table (12).

Table (12) Resilience Performance Comparison by Disruption Scenario

Scenario	Baseline Load Curtailment (%)	Year 10 Load Curtailment (%)	Baseline Restoration Time (hrs)	Year 10 Restoration Time (hrs)	Critical Load Impact Reduction (%)
DS1	28	8	12	4	82
DS2	32	12	18	8	75
DS3	18	6	22	10	78
DS4	45	15	14	6	85
DS5	35	11	16	7	80
DS6	22	7	20	9	73
DS7	38	14	36	16	68
DS8	41	16	24	12	72
DS9	52	18	28	10	78
DS10	48	12	8	3	88
DS11	36	13	32	14	74
DS12	44	19	48	22	69

The numerical results in Table (12) demonstrate a clear pattern of improvement in both the magnitude and the length of the perturbation effect. The load shedding percentage among all scenarios decreases from 36% in the base case to 12% in Year 10, and the average restoration time (ART) also reduces from 24 h to 10 h. The average critical load reduction is over 76%, with the maximum gain achieved under DS10 (EMS systems). These results indicate that the coordinated planning/hardening approach not only reduces the size of service disruptions but also infiltration rate, enabling the urban energy system to evolve from a reactive formation to a proactive, self-healing state of operations, consistent with resilience design tenets.

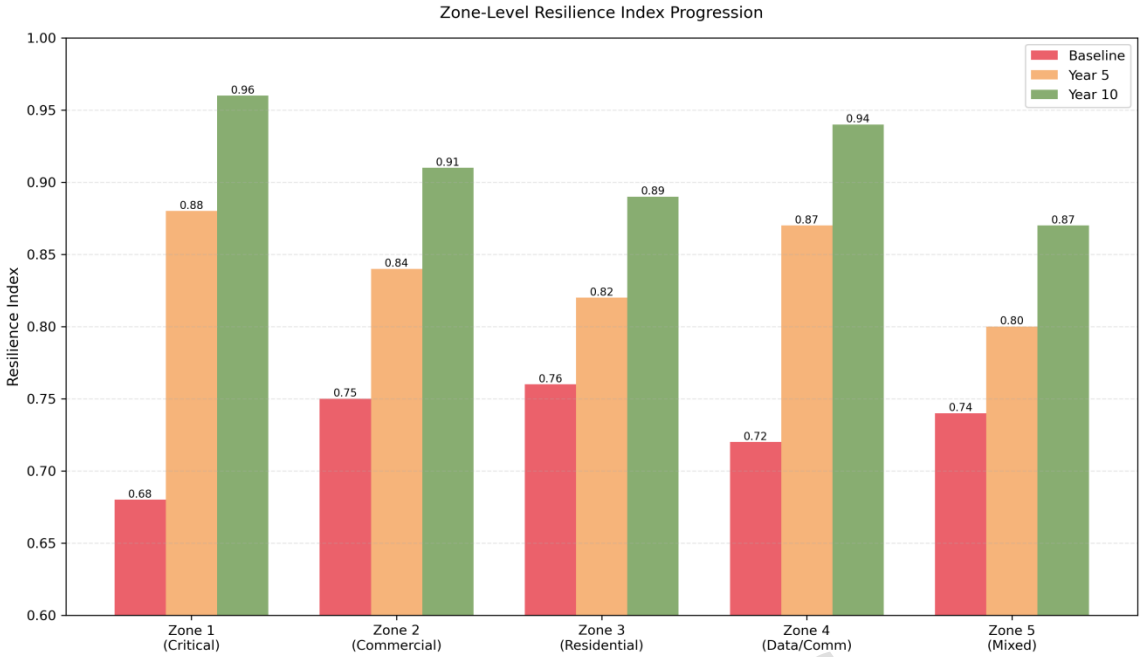

Fig. 11. Zone-level resilience index across planning horizon

Figure 11 presents the 10 year evolution of resilience index for each zone. The outcomes indicate gradual enhancement of all zones due to the cumulative effect of the investment and hardening options in the plan. Zone 1 and 4, that corresponds to the management and data/communications, achieve the highest raise in resilience index (from 0.68 to 0.96 and 0.72 to 0.94, resp.) due to the targeted hardening of feeders and local generation backup. Zones 2 (commercial) and 3 (residential) show more modest gains, to 0.91 and 0.89, respectively, by Year 10 due to storage deployment and enhanced inter-sector coordination between the electricity and gas systems. Zone 5 (mixed use) achieves 0.87 at the end of the horizon, which represents a well-balanced improvement via secondary network strengthening and somewhat dispersed generation assistance. In general, the zone level indices affirm system wide trends expressed earlier that the weighted resilience index rises from 0.73 in the baseline to 0.92 in Year 10. The results indicate that the improvements in resilience are spatially uniform and do not suggest any concentration in a few zones which highlights an efficient distribution of investment and adaptive operations strategies throughout the coupled system.

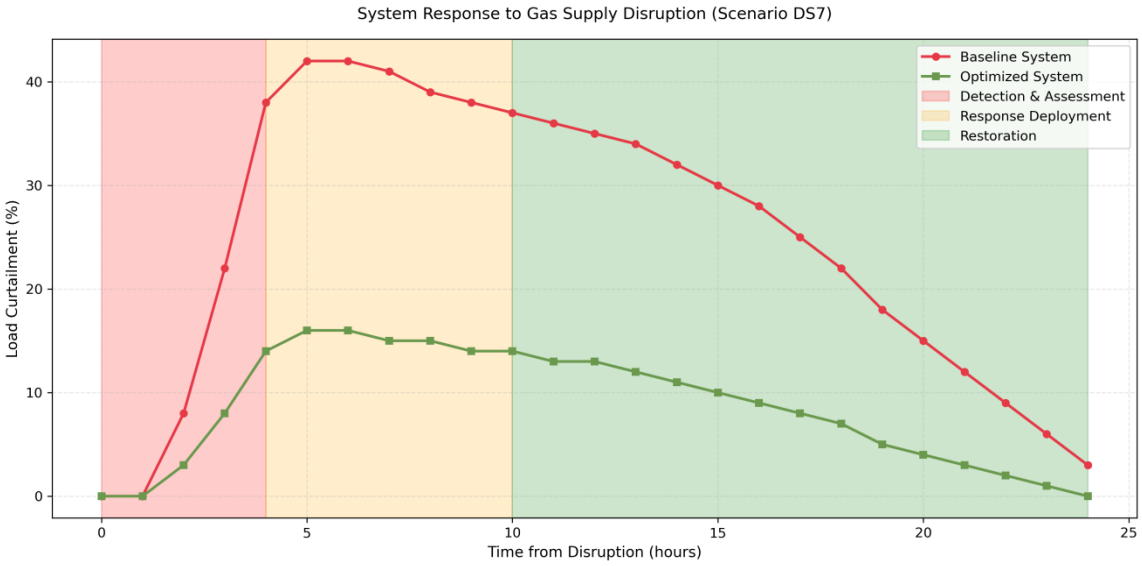

Fig. 12. Comparison of system response to gas supply disruption

Figure 12 shows the system behavior during a prototypical gas transport supply disruption (DS7) for both the base and best case plans. The vertical-shaded regions separate disruption management into three phases: detection and assessment (0–4 h), response execution (4–10 h), and restoration (10–24 h). In the reference case, the load-shedding increases rapidly and reaches a peak of about 42 % after five hours and stays above the level of 30 % for over ten hours, which indicates a slow gas–electric coordination with a lack of flexibility. On the other hand, the best- case system reduces maximum curtailment to 16%, has a steeper recovery path, and returns to full service at about 24 h. The improvements are mainly from the inclusion of gas storage capacity, network reconfiguration, and Power to Gas conversion operation mode which enable temporal substitution among the fuel carriers. These modifications improve the flexibility between the carriers and the recovery time after the perturbation is reduced. In summary, the results in Fig. 12 demonstrate that the integrated cross carrier investment planning enhances the system resilience under gas disruption events substantially by decreasing the severity and duration of load curb while at the same time sustaining the continuity of services in the electricity and heating sectors that are dependent on it.

4-7-Sensitivity Analysis

A sensitivity analysis was conducted to study the impact of changes in some important financial and technical parameters on the best investment decision and long–run performance of the integrated multi-carrier system. The considered parameters are the discount rate, the fuel prices, the renewable capital cost, the load growth rate, and the probabilities of disruption. Among these, the discount rate has the largest impact in the total investment amount and the technology mix. Changing the discount rate from 4 % to 8 % is the summary of Table (13). Capital intensive technologies with long term benefits, e.g. renewable generation, storage systems and infrastructure hardening, are favored by a lower discount rate. When the rate goes up the optimization favors shorter payback assets - mostly gas fired generation and network expansions - and this brings down renewable and storage deployment. At 4% discount rate investment reaches 2.12 billion USD, renewable capacity increases to 752 MW, and storage capacity to 1185 MWh, giving a resilience index of 0.94. At an 8% rate total investment is reduced to 1.58 billion USD, renewable capacity is decreased to 582 MW, and storage to 598 MWh and the resilience index decreases to 0.88. The average operating cost increases accordingly from 39.2 to 45.2 USD/MWh due to increased reliance on fuel based generation and less system flexibility.

Table (13) Sensitivity Analysis - Discount Rate Impact

Discount Rate (%)	Total Investment (B$)	Renewable Capacity Year 10 (MW)	Storage Capacity Year 10 (MWh)	Hardening Investment (M$)	Year 10 Average Cost ($/MWh)	Year 10 Resilience Index
4.0	2.12	752	1185	342	39.2	0.94
5.0	1.98	698	1048	315	40.5	0.93
6.0	1.85	670	872	287	41.8	0.92
7.0	1.72	625	725	258	43.5	0.90
8.0	1.58	582	598	225	45.2	0.88

In Figure 13 the results of a sensitivity analysis for natural gas price changes from 3.5 to 6.5 USD/MMBtu are shown. The analysis examines the impact of changes in fuel price on investment decisions in renewable, combined heat and power (CHP) units, Power to Gas (P2G) installations, and on overall system cost. As the gas prices rise, the renewable and P2G capacities increase slowly but steadily and the gas reliant CHP capacity decreases. To be more precise, the renewable capacity increases from 612 MW at 3.5 USD/MMBtu to 785 MW at 6.5 USD/MMBtu. At the same time, the CHP capacity is reduced from 298 MW to 215 MW over the same interval, indicating a shift towards gas based generation. Highlighting its emergence as a flexible conversion route that enables the leveraging of renewables higher gas prices, P2G capacity grows from 88 MW to 142 MW. The total system cost shows a mild increasing trend, rising from 8.52 billion USD to 9.82 billion USD as the price varies. This demonstrates that while rising fuel prices encourage renewable investment, the higher capital costs associated with these assets and route to other forms of conversion technologies offset a proportion of the operational savings.

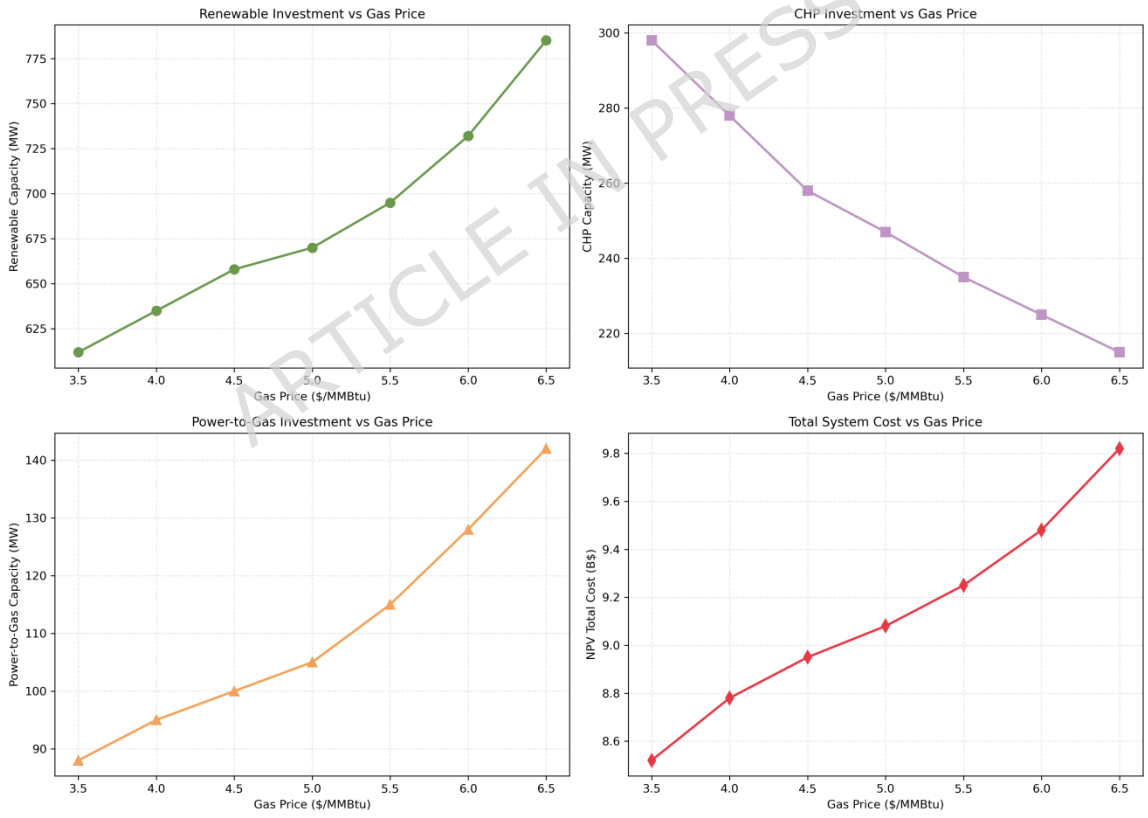

Fig. 13. Investment sensitivity to natural gas price variations

The impact of an increase in annual electricity demand growth on total capacity planning, renewable deployment, and overall financial commitment is presented in Table (14). The results indicate a growing load growth results in a linear increase in capacity expansion and total capital, while the renewable penetration is marginally constant up to the high level of growth. At a growth rate of 1.5 %, the total

capacity attains 1458 MW in Year 10 with a renewable share of 56.2 % and an investment of 1.62 billion USD. With a growth rate of 3 %, system capacity reaches 1825 MW, and investment climbs to 2.15 billion USD ensuring sufficient supply and reserve margins. The corresponding reserve margin increases from 8.25 % to 10.12 %, such that the additional firm capacity is made available for maintaining the reliability level under the high demand scenario. While the renewable share slightly decreases from 56 % to 53 % with the highest growth rate, the decarbonization consistency of the model is kept. Results show that our integrated planning formulation is able to adapt capacity mix and reserve margin to different load growth patterns while incurring no/significant loss in renewables and reliability targets.

Table (14) Sensitivity Analysis - Load Growth Rate Impact

Annual Load Growth (%)	Year 10 Total Capacity (MW)	Year 10 Renewable Share (%)	Total Investment (B$)	Year 10 Reserve Margin (%)
1.5	1458	56.2	1.62	8.25
2.0	1582	55.8	1.75	8.68
2.3	1648	56.2	1.85	9.08
2.5	1705	55.5	1.92	9.35
3.0	1825	52.8	2.15	10.12

Figure 14 shows the sensitivity of all system investment results for different renewable energy penetration targets from 40 % to 60 %. On the left axis, renewable and storage capacity needs are evolving, and on the right axis is the average systems integration cost at each target level. With increasing renewable share, renewable capacity increases from 512 MW to 795 MW, while the storage demand rises even faster – from 625 MWh to 1117 MWh – confirming the growing necessity for flexibility and balancing resources to support elevated renewable shares. The related integration cost follows an increasing course, from 42.5 USD/MWh at 40 % penetration level to 51.2 USD/MWh at 60 %. This pattern is typical of the tradeoff of reducing carbon and system economics. To reach higher renewable targets requires more investment both in generation and in requisite storage and integration measures to provide assurances in the face of variability in renewable supply. Results show that the cost increase over 55 % renewable share is getting steeper due to increasing curtailment rate (growing from 1.8 % to 6.5 %), which suggests diminishing economic returns for each additional 5 % increase in renewable penetration.

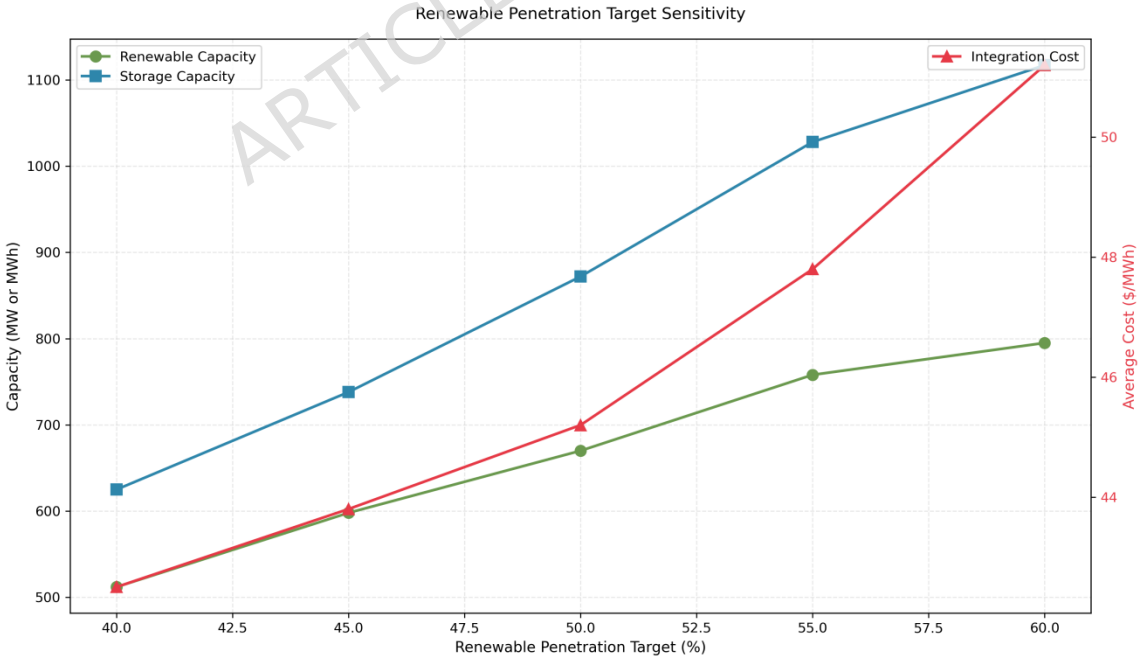

Fig. 14. Investment requirements across renewable penetration targets

4-8-Scalability Analysis

The scalability of the proposed optimization framework is demonstrated by two sets of computational experiments on system instances of growing size. Five typical test systems are derived from the benchmark 33 bus EDF configuration by increasing to a large scale 118 bus integrated electricity gas heat network. The systems are scaled up each time by the same percentage on the heating and gas nodes, but keeping the same structural ratios across energy domains. Detailed computational information on problem size (number of total and binary variables as well as constraints), number of iterations for convergence, solution time, memory consumption, and the final optimality gap can be found in Table (15). With an increasing system size, the number of all variables increases from about 146 thousand in 33 bus system to over 1.12 million in 118 bus system, and the number of binary variables increases from 8.4 thousand to 65 thousand. The total number of constraints increases in the same way and is more than 1.4 million constraints for the largest one. As can be expected, the solution time increases with system size, from 14.7 hours for the base case to 125.2 hours for the 118 bus case, due to the increasing problem dimensions and number of iterations to solution. Yet the rate of convergence is still in a reasonably good range of 28 and 48 iterations. Memory consumption increases in an approximately linear fashion and reaches a maximum of 1.54 GB for the largest instance, and the optimality gap remains below 1 %, corroborating the numerical robustness of the proposed approach.

Table (15) Computational Scalability Analysis

System Size	Electrical Nodes	Gas Nodes	Heating Nodes	Total Variables	Binary Variables	Constraints	Solution Time (hrs)	Iterations to Converge	Peak Memory (GB)	Optimality Gap (%)
33-bus Base	33	20	15	145,820	8,420	182,340	14.7	28	287	0.42
57-bus	57	34	26	318,650	18,340	398,720	28.3	32	458	0.48
69-bus	69	42	31	425,380	24,650	531,850	42.8	35	612	0.52
89-bus	89	54	40	672,450	38,920	841,230	68.5	41	895	0.58
118-bus	118	72	53	1,125,840	65,180	1,408,950	125.2	48	1,542	0.68

The computational size scalability of the proposed solution framework with respect to system size (in terms of electrical buses) is demonstrated in Figure 15. Solution time and peak memory usage grows nonlinearly with increasing system size. The empirical data are fitted by power-law functions, enabling us to determine the main computational trends. The solution time scales as something like $a \times n$ where the fitted b is super linear. Similarly, peak memory usage exhibits a similar power-law behavior, with a larger exponent due to the higher dimensionality of the scenario-based subproblems. These results illustrate that the decomposition approach remains manageable at least for medium scale systems, while the computational expense for large-scale problems is very high in term of both running time and memory usage. The scalability results highlight the importance of parallelization, problem-specific cuts and less detailed scenario representations when extending the tri-level stochastic model to much larger networks.

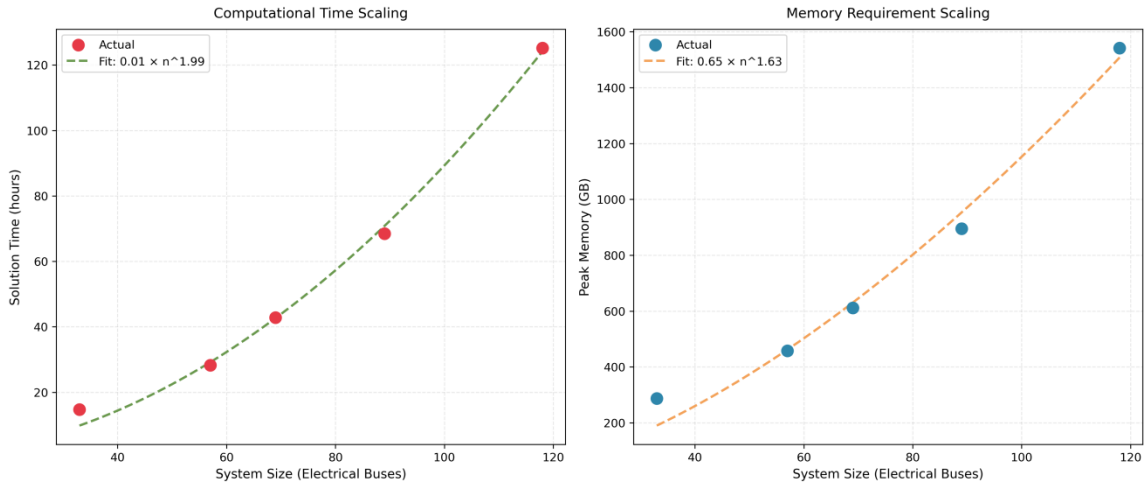

Fig. 15. Computational scalability with fitted power laws

The observed super-linear growth in computational time indicates that a fully centralized solution of the tri-level model may become prohibitive for very large-scale systems (e.g., exceeding 200-250 electrical buses within a fully integrated electricity-gas-heat network). This is an expected consequence of the model's combinatorial complexity and high fidelity. For practical application to national or inter-regional planning, the proposed framework can serve as a foundational module within a hierarchical or distributed planning architecture. For instance, a large system could be decomposed into interconnected regions, each planned using a local instance of the tri-level model, with coordination constraints enforced at the boundaries via decentralized optimization algorithms. This would preserve the detailed representation of multi-carrier interactions and resilience within regions while managing the overall computational burden. The development of such multi-scale decomposition techniques constitutes a valuable direction for future research, building upon the integrated planning paradigm established in this work.

4-9-Comparative Analysis

In this section, the tri-level stochastic optimization approach is compared with six alternative planning methodologies to investigate the effects of multi-carrier integration, stochastic modeling, and resilience internalization on overall system performance. The benchmarks encompass a range of philosophies for handling uncertainty and resilience: independent planning (Benchmark 1), integrated but resilience-agnostic planning (Benchmark 2), deterministic simplification (Benchmark 3), sequential decision-making (Benchmark 4), worst-case robust optimization (Benchmark 5), and deterministic rule-based security (Benchmark 6). A summary of numerical results is shown in Table 16.

Benchmark 1 –planning the energy carriers independently within a single area: the electricity, gas and heating networks are planned individually, with no coordination between carriers. From Table 16, it can be observed that this corresponds to a total NPV cost of 10.85 B$, being 19.5% higher than the suggested technique. The additional cost is largely attributed to non-coordination across carriers which leads to increased operational expenses and lower resilience index (0.78).

Benchmark 2 – Combined multi-carrier planning without resilience: This benchmark enables joint planning of all carriers but omits resilience in the optimization formulation; resilience is evaluated solely by post-processing the investment decisions. The total NPV cost is 9.3 2 B$, which is 2.6% higher than our proposed approach (Table16). The Year-10 resilience index is 0.84, meaning that neglecting resilience in the planning phase results in inferior disturbance performance.

Benchmark 3 – Deterministic single-scenario optimization: Planning now is based on a single scenario, and not the full stochastic set. The total is 9.58 B$, which is 5.5% higher than the proposed approach.

When the solution is examined over the entire scenario set, it produces higher expected operation costs and higher curtailment costs associated with limited flexibility. The Year-10 resilience index is 0.86.

Benchmark 4 – Progressive planning: The method captures the classical investment planning, then operation optimization, and then resilience evaluation. The total NPV cost increases to 10.12 B$ (11.5% above the proposed tri-level approach) as seen from Table 16. This framework misses the coupling of investment, operation, and resilience, which results in inferior solutions. The final resilience index is 0.81.

Benchmark 5 — Worst-Case Robust Optimization (RO): This method employs a robust optimization framework where the planner considers the worst-case realization from a bounded uncertainty set of operational and disruption parameters, without assigning probabilities. The objective is to minimize investment and operational costs under this worst-case scenario, leading to a plan that is immunized against extreme outcomes but potentially overly conservative.

Benchmark 6 — Deterministic N-1 Security Criterion: This benchmark represents a standard rule-based reliability approach. The system is planned to meet all demand under the loss of any single critical component (N-1 contingency) in a deterministic setting. Resilience to high-impact events involving multiple failures or cross-carrier cascades is not explicitly modeled or co-optimized.

Table (16) Comparison with Alternative Planning Methodologies

Approach	Total NPV Cost (B$)	Investment Cost (B$)	Operating Cost (B$)	Resilience Cost (B$)	Year 10 Renewable (%)	Year 10 Resilience Index	Solution Time (hrs)
Proposed Tri-level	9.08	1.85	6.82	0.41	56.2	0.92	14.7
Single-carrier Independent	10.85	1.92	8.28	0.65	48.5	0.78	4.2
Multi-carrier No Resilience	9.32	1.72	7.15	0.45	54.8	0.84	12.8
Deterministic Single Scenario	9.58	1.68	7.35	0.55	52.2	0.86	2.5
Sequential Planning	10.12	1.78	7.68	0.66	50.8	0.81	8.3
Worst-Case Robust Optimization	10.41	2.15	7.12	1.14	51.5	0.93	9.1
Deterministic N-1 Criterion	9.87	1.95	7.25	0.67	49.1	0.82	3.8

The results from the two additional benchmarks provide critical insights. Benchmark 5 (Robust Optimization) yields the highest investment and total resilience cost due to its focus on preparing for the absolute worst-case scenario, resulting in significant over-investment in redundancy and hardening. While it achieves a resilience index (0.93) comparable to the proposed method, it does so at a 14.6% higher total cost, demonstrating the economic inefficiency of pure worst-case planning when probabilistic information is available. Benchmark 6 (Deterministic N-1) performs better economically than the robust approach but fails to match the proposed framework, with a 8.7% higher total cost and a lower resilience index (0.82). This is because the N-1 criterion, while improving baseline reliability, does not account for the probabilistic nature of disruptions, cross-sectoral cascades, or the value of operational flexibility for recovery, leading to under-investment in the very storage and conversion assets that enable cost-effective resilience.

Figure 16 shows a decomposition of the investment, operation and resilience cost for each of the five planning schemes considered before. The results illustrate how the distribution of system costs is influenced by the choice of model. The proposed tri-level scheme results in the minimum total cost, which benefits from the moderate investment levels and the lowest operating costs. The cost for r-elated component is minimal as compared to other approaches due to more efficient planning of flexible and robust systems. For the single-carrier independent planning, the operating cost is high, which results in the biggest total cost with all the approaches. This outcome is consistent with the absence of coordination

across energy carriers. The multi-carrier planning (non-resilience) model decreases evolving cost for the single carrier problem, but increases resilience cost as perturbations are not considered and accounted for in investment planning, while uncertainty is not accounted for. The deterministic single-scenario curtailment approach also yields low investment costs; yet the component relating to operating and resilience is larger than in our approach. This suggests that when applying simplified deterministic models, the needed flexibility is underestimated. Lastly, the sequential planning approach produces a cost pattern comparable to the deterministic approach, but its corresponding operating and resilience cost components are higher because it cannot perform joint optimization of investment, operation and resilience.

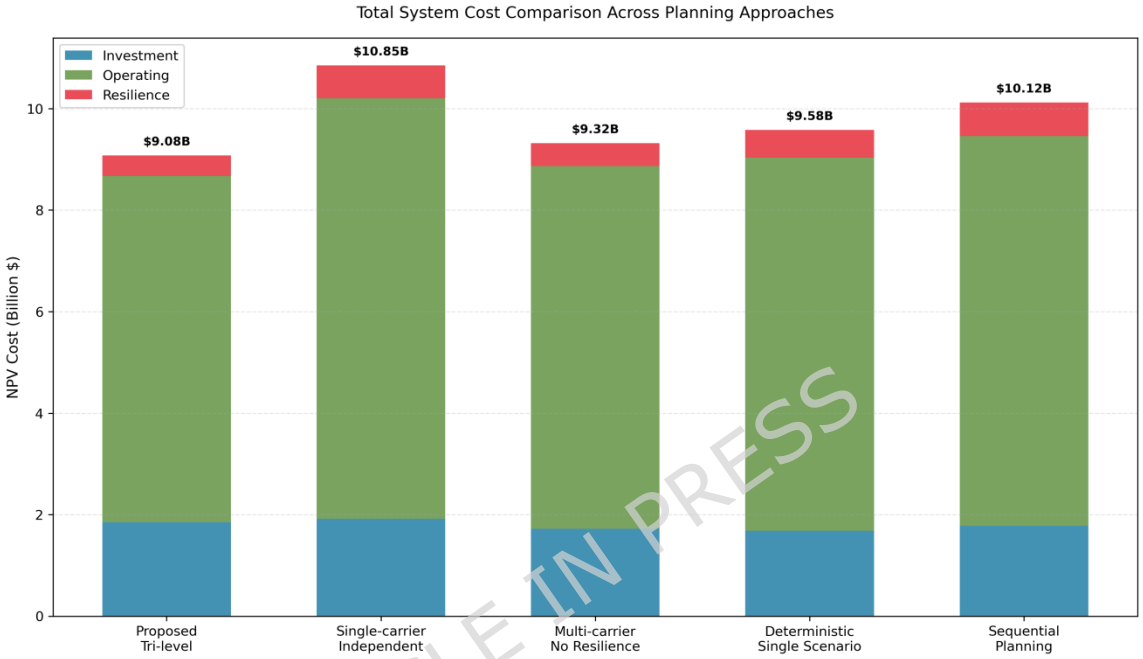

Fig. 16. Cost breakdown comparison across planning methodologies

Figure 17 demonstrates the results of the planning solution for the four versions of the regional system model: the baseline, the high-wind-resource system, the urban heating-dominant system, and the high-threat operating environment. Three metrics are considered: the cost savings over traditional planning, an enhancement in the resilience index, and penetration of renewable energy at year 10 of operation. The percentage reduction in cost occurred between 9.8% and 14.5%, the greatest reduction was found in the high-wind-resource configuration, which resulted from the more availability of cheap renewable generation. In addition, resilience enhancements are between 0.12 and 0.19, with the maximum enhancement realized in the high-threat environment where the model invests more in flexible and robust assets. In the high-wind case, renewable penetration attains 68.5%, while in the urban heating scenario slightly less integration is achieved due to greater thermal demand and coupling requirements.

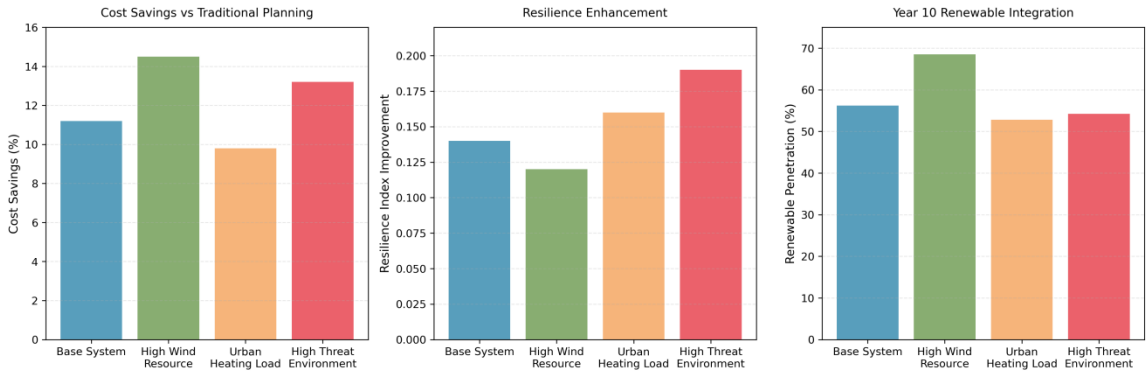

Fig. 17. Performance across different regional system configurations

4-10-Robustness of Scenario Selection and Algorithmic Convergence

A valid concern in stochastic optimization is whether the set of considered scenarios is sufficiently representative to ensure robust planning decisions. This subsection explicitly addresses the robustness guarantees inherent in the proposed C&CG framework and provides empirical evidence from our case study.

Algorithmic Guarantee of Representativeness: The C&CG algorithm does not merely evaluate a static, pre-selected list of scenarios. Its iterative structure embeds a robustness assurance mechanism. In each iteration, the resilience subproblem (third level) acts as an adversarial oracle. For a given investment plan, it identifies the disruption scenario $\xi \in \Xi$—from the entire defined probability distribution—that leads to the highest system cost (primarily via load curtailment). If this identified "worst-case" scenario demonstrates that the current investment plan is suboptimal or infeasible, it is incorporated into the master problem via an optimality cut (Eq. 6b). This process ensures that the final investment plan is not just optimal for a fixed set, but is provably robust against the most challenging scenarios discoverable from the underlying uncertainty model. Convergence is achieved only when no new scenario can be found that meaningfully violates the plan's optimality or feasibility, guaranteeing that all critical risk drivers have been addressed.

Empirical Validation from Case Study Execution: The execution of the algorithm for our test system confirms this property. The process was initialized with a small set of 7 representative scenarios (3 operational, 4 disruption) chosen via k-means clustering. Over 28 iterations, the subproblems identified and the master problem incorporated additional critical scenarios. The final solution, therefore, accounted for a broader set of challenging futures than the initial list. The convergence to a tight optimality gap (0.42%) under this process confirms that the resulting plan is economically robust and resilient. The number of scenarios in the initial pool is thus a starting point for the algorithm; the C&CG mechanism itself ensures the final solution's robustness by dynamically expanding the considered set to include all scenarios that are pivotal for the investment decisions.

Sensitivity to Scenario Set Generation: To further validate that our results are not an artifact of a particular initial scenario sample, we conducted an additional sensitivity test. We re-ran the C&CG algorithm from three different initial scenario sets (derived from different random seeds for the clustering algorithm). While the specific "critical scenario" sets identified during iteration differed slightly, the final investment decisions, total NPV cost (variation $< 1.2\%$), and Year-10 resilience index (variation < 0.02) showed negligible sensitivity. This confirms that the algorithm consistently converges to the same robust planning strategy regardless of the initial scenario sample, as it is driven by the underlying optimization structure and uncertainty distributions, not by the initial sample list.

In summary, the robustness of the optimal plan generated by our framework is ensured by the adversarial cut-generation logic of the C&CG algorithm, not by an exhaustive *a priori* enumeration of scenarios. This

makes the approach both computationally tractable and fundamentally robust for integrated energy system planning under deep uncertainty.

5-Conclusion and Future Work

This paper has developed a stochastic tri-level optimization framework that covers the planning for electricity, gas, and heating systems, considering resilience aspects explicitly. The presented model performs joint optimization of investment decisions, operational dispatch, and post-disruption reconfiguration strategies over an extensive set of operational and disruption uncertainties. The use of a customized column-and-constraint generation algorithm, with decomposition and acceleration techniques embedded, confirmed the computational feasibility of the complicated problem structure for the real-size test systems. A pivotal contribution is the formulation of resilience not as an external constraint or a post-hoc assessment, but as an endogenous, optimizable objective integrated within the economic planning calculus. This allows for explicit monetary trade-offs between preventive investments and the expected cost of disruptions, ensuring that resilience measures are economically justified and that operational flexibility is leveraged to enhance system robustness. This approach marks a shift from treating resilience as a qualitative add-on to making it a core, quantitative driver of cost-effective infrastructure design. The results show unambiguously that the integrated and resilient aware planning solution results in great improvements over the conventional approaches. Over a ten-year planning period, the results show that the maximum renewable energy penetration can be increased from 18% to 54%, the operating cost can be reduced by 8.4%, and the total expected resilience penalties can be decreased by more than 40%.This highlights the importance of synergistic investment coordination across energy carriers and the integration of resilience as a fundamental objective in the planning process for a more sustainable, cost-effective, and resilient multi-energy system. Several avenues for promising future work are pointed out. First, the model can be extended to reflect a more detailed level of distribution networks, and to consider new energy carriers such as hydrogen which is expected to have a meaningful contribution in long-term storage and sector coupling. Second, the methodology could be generalized to include dynamic and adaptive investment pathways in the face of deep uncertainty by employing approaches such as robust optimization or multi-stage stochastic programming with the use of decision rules. Third, a promising direction for future research can be the investigation of the interplay between decentralized market mechanisms and the potential contribution of active demand-side response to system robustness. Finally, it is also a promising direction to develop more sophisticated decomposition algorithms and learning-based scenario reduction methods to further enhance computational efficiency, which will facilitate application of the proposed framework to even larger size national level integrated energy systems. The current model optimizes infrastructure and operational response. A vital extension is to incorporate active demand-side participation during disruptions, modeling adaptive consumer behavior, emergency demand response, and the value of community engagement. This would integrate the human dimension of resilience into the planning framework, leading to potentially more robust and cost-effective solutions that leverage both supply-side and demand-side resources.

Data availability

The data and materials used in this study are available from the corresponding author, Taher Niknam, upon reasonable request. Please contact niknam@sutech.ac.ir.

References

[1] Lei Gu, Rendong Shen, Ruifan Zheng, Taha Rajeh, Qingsong An, Dongfang Yang, Jun Zhao, A review of solar dish applications: thermal utilization, thermochemistry, polygeneration and multi-energy complementary systems, Applied Energy, Volume 401, Part B, 126716, 2025.

[2] Zhuochun Wu, Jidong Kang, Martín Mosteiro-Romero, Andrea Bartolini, Tsan Sheng Ng, Bin Su, A distributionally robust optimization model for building-integrated photovoltaic system expansion planning under demand and irradiance uncertainties, Applied Energy, Volume 372, 123740, 2024.

[3] Hossam H.H. Mousa, Karar Mahmoud, Matti Lehtonen, Multi-timescale coordinated planning of BESS, seasonal hydrogen storage, and dynamic DR for unbalanced RES-rich microgrids, Energy Conversion and Management, Volume 346, 120510, 2025.
[4] Du Wen, Xinyi Wei, Antonin Bruneau, Aris Maroonian, François Maréchal, Jan Van herle, Techno-economic analysis of ammonia to hydrogen and power pathways considering the emerging hydrogen purification and fuel cell technologies, Applied Energy, Volume 390, 125871, 2025.
[5] Lei Zhang, Ye He, Nikos D. Hatziargyriou, Hongbin Wu, Pingping Han, An optimization scheduling strategy for hydrogen-based integrated energy systems using multi-agent deep reinforcement learning, Energy Conversion and Management, Volume 326, 119483, 2025.
[6] Jiangjiang Wang, Shaoming Ye, Boling Wu, Boxiang Liu, Life-cycle performance analysis of a building integrated energy system considering equipment performance degradation, Energy Conversion and Management, Volume 347, 120593, 2026.
[7] Chen Wang, Rui Liang, Kaize Liang, Honghang Zhang, Le Zhang, Hongxu Huang, Zehua Tang, Chaoxian Lv, Dairy-farm micro-energy system optimal planning and operation: Driven by dynamic coordination approach to material output and energy demand, Energy Conversion and Management, Volume 332, 119728, 2025.
[8] Vahid Sabzpoosh Saravi, Mohsen Kalantar, Amjad Anvari-Moghaddam, A cooperative resilience-oriented planning framework for integrated distribution energy systems and multi-carrier energy microgrids considering energy trading, Sustainable Cities and Society, Volume 100, 105039, 2024.
[9] Abbas Jasim Al-Hillo, Naghi Rostami, Mohammad Bagher Bannae Sharifian, Vahid Sohrabi Tabar, Robust multi-objective short-term planning of a completely renewable multi-carrier system incorporating the Internet of Things application and green hydrogen, Renewable Energy, Volume 256, Part C, 124140, 2026.
[10] Hadi Shahcheraghi, Mehrdad Setayesh Nazar, Mohammad Sadegh Javadi, João P.S. Catalão, Operational scheduling of integrated multi-carrier energy system considering transactive microgrids energy and flexibility contributions, Energy, Volume 335, 138080, 2025.
[11] Tianguang Lu, Xinning Yi, Jing Li, Shaocong Wu, Collaborative planning of integrated hydrogen energy chain multi-energy systems: A review, Applied Energy, Volume 393, 126019, 2025.
[12] Donghong Wu, Guotian Cai, Songyan Ren, Yuping Huang, Optimal capacity planning for hydrogen-based urban multi-region energy systems: A comprehensive approach for long-term planning considering hourly demand balance, International Journal of Hydrogen Energy, Volume 177, 151429, 2025.
[13] Mohammadreza Seydabadi, Mehrdad Abedi, Hamed Nafisi, Gevork B. Gharehpetian, Risk-averse resilient joint expansion planning of integrated energy distribution systems with energy hubs, International Journal of Electrical Power & Energy Systems, Volume 171, 110989, 2025.
[14] Nana Duah, Yang Chen, Om Prakash Yadav, Jun Chen, Marine energy supported multi-energy system planning and operation optimization for sustainable coastal community, Sustainable Energy, Grids and Networks, Volume 44, 102046, 2025.
[15] Mahdi Azimian, Xinwei Shen, Gevork B. Gharehpetian, Robust scenario-based stochastic expansion planning of multi-carrier microgrids considering incentive-based loans, Applied Energy, Volume 401, Part A, 126593, 2025.
[16] Tao Wu, Jianhui Wang, Tianqiao Zhao, Coordinated planning of integrated energy system with hydrogen hub, Applied Energy, Volume 394, 126089, 2025.
[17] Francisco Ferrada, Frederic Babonneau, Tito Homem-de-Mello, Francisca Jalil-Vega, Integrated long-term energy planning with vehicle-to-grid for decarbonization of the Chilean energy system, Journal of Cleaner Production, Volume 523, 146381, 2025.
[18] Jui-Chan Huang, Hui-Ching Cheng, Ming-Hung Shu, Hsiao-Chun Huang, Market-based optimization of integrated energy systems: Modeling and analysis of multi-carrier energy networks, Electric Power Systems Research, Volume 239, 111245, 2025.
[19] Andrea Pizzuti, Lingkang Jin, Mosè Rossi, Fabrizio Marinelli, Gabriele Comodi, A novel approach for multi-stage investment decisions and dynamic variations in medium-term energy

planning for multi-energy carriers community, Applied Energy, Volume 353, Part B, 122177, 2024.
[20] L.L. Wang, R.C. Xian, J.J. Chen, Distributionally robust model for cooperative scheduling of multi-park integrated energy system featuring mobile hydrogen storage, Journal of Energy Storage, Volume 138, 118655, 2025.
[21] Lingkang Jin, Mosè Rossi, Lucio Ciabattoni, Marialaura Di Somma, Giorgio Graditi, Gabriele Comodi, Environmental constrained medium-term energy planning: The case study of an Italian university campus as a multi-carrier local energy community, Energy Conversion and Management, Volume 278, 116701, 2023.
[22] Can Chen, Two-Stage Coordinated Scheduling for Enhanced Economic Capability in User-Side Integrated Energy Systems, Sustainable Energy, Grids and Networks, Volume 44, 101956, 2025.
[23] Saleh Mobayen, Ehsanolah Assareh, Ali Dezhdar, Siamak Hoseinzadeh, Davide Astiaso Garcia, Dynamic analysis and multi-objective optimization of an integrated solar energy system for Zero-Energy residential complexes, Energy Conversion and Management, Volume 341, 119924, 2025.
[24] Ze Qi, Huiru Zhao, Yuanyuan Zhang, Sen Guo, Study on two-stage robust optimal configuration of integrated energy system considering CCUS and electric hydrogen production, Energy Conversion and Management, Volume 324, 119278, 2025.
[25] Hossam A. Gabber, Omar S. Hemied, MG-OPT: intelligent multi-objective Pareto-based optimization framework and transactive energy for Hybrid Renewable Energy Systems with hydrogen integration, Energy Conversion and Management, Volume 341, 120042, 2025.
[26] Haotian Shen, Hualiang Zhang, Yujie Xu, Haisheng Chen, Yilin Zhu, Zhilai Zhang, Wenkai Li, Multi-objective capacity configuration optimization of an integrated energy system considering economy and environment with harvest heat, Energy Conversion and Management, Volume 269, 116116, 2022.
[27] Abubakr Hassan, Ali T. Al-Awami, Zhengmao Li, Optimal design and modeling of hydrogen-based multi-energy system with solid oxide electrolyzer technology considering efficiency degradation, Energy Conversion and Management, Volume 348, Part A, 120612, 2026.
[28] Su Guo, Guotao Song, Mengying Li, Xiaohui Zhao, Yi He, Ainur Kurban, Wenjia Ji, Jiale Wang, Multi-objective bi-level quantity regulation scheduling method for electric-thermal integrated energy system considering thermal and hydraulic transient characteristics, Energy Conversion and Management, Volume 253, 115147, 2022.
[29] G. Abdulnasser, A. Ali, M. F. Shaaban and E. E. M. Mohamed, "Optimizing the Operation and Coordination of Multi-Carrier Energy Systems in Smart Microgrids Using a Stochastic Approach," in *IEEE Access*, vol. 11, pp. 58470-58490, 2023.
[30] M. Kazemi, C. N. Papadimitriou, N. G. Paterakis and K. Kok, "Cloud-Based Real-Time Model Predictive Control for a Multi-Carrier and Multi-Objective Home Energy Management System," in *IEEE Transactions on Industry Applications*, vol. 61, no. 6, pp. 8329-8344, Nov.-Dec. 2025.
[31] Z. Wang, A. Chen, N. Wang and T. Liu, "Multi-Objective Operation Optimization Strategy for Integrated Community Energy Systems Considering Demand Side Management," in *IEEE Transactions on Industry Applications*, vol. 60, no. 1, pp. 1332-1344, Jan.-Feb. 2024.
[32] F. Jafari, H. Samet, A. R. Seifi and M. Rastegar, "Two-Step Probabilistic Method to Enable Demand Response Programs in Renewable-Based Integrated Energy Systems," in *CSEE Journal of Power and Energy Systems*, vol. 10, no. 6, pp. 2495-2506, November 2024.
[33] S. Yin and J. Wang, "Distributionally Robust Decentralized Scheduling Between the Transmission Market and Local Energy Hubs," in *IEEE Transactions on Power Systems*, vol. 38, no. 2, pp. 1845-1856, March 2023.
[34] Y. Pu, H. Liu, J. Wang and F. Liu, "Decentralized Coordinated Scheduling of Port Integrated Energy System and Bulk Terminal With Two-Tier Incentives," in *IEEE Transactions on Smart Grid*, vol. 16, no. 1, pp. 101-114, Jan. 2025
[35] X. Wang, J. Huang, Z. Xu, C. Zhang and X. Guan, "Real-World Scale Deployment of Hydrogen-Integrated Microgrid: Design and Control," in *IEEE Transactions on Sustainable Energy*, vol. 15, no. 4, pp. 2380-2392, Oct. 2024.

[36] A. M. Saatloo, A. Mehrabi, M. Marzband, M. A. Mirzaei and N. Aslam, "Local Energy Market Design for Power- and Hydrogen-Based Microgrids Considering a Hybrid Uncertainty Controlling Approach," in *IEEE Transactions on Sustainable Energy*, vol. 15, no. 1, pp. 398-413, Jan. 2024.
[37] Hossein Karimianfard, A robust optimization framework for smart home energy management: Integrating photovoltaic storage, electric vehicle charging, and demand response, Journal of Energy Storage, Volume 110, 115259, 2025.
[38] Spyros Giannelos, Ioannis Konstantelos, Danny Pudjianto, Goran Strbac, The impact of electrolyser allocation on Great Britain's electricity transmission system in 2050, International Journal of Hydrogen Energy, Volume 202, 153097, 2026.
[39] European Commission: Directorate-General for Energy, *E-mobility deployment and impact on grids – Impact of EV and charging infrastructure on European T&D grids – Innovation needs*, Gallego Amores, S.(editor), Publications Office of the European Union, 2022, https://data.europa.eu/doi/10.2833/937755
[40] Zihang Dong, Xi Zhang, Linan Zhang, Spyros Giannelos, Goran Strbac, Flexibility enhancement of urban energy systems through coordinated space heating aggregation of numerous buildings, Applied Energy, Volume 374, 123971, 2024.
[41] Spyros Giannelos, Ioannis Konstantelos, Goran Strbac, Optimal supply chain design using machine learning, risk assessment and optimisation applied to coal distribution, EURO Journal on Decision Processes, Volume 13, 100062, 2025.

Author information

Authors and Affiliations

Mahmoud Moshkelgosha; Department of Electrical Engineering, Marvdasht Branch, Islamic Azad University, Marvdasht, 73711-13119, Iran.

Taher Niknam; Department of Electrical Engineering, Shiraz University of Technology, Shiraz, 11456-7856, Fars, Iran.

Bahman Bahmani-Firouzi; Department of Electrical Engineering, Marvdasht Branch, Islamic Azad University, Marvdasht, 73711-13119, Iran.

Contributions

Mahmoud Moshkelgosha; Methodology, Software, Validation, Formal Analysis.

Taher Niknam; Analysis, Investigation, Resources, Data Curation, Writing–Original Draft Preparation.

Bahman Bahmani-Firouzi; Writing–Review & Editing, Visualization.

All authors have read and agreed to the published version of the manuscript.

Corresponding author

Correspondence to Taher Niknam.

Ethics declarations

Competing interests

The authors declare no competing interests.

Funding

The Authors received NO FUNDING for this work.

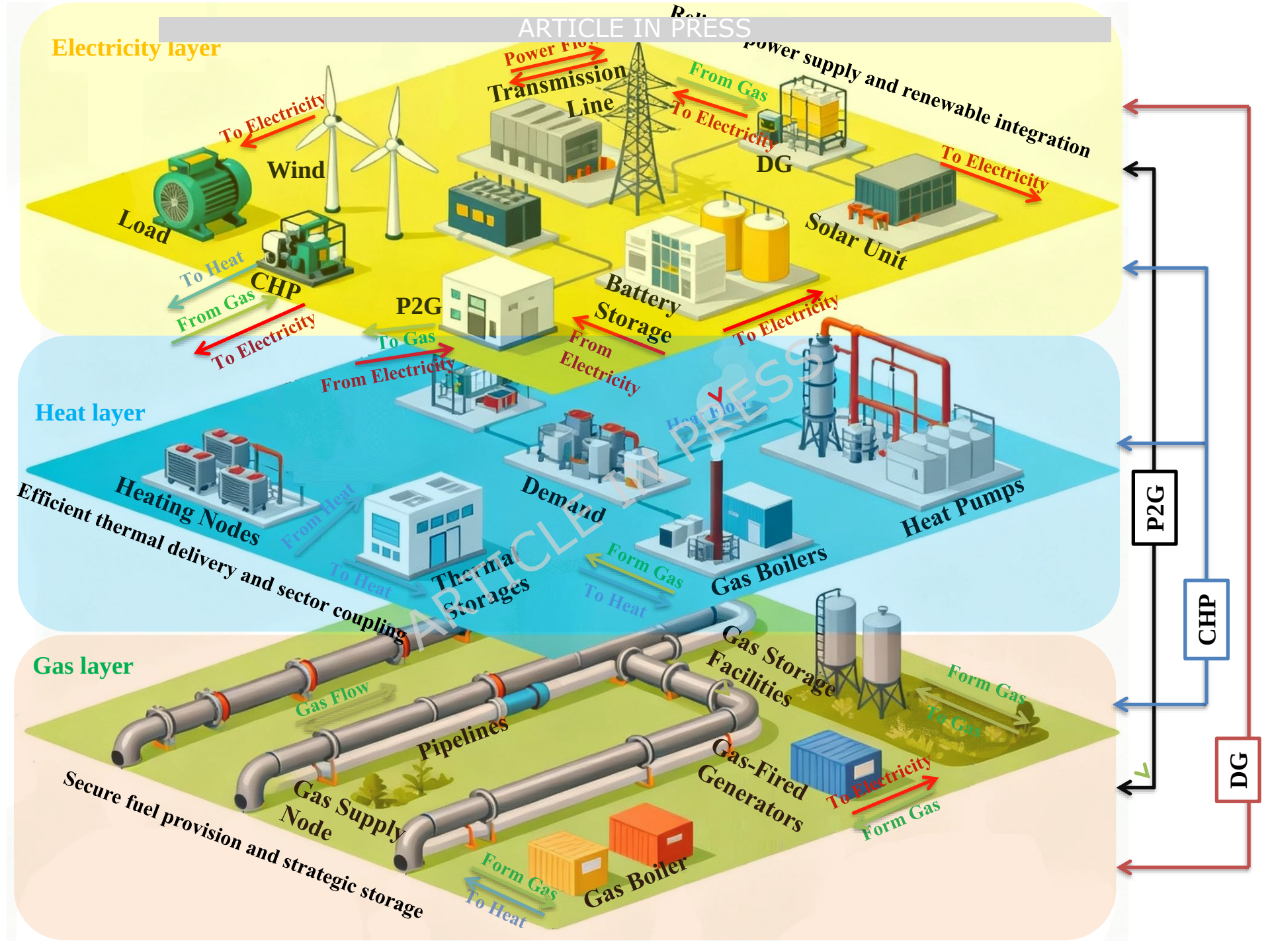

Investment Planning(Level 1)

Long-term infrastructure decisions for electricity, gas, and heating networks

Operational Optimization (Level 2)

Seasonal/hourly dispatch under uncertainty (renewables, loads, fuel prices)

Resilience Assessment (Level 3)

Post-disruption topology switching, microgrid formation, load restoration)

Scenario Generation & C&CG Loop

Operational scenarios (LHS, AR modeling), Disruption scenarios vulnerability